INSTITUTE
FOR
AEROSPACE STUDIES
UNIVERSITY OF TORONTO

AN ANALYSIS OF SHOCK STRUCTURE AND NONEQUILIBRIUM LAMINAR BOUNDARY LAYERS INDUCED BY A NORMAL SHOCK WAVE IN AN IONIZED ARGON FLOW

by

W. S. Liu

October, 1975

UTIAS Report No. 198
CN ISSN 0082-5255

Approved for public release; distribution unlimited.

Qualified requestors may obtain additional copies from the Defense Documentation Center, all others should apply to the National Technical Information Service.

Conditions of Reproduction:

Reproduction, translation, publication, use and disposal in whole or in part by or for the United States Government is permitted.

UNCLASSIFIED

SECURITY CLASSIFICATION OF THIS PAGE (When Data Entered)

REPORT DOCUMENTATION PAGE

READ INSTRUCTIONS BEFORE COMPLETING FORM

1. REPORT NUMBER: [illegible] 76-1329

2. GOVT ACCESSION NO.

3. RECIPIENT'S CATALOG NUMBER (9)

4. TITLE (and Subtitle) (6)
AN ANALYSIS OF SHOCK STRUCTURE AND NONEQUILIBRIUM LAMINAR BOUNDARY LAYERS INDUCED BY A NORMAL SHOCK WAVE IN AN IONIZED ARGON FLOW.

5. TYPE OF REPORT & PERIOD COVERED
INTERIM Rept'y.

6. PERFORMING ORG. REPORT NUMBER
Report No 198.

7. AUTHOR(s) (10)
W. S. LIU

8. CONTRACT OR GRANT NUMBER(s) (14) UTIAS-198 (15) AF-AFOSR-2274-72

9. PERFORMING ORGANIZATION NAME AND ADDRESS
UNIVERSITY OF TORONTO,
INSTITUTE FOR AEROSPACE STUDIES, 4925 DUFFERIN ST.
DOWNSVIEW, ONTARIO, CANADA M3H 5T6

10. PROGRAM ELEMENT, PROJECT, TASK AREA & WORK UNIT NUMBERS (16)
AF-9781
61102F (17) 9781Ø3

11. CONTROLLING OFFICE NAME AND ADDRESS
AIR FORCE OFFICE OF SCIENTIFIC RESEARCH/NA
BUILDING 410
BOLLING AIR FORCE BASE, D C 20332

12. REPORT DATE (11) Oct 75 (12)

13. NUMBER OF PAGES
101 104p.

14. MONITORING AGENCY NAME & ADDRESS (if different from Controlling Office) (18) AFOSR (19) TR-76-Ø329

15. SECURITY CLASS. (of this report)
UNCLASSIFIED

15a. DECLASSIFICATION DOWNGRADING SCHEDULE

16. DISTRIBUTION STATEMENT (of this Report)

Approved for public release; distribution unlimited.

17. DISTRIBUTION STATEMENT (of the abstract entered in Block 20, if different from Report)

18. SUPPLEMENTARY NOTES

19. KEY WORDS (Continue on reverse side if necessary and identify by block number)
IONIZED ARGON SHOCK STRUCTURE
NONEQUILIBRIUM FLOWS
IONIZED ARGON BOUNDARY LAYERS
COLLISION CROSS-SECTIONS
IONIZED ARGON CORNER-EXPANSION FLOWS AND INTERACTIONS
SHOCK TUBE FLOWS
INTEGRAL AND SIMILARITY METHODS
INTERFEROMETRY

20. ABSTRACT (Continue on reverse side if necessary and identify by block number)
An analytical study was made to describe the structure of a strong normal shock wave moving into argon and the nonequilibrium flow of partially ionized argon in the laminar boundary layers induced behind the shock wave on the shock-tube walls and over a flat plate. The subsequent interaction of the laminar boundary layer with a corner-expansion flow was also considered. In order to determine the shock structure, the ionization and relaxation processes were based on a two-step model of the collisional processes. The excitation (or ionization) cross-section constant for the argon atom-atom collisions was determined to be

DD FORM 1 JAN 73 1473 EDITION OF 1 NOV 65 IS OBSOLETE

UNCLASSIFIED 178 920

3.5×10^{-20} cm^2/eV from a comparison of theoretical and experimental shock-structure data. The effects of a small amount of hydrogen impurity in the argon test gas on shock-wave structure was evaluated and discussed, as the hydrogen impurity can markedly reduce the total relaxation length. A study of this effect was required in connection with stabilizing the experimental shock waves. An integral method was used in the analysis to study both the shock induced non-stationary laminar boundary layer on the shock-tube walls and the quasi-steady flat-plate laminar boundary layer for an ionized argon flow. The frozen, equilibrium and nonequilibrium flow solutions were obtained and compared with some existing experimental results. The calculated results based on the integral method were found to be in agreement with the experimental data for the shock-induced wall boundary layer, but they did not agree with the experimental data for the flat-plate quasi-steady boundary layer. The cold-wall similarity method of Sullivan was extended to apply to the interaction of a laminer boundary layer with a corner-expansion wave for a supersonic frozen flow. The validity of the extended method is discussed.

AN ANALYSIS OF SHOCK STRUCTURE AND NONEQUILIBRIUM LAMINAR BOUNDARY LAYERS INDUCED BY A NORMAL SHOCK WAVE IN AN IONIZED ARGON FLOW

by

W. S. Liu

Submitted July, 1974

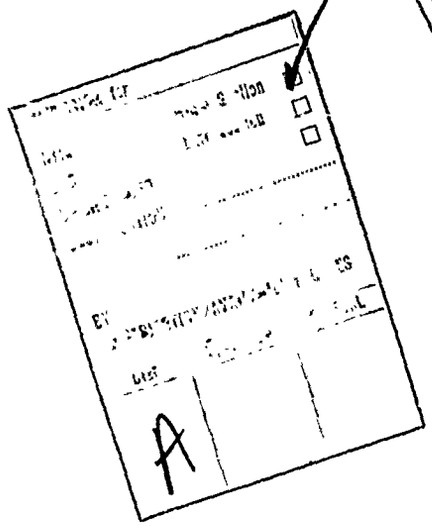

October, 1975

UTIAS Report No. 198

Acknowledgements

I am deeply indebted to Dr. I. I. Glass for the opportunity to do this research. I particularly appreciate his stimulating guidance, helpful suggestions and critical reading of the manuscript. The discussions on the theory and experiment that I received from B. T. Whitten and P. I. Brimelow are acknowledged with thanks. I also appreciated the discussions with Dr. K. Teshima, Department of Aeronautical Engineering, Kyoto University and Centre for Research in Experimental Space Science, York University (CRESS), on shock structure and ionization processes. The assistance received from Dr. J. J. Gottlieb in proofreading the original and final manuscripts is acknowledged with thanks.

The financial assistance from both AFOSR, under grant number AF-AFOSR 72-2274C, and the National Research Council of Canada is gratefully acknowledged.

Summary

An analytical study was made to describe the structure of a strong normal shock wave moving into argon and the nonequilibrium flow of partially ionized argon in the laminar boundary layers induced behind the shock wave on the shock-tube walls and over a flat plate. The subsequent interaction of the laminar boundary layer with a corner-expansion flow was also considered.

In order to determine the shock structure, the ionization and relaxation processes were based on a two-step model of the collisional processes. The excitation (or ionization) cross-section constant for the argon atom-atom collisions was determined to be 3.5×10^{-20} cm^2/ev from a comparison of theoretical and experimental shock-structure data.

The effects of a small amount of hydrogen impurity in the argon test gas on shock-wave structure was evaluated and discussed, as the hydrogen impurity can markedly reduce the total relaxation length. A study of this effect was required in connection with stabilizing the experimental shock waves.

An integral method was used in the analysis to study both the shock induced nonstationary laminar boundary layer on the shock-tube walls and the quasi-steady flat-plate laminar boundary layer for an ionized argon flow. The frozen, equilibrium and nonequilibrium flow solutions were obtained and compared with some existing experimental results. The calculated results based on the integral method were found to be in agreement with the experimental data for the shock-induced wall boundary layer, but they did not agree with the experimental data for the flat-plate quasi-steady boundary layer.

The cold-wall similarity method of Sullivan was extended to apply to the interaction of a laminar boundary layer with a corner-expansion wave for a supersonic frozen flow. The validity of the extended method is discussed.

TABLE OF CONTENTS

Notation

a_n	n^{th} polynomial constant for the velocity profile (Chapter 4)
a_∞	speed of sound (Chapter 5)
A	cross-sectional area of a shock tube
b_n	n^{th} polynomial constant for the enthalpy profile (Chapter 4)
B	magnetic field intensity
B_n	n^{th} constant used in Eq. 4.39b
c_n	n^{th} polynomial constant for the degree of ionization profile (Chapter 4)
C	ratio $\rho\mu/\rho_e\mu_e$
C_n	n^{th} constant used in Eq. 4.39c
C_∞	defined by Eq. 5.2b
Cp	specific heat at constant pressure
C^*	defined by Eq. 3.31
C_f	skin friction coefficient defined by Eq. 5.18
D_{am}	ambipolar diffusion coefficient
e	electron charge
E	electric field intensity
f	velocity ratio defined by Eq. 4.22
f'_B	velocity ratio defined in Section 4.8
F_n	n^{th} integral form defined by Eq. 4.23 (n = 1, 2 or 3)
g	total enthalpy ratio defined by Eq. 4.22
G_{ji}	defined by Eq. 4.2
G(x)	defined by Eq. 5.3
h	enthalpy (specific)
H	enthalpy (total)
I	ionization energy

J	an integral defined by Eq. 4.44
k	Boltzman constant
k	production rate used in Chapter 3
K_{eq}	equilibrium constant of the production rate
κ	thermal conductivity
K	constant defined by Eq. 4.23
L	characteristic length
Le	Lewis number
m	mass
M	Mach number
n	particle number density
p	pressure
P_{ij}	pressure tensor
Pr	Prandtl number
Q	collision cross-section
r	u_w/u_e
R	gas constant
Sc	Schmidt number
S^*	excitational cross-section constant
t	time
T	temperature
u	particle velocity in the x-direction
v	particle velocity in the y-direction
V_d	drift velocity
$\dot{w}$	mass production rate
x	direction parallel to the shock-tube wall
y	direction normal to the shock-tube wall
z	ratio of the degree of ionization defined by Eq.4.22

α	degree of ionization
β	defined by Eq. 4.50a
γ^*	isentropic specific heat ratio for a partially frozen flow
δ	boundary layer thickness
ϵ	internal energy
λ	defined by Eq. 4.27
μ	viscosity
ν	collisional frequency
ρ	density
η	coordinate defined by Eq. 4.20
η_B	coordinate defined by Eq. 4.62b
ξ	coordinate defined by Eq. 4.20
ξ_B	coordinate defined by Eq. 4.62b
$\Delta\phi$	potential between the wall and the plasma

Subscripts

a	atom
Ar	argon
A_r^+	argon ion
e	electron (Chapter 3)
e	boundary layer edge (Chapters 4 and 5)
f	ionization or forward reaction (Chapter 3)
H	hydrogen
H^+	hydrogen ion
i	ion
I	ionization
r	recombination or backward reaction
s	sheath region (Chapter 4)
s	shock (Chapter 3)

Superscripts

*	excitation
+	ion
el	elastic collision

1. INTRODUCTION

The structure of a strong shock wave in an ionizing gas, and the associated nonequilibrium boundary layer flow behind such a shock, have received considerable attention during the past decade. Research into shock structure has determined how elastic and inelastic collisions among atoms, ions and electrons can influence the ionization process. Shock-structure measurements present an opportunity for an indirect determination of excitation (or ionization) cross-sections for heavy gas particles.

An understanding of boundary-layer flows in a partially ionized gas is helpful in designing a successful reentry into the Earth's atmosphere at supersonic and hypersonic conditions. If the term boundary layer can be applied to any region of a continuum flow within which the transport of mass, momentum and energy by diffusive mechanisms is important, then the boundary layer of an ionizing gas can be seen to be generally more complex than that normally encountered in a non-ionized aerodynamic type of flow. The presence of ions and electrons introduces new transport mechanisms in the boundary layer. Additionally, the magnitude of the various transport properties of a partially-ionized gas can be markedly different from a perfect gas. Even today, after many years of research, boundary layer flows of a partially-ionized gas are not fully understood, experimentally or theoretically.

Experiments were recently conducted at UTIAS, using a hypervelocity shock tube. These experiments provided unique and reliable data (interferometric) on both the structure of a strong shock wave in argon and on the shock-induced, nonequilibrium boundary-layer flows in ionized argon, in order to compare with the analyses.

In Chapter 2 the general equations of motion for a partially ionized gas have been reviewed briefly. A simple model for studying initial ionization and relaxation processes behind strong shock waves in an argon flow is given in Chapter 3. The excitation (or ionization) cross-section constant for argon atom-atom collisions can be and is determined from a comparison of theoretical and experimental results. The constant determined herein is more reliable than the value obtained by Kelly (Ref. 12), which has been widely accepted for previous theoretical calculations. The impurity effect of hydrogen molecules on shock structure in argon is also determined and discussed, and the theoretical and experimental results are compared.

The laminar, nonstationary, shock tube-wall boundary layer behind a normal shock wave, and the quasi-steady flat-plate boundary layer in partially ionized argon, are both considered in Chapter 4. The method of solution was based on the Karman-Pohlhausen integral method. The integral and similarity solutions are compared and the results discussed. Theoretical calculations for nonequilibrium, frozen and equilibrium flows are compared with UTIAS experimental data.

In Chapter 5 the cold-wall similarity method of Sullivan is adopted and extended, in order to treat the interaction of a laminar boundary layer with a corner-expansion wave in a partially ionized supersonic argon flow. The flow was assumed to be frozen both before and after the corner expansion. Actually, this assumption is not valid, as

deduced from experimental results (see Chapter 5). However, the assumption greatly simplifies the calculations, and it provides a rough estimation of the variations of pressure, density, temperature and Mach number as a function of turning angle at the edge of the boundary layer. The validity of this oversimplified model is discussed.

In the last chapter discussions are given on the significance of the theoretical models.

2. GENERAL EQUATIONS OF MOTION

2.1 Introduction

The general formulation of the gasdynamic conservation equations for individual species in a nonequilibrium partially ionized gas mixture has been reviewed by Appleton and Bray (Ref. 1). The conservation equations for the electrons and the overall conservation equations were developed for a three-component plasma consisting of neutral atoms, singly ionized ions and electrons. In this formulation the main assumption is that each of the three components has a Maxwellian velocity distribution. Also, the electrons can have a temperature that is different from the heavy particles and they can drift relative to them.

The nonequilibrium electron temperature is of interest in gasdynamic problems involving ionized gases, namely, ionization and relaxation processes in shock waves and in expansion flows in rarefaction waves, nozzles (Ref. 2) and at corners. Nonequilibrium phenomena of electron (or ion) mass production are also of interest in shock structure, boundary layer and expansion-wave (Ref. 3) problems. Recently, Igra (Ref. 4) reviewed briefly the relevant formulations and atomic processes, especially the three-body recombination process. The latter was studied in some detail.

In this chapter the basic equations are presented for a nonequilibrium laminar boundary-layer flow induced behind a normal shock wave on the shock-tube wall or over a sharp leading edge flat plate. The basic equations for an ionized argon plasma flow are based on the general formulation (Ref. 1) of the conservation equations.

2.2 General Equations of Motion for an Ionized Gas

An ionized monatomic gas or plasma is considered which consists of a mixture of atoms, singly ionized ions and electrons. For each species the macroscopic balance equations can be expressed (Ref. 1) by using the plasma macroscopic properties, as shown below,

$$\frac{\partial}{\partial t}\left[n_s \langle \phi_s \rangle\right] + \frac{\partial}{\partial x^j}\left[n_s \langle \phi_s V_s^{\,j} \rangle\right] = I(\phi_s) \qquad (2.1)$$

The quantity $\langle \phi_s \rangle$ is the average of the property ϕ_s, n_s is the number density of species s, $I(\phi_s)$ is the source term of property ϕ_s, and V_s is the total

velocity of a particle of species s. The source term expresses the change in $< \phi_s >$ as a result of both external influences (i.e., electric, magnetic and gravitational fields) and internal influences (i.e., chemical reactions, heat conduction, diffusion and viscosity).

In this analysis, for a mixture of atoms, ions and electrons, it will be assumed that each species has a Maxwellian velocity distribution with an appropriate temperature.

The equations for mass-production rate, momentum and energy for the electron gas are given below:

$$\frac{\partial n_e}{\partial t} + \frac{\partial}{\partial x^j}\left[n_e\, u_e{}^j\right] = \frac{\dot{w}_e}{m_e} \tag{2.2}$$

$$\frac{\partial p_e}{\partial x^j} = -\, n_e\, e\left[E^i + (\bar{u}_e \times \bar{B})^i\right] + n_e\, m_e(\nu_{ea} + \nu_{ei})\,(u^i - u_e{}^i) \tag{2.3}$$

$$\frac{\partial \epsilon_e}{\partial t} + \frac{\partial}{\partial x^j}\left[(\epsilon_e + p_e)u_e{}^j\right] = u_e{}^j \frac{\partial p_e}{\partial x^j} + \frac{dn_e}{dt} I_1 + Q_{rad} + 2n_e \frac{m_e}{m_a}(\nu_{ea} + \nu_{ei})\left[\frac{3}{2} k(T - T_e) + \frac{1}{2} m_a(u^i - u_e{}^i)^2\right] \tag{2.4}$$

The subscripts e, a, and i denote electron, atom and ion, respectively; u and u_e are the velocities of the heavy particles (atoms and ions) and electrons, respectively; $\dot{w}_e$ is the rate of creation (or disappearance) of electrons; m_a and m_e are the masses of the heavy particles (mass of an atom is approximately equal to that of an ion) and electrons, respectively; e is the electron charge; $\bar{E}$ and $\bar{B}$ are the electric and magnetic fields, respectively; ϵ is the internal energy; ν_{ea} and ν_{ei} are the respective collisional frequencies between electrons and atoms and between electrons and ions; Q_{rad} is the radiation source term; T and T_e are the respective temperatures of heavy particles and electrons; p_e is the partial (hydrostatic) pressure of electrons; and I_1 is the net energy gained by the electrons per event of the three-body recombination process.

The equations of continuity, momentum and energy for the whole plasma are obtained by summing the corresponding equations for all the plasma constituents. The following definitions and relationships are used.

$$p = \sum_s p_s$$

$$\epsilon = \sum_s \epsilon_s \qquad \text{where s equals e, a and i}$$

$$e = \sum_s e_s$$

$$\epsilon = \frac{3}{2}\left[n_e\, k\, T_e + (n_a + n_e)\, k\, T\right]$$

$$\epsilon + p = \frac{5}{2}\left[n_e\, k\, T_e + (n_a + n_e)\, k\, T\right]$$

$$p = (n_e + n_a)\, k(T + \alpha\, T_e) \tag{2.5}$$

$$\alpha = \frac{n_e}{n_e + n_a}$$

$$e \simeq m_a(n_a + n_e)$$

The degree of ionization of the plasma is denoted by the symbol α.

The equations of motion for the entire plasma are then written as follows:

$$\frac{\partial e}{\partial t} + \frac{\partial}{\partial x^j}\left[e\, u^j\right] = 0 \tag{2.6}$$

$$\rho \frac{Du^i}{Dt} = \frac{\partial P_{ij}}{\partial x^j} + (n_i - n_e)\, e[E^i + (\vec{u} \times \vec{B})^i] + n_e\, e[(\vec{u} - \vec{u}_e) \times B]^i \tag{2.7}$$

$$\rho \frac{DH_1}{Dt} + \frac{DP_{ij}}{Dt} = - n_e\, e[(\vec{u} - \vec{u}_e) \times \vec{B}]^i\, u^i + n_e\, e[u^i - u_e^i]\, E^i + \frac{\partial}{\partial x^j}\left[(\epsilon_e + p_e)\,(u^i - u_e^i)\right] + Q_{rad} - \frac{dn_e}{dt} I_1 \tag{2.8}$$

where, P_{ij} is the pressure tensor defined as

$$P_{ij} = - p\delta_{ij} + \tau_{ij} \tag{2.9}$$

and τ_{ij} is the viscous stress tensor, which contributes to the plasma dissipation. H_1 in Eq. 2.8 is defined by

$$H_1 = \frac{5}{2}\frac{k}{m_a}(T + \alpha\, T_e). \tag{2.10}$$

We should note that if the viscous effects can be neglected (i.e., $\tau_{ij} = 0$), then Eqs. 2.8 and 2.9 reduce to the equations given by Appleton and Bray (Ref. 1). Additionally, the pertinent set of equations for other simpler problems can be obtained from the general equations - Eqs. 2.2 to 2.8.

2.3 Equations for a One-Dimensional Inviscid Flow of an Ionized Gas

For studies of shock structure and expansion nozzle flows, the variation of dynamic and thermodynamic quantities in the direction normal to the flow direction are normally small compared with those in the flow direction. Hence these problems can be treated as one-dimensional.

Actually, the flow for the shock-structure problem is nonstationary. However, a nonstationary flow can be readily reduced to a steady flow. Let $(\bar{x}, \bar{y})$ be a coordinate system fixed with respect to the wall, and let $(\bar{u}, \bar{v})$ be velocities parallel to $(\bar{x}, \bar{y})$. The flow is unsteady in this $(\bar{x}, \bar{y})$-coordinate system. Let (x, y) represent another coordinate system which moves with the same speed as the shock wave, and let the velocities parallel to the x- and y-coordinates be denoted by u and v respectively. In this coordinate system the flow is steady. The transformation relating the two coordinate systems is given below.

$$\begin{aligned} \bar{x} &= x - u_e t \\ \bar{y} &= y \\ \bar{u} &= u - u_w \\ \bar{v} &= v \end{aligned} \tag{2.11}$$

The velocity of the wall, u_w, equals the negative value of the shock velocity, u_s. Under this transformation, nonstationary flows for shock structure and boundary layers behind a moving shock can be conveniently treated as quasi-steady flows (see Fig. 1).

For treating the shock-structure problem two assumptions are made: (1) no electric or magnetic fields exist ($\vec{E} = \vec{B} = \vec{0}$), (2) $u_e = u$. Note that the magnitude of the electric field can be predicted by the following expression.

$$E^i \simeq - \frac{1}{n_e e} \frac{\partial p_e}{\partial x^i}$$

which is negligible for the present study. In a similar fashion the magnetic field can be shown to be even less important. Due to the very small electron mass, the effects of diffusion ($u_e \neq u$) are small and can be neglected. The preceding two assumptions, which can be justified for many types of nonequilibrium shock-structure problems, have been widely accepted by previous researchers.

For the present shock-structure study, the translational transition region of the shock front has been neglected, since its thickness is negligibly small compared with that of the following relaxation region. It should be

noted that if the translational transition region of the shock front is considered, gradients in the flow variables are large and the effects of viscosity $[\frac{\partial}{\partial x}(\mu \frac{\partial u}{\partial x})]$, and heat conduction, $[\frac{\partial}{\partial x}(\kappa_a \frac{\partial T}{\partial x})]$ and $[\frac{\partial}{\partial x}(\kappa_e \frac{\partial T}{\partial x})]$, must be included.

For a steady one-dimensional and inviscid flow of a singly ionized gas, Eqs. 2.2 to 2.8 reduce to the following expressions.

Conservation of electron mass:

$$\frac{d}{dx}(n_e u) = \frac{dn_e}{dt} \tag{2.12}$$

$$\frac{d}{dx}(\frac{5}{2} n_e k T_e u) = 3 n_e \frac{m_e}{m_a}(\nu_{ea} + \nu_{ei}) k(T - T_e) - \frac{dn_e}{dt} I + Q_{rad} + k u[n_e \frac{dT_e}{dx} + T_e \frac{dn_e}{dx}] \tag{2.13}$$

Conservation of total mass:

$$\frac{d}{dx}(\rho u A) = 0 \tag{2.14}$$

Total momentum:

$$\rho u \frac{du}{dx} = - \frac{dp}{dx} \tag{2.15}$$

Conservation of energy:

$$\rho u \frac{dH_1}{dx} - u \frac{dp}{dx} = Q_{rad} - \frac{dn_e}{dt} I \tag{2.16}$$

The Boltzmann constant is denoted by k, A is the shock-tube cross-sectional area or expansion nozzle cross-section, I denotes the ionization energy of the atom, and

$$\begin{aligned} p &= \rho \frac{k}{m_a}(T + \alpha T_e), \\ H_1 &= (\epsilon + p)/\rho, \\ \epsilon &= \frac{3}{2}[n_e k T_e + (n_a + n_e) k T]. \end{aligned} \tag{2.17}$$

These basic equations contain five dependent variables: $n_e(x)$, $n_a(x)$, $T(x)$, $T_e(x)$ and $u(x)$. Any numerical solution will depend on the model adopted to describe the atomic processes for $\frac{dn_e}{dt}$ and Q_{rad}.

In the case of the shock-structure problem, if the cross-sectional area of the shock tube is sufficiently large, then the effects of the wall boundary layer on reducing the total area will be negligibly small. Therefore,

A in Eq. 2.14 can be taken to be constant. The effect of the wall boundary layer can be included simply by assuming the variation of the cross-sectional area outside the boundary layer is a given function of distance (x). Let A_o be the initial area at distance x equal to zero, then

$$A(x) = A_o F(x) \tag{2.18}$$

where F(x) can be calculated by using boundary-layer theory.

The basic difference between shock-structure and expansion nozzle problems is in the atomic collision processes. For the shock-structure problem the initial ionization processes due to atom-atom collisions are dominant. By contrast, in the expansion-nozzle problem, the three-body recombination process dominates in the entire relaxation region. The former case provides an opportunity to determine the excitation (or ionization) cross-section for an atom-atom collision, and the latter case allows one to determine the excitation cross-section for electron-atom collisions or the recombination rate constant.

2.4 Equations for the Laminar Boundary Layer Flow Induced by a Strong Shock Wave

For a two-dimensional problem, Eqs. 2.2 to 2.8 contain fourteen independent variables: n_e, n_a, T_e, T, u, v, u_e, v_e, E_x, E_y, E_z, B_x, B_y and B_z. Because of the complexity of the equations, no numerical solutions appear to exist. The less general two-dimensional inviscid plasma flow with the assumptions, $T = T_e$, $u_e = u$, $v_e = v$, $\vec{E} = \vec{B} = \vec{0}$ and $Q_{rad} = 0$ has been solved by many researchers. For example, Glass and Takano (Ref. 3) deal with the problem of a corner-expansion flow.

The occurrence of an appreciable degree of ionization in a gas flow introduces some features that are markedly different from those normally encountered in a perfect-gas flow or in a flow with chemical dissociation, primarily because of the presence of ions and electrons. The reasons are given as follows:

1. The extremely low mass of the electron yields a species possessing a thermal conductivity that can be much higher than that of any other species present in the mixture.

2. The collisional energy-transfer process between electrons and heavy particles is relatively slow and gives rise to the possible situation in which the electrons may have a temperature different from that of the heavy species.

The detailed analysis of an appreciably ionized gas is necessarily complex.

In general, it is well known that three rather distinct regions exist near the surface of a plasma flow:

1. Away from the wall the gas is quasi-neutral, the ion diffusion velocity is small, and the behaviour of the gas in this region is described by continuum equations.

2. Near the surface but not adjacent to it the gas remains quasi-neutral, but the ion diffusion velocity is comparable to the ion sound velocity and the usual equations are not valid (the region will be referred to as the "transition region".

3. Adjacent to the surface of the wall a space charge sheath exists within the gas which is no longer quasi-neutral.

A major difficulty exists in connection with the latter two regions, because it is necessary to solve the Boltzmann equation for each species. In Fig. 2 the flow regimes near a cold surface and the order of thickness of each regime are indicated.

In the case of a partially ionized gas, a sheath formed next to the wall is thin compared to the boundary layer thickness. Hence, the ionized gas in the boundary layer should be electrically neutral and the concept of ambipolar diffusion can be adopted (described in Section 4.3).

The present section is specifically concerned with the basic equations for a nonequilibrium boundary-layer development on the cold wall surface. The basic assumptions are: (1) steady flow, (2) laminar flow (3) no continuum radiation losses, (4) all species have the same mass motion velocity, (5) free-stream conditions are constant along the flow direction, (6) no electric or magnetic fields exist, (7) $T = T_e$. Note that when the boundary layer is inside the relaxation zone, assumption (7) may be invalid. Under these assumptions, the basic equations for the boundary layer flow are given below (Ref. 47).

Continuity equation:

$$\frac{\partial}{\partial x}(\rho u) + \frac{\partial}{\partial y}(\rho v) = 0 \tag{2.19}$$

Momentum equation:

$$\rho u \frac{\partial u}{\partial x} + \rho v \frac{\partial u}{\partial y} = - \frac{dp}{dx} + \frac{\partial}{\partial y}\left(\mu \frac{\partial u}{\partial y} \right) \tag{2.20}$$

Energy equation:

$$\rho u \frac{\partial H}{\partial x} + \rho v \frac{\partial H}{\partial y} = \frac{\partial}{\partial y}\left[- q_c - q_d + \mu \frac{\partial}{\partial y}\left(\frac{u^2}{2} \right) \right] \tag{2.21}$$

Conservation of species:

$$\rho u \frac{\partial \alpha}{\partial x} + \rho v \frac{\partial \alpha}{\partial y} = \frac{\partial}{\partial y}\left[- \rho_i V_i \right] + \dot{w}_i \tag{2.22}$$

In these expressions, the respective symbols μ, H, q_c, q_d, V_i, ρ_i and $\dot{w}_i$ denote viscosity, stagnation enthalpy, conductive heat flux, diffusive energy flux, ion diffusion velocity normal to the wall, ion density, and net production rate of ions.

For an electrically neutral, singly ionized, monatomic gas consisting of atoms, ions and electrons, all at the same temperature, the equilibrium-thermodynamic relations and the equation of state for the mixture are given below.

$$p = \rho R T (1 + \alpha) \tag{2.23}$$

$$H = \frac{5}{2} R T (1 + \alpha) + \alpha I + \frac{u^2}{2} \tag{2.24}$$

where, I denotes the ionization energy. Note, the enthalpy due to excitational effects is neglected.

The conductive heat flux (q_c) is given as follows:

$$\begin{aligned} q_c &= - \kappa \frac{\partial T}{\partial y} \\ &= - \frac{\kappa}{\bar{c}_p} \left[\frac{\partial H}{\partial y} - \frac{\partial}{\partial y} \left(\frac{u^2}{2} \right) - (I + \frac{5}{2} R T) \frac{\partial \alpha}{\partial y} \right] \end{aligned} \tag{2.25}$$

where $\bar{c}_p$ is the "frozen" specific heat at constant pressure and defined below.

$$\bar{c}_p = \frac{5}{2} R (1 + \alpha) \tag{2.26}$$

R is the gas constant for the atom and κ is the thermal conductivity for the mixture if no chemical reactions took place.

The diffusive energy flux for ambipolar diffusion (q_d) is given by the following expression:

$$q_d = - \rho D_{am} [I + \frac{5}{2} R T] \frac{\partial \alpha}{\partial y} \tag{2.27}$$

where D_{am} is the ambipolar diffusion coefficient.

The diffusive mass flux of ions ($\rho_i V_i$) for ambipolar diffusion by ion-electron pairs is governed by Fick's law, as given below.

$$\rho_i V_i = - \rho D_{am} \frac{\partial \alpha}{\partial y} \tag{2.28}$$

By introducing the Prandtl and Lewis numbers defined by

$$\begin{aligned} P_r &= \frac{\mu \bar{c}_p}{\kappa} \\ L_e &= \frac{\rho D_{am} \bar{c}_p}{\kappa} \end{aligned} \tag{2.29}$$

the ion (or electron) concentration and energy conservation equations take the following form:

$$\rho u \frac{\partial \alpha}{\partial x} + \rho v \frac{\partial \alpha}{\partial y} = \frac{\partial}{\partial y} \left[\mu \frac{L_e}{P_r} \frac{\partial \alpha}{\partial y} \right] + \dot{w}_i \tag{2.30}$$

$$\rho u \frac{\partial H}{\partial x} + \rho v \frac{\partial H}{\partial y} = \frac{\partial}{\partial y}\left[\frac{\mu}{P_r} \frac{\partial H}{\partial y} + \mu \left(1 - \frac{1}{P_r}\right) \frac{\partial}{\partial y}\left(\frac{u^2}{2}\right) \right.$$

$$\left. + \frac{\mu}{P_r} (L_e - 1) \left(I + \frac{5}{2} R T\right) \frac{\partial \alpha}{\partial y} \right] . \qquad (2.31)$$

In general the Prandtl and Lewis numbers are functions of the gas temperature (T) and degree of ionization (α), as shown in Section 4.2. This temperature and degree of ionization dependence couples Eqs. 2.19 and 2.20 to Eqs. 2.30 and 2.31, making it difficult to obtain a solution.

3. SHOCK STRUCTURE AND INITIAL IONIZATION PROCESSES

3.1 Introduction

Experimental and theoretical investigations of ionization rates and relaxation processes behind strong shock waves moving in monatomic gases can be found in Refs. 5 to 19. It is now well established that when a strong shock wave raises the temperature of atoms from a low temperature (about 300°K) to a high temperature (over 10,000°K), the initial ionization is due to atom-atom collisions. The rate of ionization is controlled by the rate of excitation from the ground state to the first excited level. Ultimately when the number of electrons becomes sufficiently large, electron-atom and ion-electron-electron collisions dominate the excitation, ionization and recombination processes (see Eq. 3.1), and the rate of ionization is controlled by the rate of energy transfer between the heavy particles and the electrons. The radiative processes will be important (Ref. 5) for a low electron number density (e.g., at $T \simeq 3200°K$ and $n_e < 10^{12}$ cm^{-3}). Treatments of relaxation phenomena in radiating argon-plasma flows can be found in Refs. 6, 7, 8 and 9. For specific conditions of a shock Mach number of 15 and an initial pressure of 1 torr, Kamimoto et al (Ref. 9) have shown that the effect of radiation on the relaxation profiles is negligible. Oettinger and Bershader (Ref. 6) have shown that the effect of radiation is negligibly small only until the end of the relaxation zone. Thereafter radiative emission becomes appreciable.

In general, the excitation cross-section for atom-atom collisions is well known. The shock tube presents an opportunity for indirect measurements to be made of the excitation (or ionization) cross-section of heavy gas particles. Recently, Harwell and Jahn (Ref. 10) have employed a transverse microwave probe to determine the cross-section constant of proportionality, $S^*_{Ar\text{-}Ar}$, as equal to 7×10^{-19} cm^2/eV, for argon inelastic atom-atom collisions. Morgan and Morrison (Ref. 11) have made a theoretical reassessment of the ionization mechanism and referred to earlier experimental measurements. They showed that a best fit curve to the ionization relaxation time measurements of Petschek and Byron (Ref. 5) was obtained by reducing Harwell and Jahn's value (Ref. 10) for $S^*_{Ar\text{-}Ar}$ by a factor of ten. Kelly (Ref. 12) has reduced the impurity level for his experiments and obtained a value for $S^*_{Ar\text{-}Ar}$ of $1.2 \times 10^{-19} \pm 15\%$ cm^2/eV, which has been widely accepted by many researchers (Refs. 2, 7, 10 and 13) for their theoretical calculations. However, we must point out that there are two important effects which must

be considered in regard to Kelly's experiments: (1) the range of the shock Mach number was between 7 and 10, which is too low, and (2) the relatively small cross-sectional area of the shock tube (5cm x 5cm) makes the wall boundary layer effect important (i.e., $dA/dx \neq 0$). On the other hand, McLaren and Hobson (Ref. 14) have used double electrostatic probes to measure the ionization rates and they obtained a value for $S^*_{Ar\text{-}Ar}$ of 2.5×10^{-20} cm^2/eV, which is lower than the value suggested by Morgan and Morrison (Ref. 11). Although many experiments have been made with argon to determine the initial ionization processes, the excitation cross-section for argon atom-atom collisions has not been determined with great accuracy.

An experimental investigation (Ref. 15) of the initial ionization processes in a strong shock wave in argon and in a mixture of argon and hydrogen (0.4% by partial pressure) was made recently in the UTIAS 4-in x 7-in hypervelocity shock tube. This investigation provided the most reliable data for determining $S^*_{Ar\text{-}Ar}$. Considerable care was taken to reduce the impurity levels to approximately 10^{-4} torr. Therefore at an initial pressure of about 5 torr for the present experiments the impurity level was about 20 parts per million or less. The large cross-sectional area made the effect of the wall boundary layer negligible during the experiments. The purpose of the present chapter is to propose a simple, theoretical model from which the excitation cross-section constant of proportionality for argon atom-atom collisions can be determined from the experimental results (Ref. 15). The effect of the small hydrogen impurity in the argon test gas on the ionization rate is calculated, compared with experimental work (Ref. 15) and discussed.

In the present study the transition through the translational shock front is neglected since its thickness is negligibly small compared with that of the relaxation region. In the translation transition region in the flow variables are large and the effects of viscosity $\left[\frac{\partial}{\partial x}\left(\mu \frac{\partial u}{\partial x}\right)\right]$, and heat conduction $\left[\frac{\partial}{\partial x}\left(\kappa_a \frac{\partial T}{\partial x}\right)\right]$ and $\left[\frac{\partial}{\partial x}\left(\kappa_e \frac{\partial T}{\partial x}\right)\right]$, must be considered. However, as only the relaxation region is considered, where the gradients are small (see Figs. 6 and 7), the viscous and heat conduction dissipative processes can be neglected. Then the only important processes in the flow are the collisional processes.

3.2 Collisional Ionization Rates

Petschek and Byron (Ref. 5) and Harwell and Jahn (Ref. 10) have shown that excitation from the ground state to the first-excited state is rate controlling for the overall ionization process. This two-step process is based on the fact that the cross-section for excitation from the ground state is greater than that for ionization from the ground state. This familiar two-step collisional ionization model is adopted herein. Of course, the multi-step collisional radiative ionization models of Hollenbach and Salpeter (Ref. 16), Kamimoto et al (Ref. 9) and Bates et al (Ref. 17) are the most accurate. However, many unknowns are contained in those models and some simplifying assumptions are required before actual calculations can be made. For example, there are three unknowns in the ladder-climbing model of Hollenbach and Salpeter, where transitions to neighbouring levels are only allowed. Kamimoto et al have shown that the results for argon atom and electron number densities as calculated by a two-step model are

nearly the same as those calculated using a multi-step model, except that the relaxation time based on the multi-step model was somewhat longer.

The collisional-ionization kinetics of singly ionized argon are postulated to take place according to the following equations:

$$Ar + X \rightleftharpoons A_r^* + X \tag{3.1a}$$

$$A_r^* + X \rightleftharpoons A_r^+ + e + X \tag{3.1b}$$

$$Ar + X \underset{k_r}{\overset{k_f}{\rightleftharpoons}} A_r^+ + e + X \tag{3.1c}$$

The two-step model is represented by Eqs. 3.1a and 3.1b for the overall reaction path given by Eq. 3.1c; X denotes either the argon atom (A_r) or an electron (e).

For this collision process one can express the electron-production rates $(\dot{n}_e)_a$ and $(\dot{n}_e)_e$ in terms of recombination rates and equilibrium constants (Ref. 13), as illustrated below:

$$(\dot{n}_e)_a = k_{fa}\, n_a^2 - k_{ra}\, n_a\, n_e^2$$

$$= k_{ra}\,(T_a)\, n_a \left[K_{eq}\,(T_a)\, n_a - n_e^2\right] \tag{3.2}$$

$$(\dot{n}_e)_e = k_{fe}\, n_a\, n_e - k_{re}\, n_e^3$$

$$= k_{re}\,(T_e)\, n_e \left[K_{eq}\,(T_e)\, n_a - n_e^2\right] \tag{3.3}$$

The electron-production rate due to atom-atom collisions is denoted by $(\dot{n}_e)_a$ and that due to atom-electron collisions is denoted by $(\dot{n}_e)_e$, and the subscripts a and e denote atoms and electrons, respectively. The two equilibrium constants are defined by the following expressions:

$$K_{eq}\,(T_a) = \frac{n_{e,eq}^2\,(T_a)}{n_{a,eq}\,(T_a)} \tag{3.4a}$$

$$K_{eq}\,(T_e) = \frac{n_{e,eq}^2\,(T_e)}{n_{e,eq}\,(T_e)} \tag{3.4b}$$

The calculations of k_{ra} and k_{re} require a knowledge of the dependence of the inelastic-collision cross-section for the first-excited level (σ^*_{ax}) and on the kinetic energy (ϵ_x). A reasonably good approximation is given below:

$$\sigma^*_{ax} = S^*_{ax} (\epsilon_x - \epsilon^*_a) \text{ with } \epsilon_x \geq \epsilon^*_a \tag{3.5}$$

where S^*_{ax} is the constant of proportionality of the first-excitation collision cross-section between atom a, and particle x, and ϵ^*_a is the excitation energy of the first level.

By applying Eq. 3.5, k_{ra} and k_{re} can be expressed (as in Refs. 11 and 13) in terms of S^*_{ax} for argon atoms as shown below:

$$k_{ra}(T_a) = 4.835 \times 10^{-18} S^*_{Ar\text{-}Ar} \left(\frac{T^*}{T_a} + 2 \right) \exp \left(\frac{T_I - T^*}{T_a} \right) \frac{cm^6}{sec} \tag{3.6}$$

$$k_{re}(T_e) = 1.843 \times 10^{-15} S^*_{Ar\text{-}e} \left(\frac{T^*}{T_e} + 2 \right) \exp \left(\frac{T_I - T^*}{T_e} \right) \frac{cm^6}{sec} \tag{3.7}$$

T^* and T_I are the first-excitation and ionization temperatures respectively for an argon atom, and S^* is in units of cm^2/eV. (Note that k_{ra} in Eq. 3.6 has now been divided by a factor of 2 to avoid counting like-like collisions twice.)

A schematic diagram of the collision processes from the Rankine-Hugoniot translational shock front through the relaxation region appears in Fig. 3. The boundary layer formation in this region is also indicated. Radiation losses give rise to a somewhat nonuniform equilibrium flow. It is important to take this loss into account during the calculation of the physical properties of the flow.

3.3 Governing Equations

The theoretical approach to solving the shock structure is similar to that described in Ref. 13, except the correct equations given in Section 2.3 are used. Note that the conservation equations of electron energy described in Ref. 13 are only an approximation for Eq. 2.13. The governing equations are obtained from Eqs. 2.12 to 2.16, as given below:

$$\frac{d}{dx}(n_e u) = \frac{dn_e}{dt} = \dot{n}_e \tag{3.8}$$

$$\frac{dT_e}{dx} = 2 \left(\frac{m_e}{m_a} \right) \frac{\nu_{ea} + \nu_{ei}}{u} (T - T_e) - \frac{2T_e}{3u} \frac{du}{dx} - \frac{2}{3} \frac{(\dot{n}_e)_e}{un_e} (T_x + \frac{3}{2} T_e) \tag{3.9}$$

$$\rho u = \rho_1 u_1 \tag{3.10}$$

$$p + \rho u^2 = p_1 + \rho_1 u_1^2 \tag{3.11}$$

$$\frac{5}{2} R(T + \alpha T_e) + \alpha R T_I + \frac{1}{2} u^2 = \frac{5}{2} R T_1 + \frac{u_1^2}{2} \tag{3.12}$$

The subscript 1 refers to the state of the gas in front of the translational shock front, ν_{ea} and ν_{ei} denote the elastic collision frequencies for the pairs electron-atom and electron-ion respectively, which can be expressed in terms of the elastic-collision cross-sections σ_{ea}^{el} and σ_{ei}^{el}, as shown below:

$$\nu_{ea} = \frac{(1-\alpha)\rho}{m_a} \left(\frac{8kT_e}{\pi m_e} \right)^{\frac{1}{2}} \sigma_{ea}^{el} \tag{3.13a}$$

$$\nu_{ei} = \frac{\alpha\rho}{m_a} \left(\frac{8kT_e}{\pi m_e} \right)^{\frac{1}{2}} \sigma_{ei}^{el} \tag{3.13b}$$

The degree of ionization (α) is defined by Eq. 2.5.

From the fact that $\dot{n}_e = n_e(\dot{\alpha}/\alpha)$, Eqs. 3.2 and 3.3 yield the following expressions.*

$$\dot{\alpha}_a(T) = (1 - \alpha) \left[\frac{\rho}{m_a} \right]^2 k_{ra}(T) \left[\frac{\alpha_{eq}^2(T)}{1 - \alpha_{eq}(T)} (1 - \alpha) - \alpha^2 \right] \tag{3.14a}$$

$$\dot{\alpha}_e(T_e) = \alpha \left(\frac{\rho}{m_a} \right)^2 k_{re}(T_e) \left[\frac{\alpha_{eq}^2(T_e)}{1 - \alpha_{eq}(T_e)} (1 - \alpha) - \alpha^2 \right] \tag{3.14b}$$

The conservation of electron mass, Eq. 3.8, becomes

$$\frac{d\alpha}{dx} = (\dot{\alpha}_a + \dot{\alpha}_e)/u \tag{3.15}$$

where $\dot{\alpha}_a$ and $\dot{\alpha}_e$ denote production rates due to atom-atom and atom-electron collisions, respectively.

The equilibrium value of the degree of ionization, $\alpha_{eq}(T)$, can be obtained from the following equation (Ref. 3):

$$\frac{\alpha_{eq}^2}{1 - \alpha_{eq}} = \frac{\rho_I}{\rho} \left[\frac{T}{T_I} \right]^{3/2} \exp(-T_I/T) \tag{3.16}$$

The characteristic density for ionization ρ_I is defined by Eq. 2.24 of Ref. 3 (see Table 1 of this report).

*Note that Eqs. 15 and 16 of Ref. 13 are incorrect.

The value of du/dx which appears in Eq. 3.9 is obtained easily from Eqs. 3.10 to 3.12, and it is given below,

$$\frac{du}{dx} = -\frac{6}{5}\frac{u\,T_I}{M_s^2\,T_1}\left[9\left(1-\frac{1}{M_s^2}\right)^2+\frac{96\alpha}{5M_s^2}\frac{T_I}{T}\right]^{-\frac{1}{2}}\frac{d\alpha}{dx} \qquad (3.17)$$

3.4 Model Calculations and Comparison with Experimental Results for Pure Argon

For the present calculations the same collisional cross-section employed by Petschek and Byron (Ref. 5) with $S^*_{Ar\text{-}e}$ equal to 7.0×10^{-18} cm^2/eV was used. The values of σ^{el}_{ea} have been taken from Refs. 11 and 13. The initial conditions employed for the calculations for a shock wave in pure argon are summarized in Table 2, which coincide with those used in the experimental work in the UTIAS 4-in x 7-in hypervelocity shock tube (Refs. 15 and 18).

The first-order differential equations (Eqs. 3.9 and 3.15) were solved by using a standard Runge-Kutta method (see Appendix A). The initial condition for α was taken as $\alpha(0) \simeq 0$. The initial value of the electron temperature is somewhat ambiguous. Three values of the initial electron temperature are given as follows:

1. $T_e(0) = T_1$ ($\simeq 300°K$),
2. $T_e(0) = T(0)$, and
3. local steady-state value.

However, it should be noted that these different initial values would not affect the values of the other physical quantities, as the initial number density of the electrons is very small, or α is approximately zero.

For a strong shock wave moving in pure argon (Case I of Table 2), predicted and experimental variations of the degree of ionization (α) with distance (x) through the relaxation region are shown in Fig. 4. The degree of ionization initially increases rather slowly from zero at the shock front (x = 0) and eventually rises rapidly to its equilibrium value (α_e = 0.158). The dashed line corresponds to a solution using the value of $S^*_{Ar\text{-}Ar}$ equal to 0.6×10^{-19} cm^2/eV. It can be seen that this predicted variation for α has the same features as displayed by the experimental data (Ref. 15), but the predicted relaxation length (or time) is significantly shorter. It would be even worse for larger values of $S^*_{Ar\text{-}Ar}$. In addition, a number of calculations with different $S^*_{Ar\text{-}Ar}$ values showed that the relaxation length increased with decreasing values of $S^*_{Ar\text{-}Ar}$. The continuous line in Fig. 4, corresponding to a solution with a lower $S^*_{Ar\text{-}Ar}$ value of 3.5×10^{-20} cm^2/eV, which is in good agreement with the experimental data. Hence, from such a comparison the excitational cross-section constant for argon atom-atom collisions ($S^*_{Ar\text{-}Ar}$) has been determined to be 3.5×10^{-20} cm^2/eV. This newly determined value is used for the remainder of the calculations.

The predicted and measured variation of density through the relaxation region is shown in Fig. 5. The predicted and measured density profiles are in good agreement, adding further verification to the acceptance of the new value for $S^*_{Ar\text{-}Ar}$.

The atom-temperature (T) and electron-temperature (T_e) variations through the relaxation zone are displayed in Fig. 6. Although three different initial electron temperatures were selected, the electron-temperature profile is affected by this choice only in the small initial part of the relaxation region, as shown in the figure.

The flow velocity and pressure variations in the relaxation region are given in Fig. 7, and in Fig. 8 the variations of electron number density (n_e) and ionization production rates are shown. It can be seen that the ionization production rate due to atom-atom collisions ($\dot{\alpha}_a$) is very large in the initial stage of the ionization process as compared with that due to atom-electron collisions ($\dot{\alpha}_e$), and the collision process is controlled by atom-atom collisions. The ionization production rate $\dot{\alpha}_e$ increases very rapidly as the number of electrons increase. After $\dot{\alpha}_e$ exceeds $\dot{\alpha}_a$, then $\dot{\alpha}_a$ quickly decreases and the collision process is controlled by atom-electron collisions. Eventually $\dot{\alpha}_e$ reaches a maximum and then falls off rapidly, and the collision process is controlled by three-body recombination (electron-electron-ion) and radiation processes.

Additional predicted and measured results (Ref. 15) for the density and degree of ionization variations through the relaxation zone are given in Fig. 9. These results for Case II, Table 2, are not too different from those of Case I, and the predicted and measured data are in fair agreement.

For Case III, Table 2, for which the shock strength and degree of ionization are both less, the predicted and measured degree of ionization profiles for the relaxation region are compared in Fig. 10. The agreement is not as good as for Cases I and II. This disagreement, however, is most likely due to inaccurate experimental measurements. Brimelow (Ref. 15) has mentioned that it was difficult to obtain accurate data from interferograms that exhibit small fringe shifts, as is the case when the degree of ionization is small. However, it should be noted that the analysis predicts the correct relaxation length.

t should be pointed out that the analysis overpredicts the relaxation lengths as measured by Oettinger and Bershader (Ref. 6). The initial conditions for both Brimelow's work (Ref. 15) and Oettinger and Bershader (Ref. 6) were the same. However, the measured relaxation lengths of Oettinger and Bershader were shorter. The reason for the different lengths is not clear. The shock tube used by Oettinger and Bershader had a smaller cross-section and its impurity level is not known.

In some of the interferometric results of Brimelow (Ref. 15), it was found that the degree of ionization was larger near the shock-tube wall than at the centre of the freestream, and relaxation lengths were shorter near the wall. At the present time it is difficult to explain this phenomenon. It may be possible that a two-dimensional model incorporating the viscous effect and impact phenomena between ions (or electrons) and a solid surface would be required to explain the above-mentioned phenomenon, or perhaps impurity gradients (e.g., water molecules) closer to the wall may account for it.

3.5 Effects of Hydrogen Impurity on the Ionization Processes

The effects of impurities in the test gas on the structure of shock waves was studied initially by Morgan and Morrison (Ref. 11). In this section, the effects of a small addition of hydrogen (impurity) to the argon test gas on the shock wave structure is considered in some detail.

The initial ionization of hydrogen in a strong shock wave has been studied by Belozerov and Measures (Ref. 19). From a comparison of theoretical and experimental results they have determined S^*_{H-H} to be 3.57×10^{-18} cm^2/eV, which is about 1/15 that of the corresponding cross-section for electron-atom excitation collisions where S^*_{H-e} equals 5.1×10^{-17} cm^2/eV. They showed that the electron temperature is nearly identical to the atom temperature everywhere in the relaxation region except for a very small region near the shock front ($x \simeq 0$). This result is quite different from a similar solution for an argon test gas (see Section 3.4). The reasons are as follows: first, the mass of the hydrogen atom is 1/40 that of the argon atom, and second, there is no Ramsauer effect (Ref. 19) for the electron-hydrogen atom elastic collisions. The latter effect reduces the cross-section for elastic electron-argon atom collisions.

Chang (Ref. 20) has shown that for certain shock velocities it is possible to consider the different relaxation processes (e.g., translation, vibration, dissociation, and ionization) independently for hydrogen molecules. For the present work we can assume that ionization of the hydrogen molecules behind a strong shock starts effectively after dissociation is complete. Also, the relaxation length for the dissociation process is very small compared with ionization. With these assumptions there appears to be no difference between hydrogen and monatomic argon in the theoretical description of the ionization process. The only difference in the ionization processes between pure hydrogen and argon is that the initial conditions for hydrogen will correspond to those for a fully dissociated gas behind the shock front. These required conditions have been given by Belozerov and Measures (Ref. 19). For the present case (Case IV of Table 2), since we will consider only a small amount of hydrogen impurity (0.4% by pressure) in the argon test gas, the assumption is made that the initial conditions for hydrogen and argon are identical.

The following reactions are considered for the collisional ionization processes.

(a) $A_r + A_r \underset{k_r}{\overset{k_f}{\rightleftharpoons}} A_r^+ + e + A_r$

(b) $A_r + e \rightleftharpoons A_r^+ + e + e$

(c) $A_r + H \rightleftharpoons A_r^+ + e + H$

(d) $H + A_r \rightleftharpoons H^+ + e + A_r$

(e) $H + H \rightleftharpoons H^+ + e + H$

(f) $H + e \rightleftharpoons H^+ + e + e$

Processes (a) and (b) for pure argon have been discussed previously in Section 3.4.

The production rates due to atom-atom collisions (a, c, d, and e) and atom-electron collisions (b and f) can be expressed as follows:

$$(\dot{n}_e)_a^{Ar\text{-}Ar} = k_{fa}^{Ar\text{-}Ar}(T)\, n_{a,Ar}^2 - k_{ra}^{Ar\text{-}Ar}(T)\, n_{a,Ar}\, n_{e,Ar}^2 \tag{3.19a}$$

$$(\dot{n}_e)_e^{Ar\text{-}e} = k_{fe}^{Ar\text{-}e}(T_e)\, n_{a,Ar}\, n_{e,Ar} - k_{re}^{Ar\text{-}e}(T_e)\, n_{e,Ar}^3 \tag{3.19b}$$

$$(\dot{n}_e)_a^{Ar\text{-}H} = k_{fa}^{Ar\text{-}H}(T)\, n_{a,Ar}\, n_{a,H} - k_{fa}^{Ar\text{-}H}(T)\, n_{a,H}\, n_{e,Ar}^2 \tag{3.19c}$$

$$(\dot{n}_e)_a^{H\text{-}Ar} = k_{fa}^{H\text{-}Ar}(T)\, n_{a,H}\, n_{a,Ar} - k_{ra}^{H\text{-}Ar}(T)\, n_{a,Ar}\, n_{e,H}^2 \tag{3.19d}$$

$$(\dot{n}_e)_a^{H\text{-}H} = k_{fa}^{H\text{-}H}(T)\, n_{a,H}^2 - k_{ra}^{H\text{-}H}(T)\, n_{a,H}\, n_{e,H}^2 \tag{3.19e}$$

$$(\dot{n}_a)_e^{H\text{-}e} = k_{fe}^{H\text{-}e}(T_e)\, n_{a,H}\, n_{e,H} - k_{re}^{H\text{-}e}(T_e)\, n_{e,H}^3 \tag{3.19f}$$

where it should be noted that $(\dot{n}_e)_a^{Ar\text{-}H} \neq (\dot{n}_e)_a^{H\text{-}Ar}$.

The forward rate coefficients $k_{fa}^{A\text{-}B}$ between atoms A and B and $k_{fe}^{A\text{-}e}$ between atom A and an electron can be written in terms of the excitational cross-section constants $S_{A\text{-}B}^*$ and $S_{A\text{-}e}^*$ as shown below (Ref. 11):

$$k_{fa}^{A\text{-}B}(T) = S_{A\text{-}B}^* \left[\frac{32}{\pi} \left(\frac{m_A + m_B}{m_A\, m_B} \right) \right]^{1/2} (kT)^{3/2} \left(\frac{T_A^*}{2T} + 1 \right) \exp\left(\frac{-T_A^*}{T} \right) \tag{3.20}$$

$$k_{fe}^{A\text{-}e}(T) = S_{A\text{-}e}^* \left[\frac{32}{\pi} \left(\frac{m_A + m_e}{m_A\, m_e} \right) \right]^{1/2} (kT_e)^{3/2} \left(\frac{T_A^*}{2T_e} + 1 \right) \exp\left(\frac{-T_A^*}{T_e} \right) \tag{3.21}$$

These rates must be divided by two for like-like collisions to avoid a double count.

The forward and recombination rates are related to the equilibrium constants as indicated below:

$$k_{ra}^{A\text{-}B} = k_{fa}^{A\text{-}B}(T)/K_{eq}^{A\text{-}B}(T) \tag{3.22}$$

$$k_{re}^{A\text{-}e} = k_{fe}^{A\text{-}e}(T_e)/K_{eq}^{A\text{-}e}(T_e) \tag{3.23}$$

The equilibrium constants are defined below:

$$K_{eq}^{Ar\text{-}Ar}(T) = \frac{n_{e,Ar,eq}^2(T)}{n_{a,Ar,eq}(T)} \tag{3.24}$$

$$K_{eq}^{Ar\text{-}H}(T) = K_{eq}^{Ar\text{-}Ar}(T)$$

$$K_{eq}^{H\text{-}Ar}(T) = K_{eq}^{H\text{-}H} \tag{3.26}$$

$$K_{eq}^{H\text{-}H}(T) = \frac{n_{e,H,eq}^2(T)}{n_{a,H,eq}(T)} \tag{3.27}$$

$$K_{eq}^{Ar\text{-}e}(T_e) = \frac{n_{e,Ar,eq}(T_e)}{n_{a,Ar,eq}(T_e)} \tag{3.28}$$

$$K_{eq}^{H\text{-}e}(T_e) = \frac{n_{e,H,eq}(T_e)}{n_{a,H,eq}(T_e)} \tag{3.29}$$

The definition of the degree of ionization for the mixture is as follows:

$$\alpha = \frac{n_{e,Ar} + n_{e,H}}{n_{e,Ar} + n_{e,H} + n_{a,Ar} + n_{a,H}} \tag{3.30}$$

If we define a ratio C* as shown below,

$$C^* = \frac{2n_{e,H} + n_{a,H}}{2n_{e,Ar} + n_{a,Ar}} \tag{3.31}$$

then α can be expressed in terms of C* as follows:

$$\alpha = \frac{\alpha_{Ar}}{1 + \frac{C^*(1+\alpha_{Ar})}{(1+\alpha_H)}} + \frac{\alpha_H}{1 + \frac{(1+\alpha_H)}{C^*(1+\alpha_{Ar})}} \tag{3.32}$$

where α_{Ar} and α_H are defined below,

$$\alpha_{Ar} = \frac{n_{e,Ar}}{n_{e,Ar} + n_{a,Ar}} \tag{3.33}$$

$$\alpha_{H} = \frac{n_{e,H}}{n_{e,H} + n_{a,H}} \tag{3.34}$$

For the present calculations the excitation collision cross-section for atomic hydrogen by electron impact is given by,

$$\sigma^*_{H\text{-}e} = 5.1 \times 10^{-17} \, (10.2 - E) \text{cm}^2 \tag{3.35}$$

and

$$S^*_{H\text{-}H} = 7.0 \times 10^{-2} \, S^*_{H\text{-}e}$$

as obtained by Belozerov and Measures (Ref. 19) from a comparison of theoretical and experimental results. $S^*_{Ar\text{-}H}$ and $S^*_{H\text{-}Ar}$ are still unknowns for the present work. However, the method used by Kelly (Ref. 12) in his treatment of the argon-xenon case by assuming $S^*_{Ar\text{-}H} = S^*_{Ar\text{-}Ar}$ and $S^*_{H\text{-}Ar} = S^*_{H\text{-}H}$ is adopted herein. This assumption would be invalid for a high impurity level of H due to the small mass ratio between H and Ar. However, it can be accepted for the present work as the impurity level in the test gas (argon) is small.

Calculations were made for Case IV of Table 2 for the relaxation zone behind a strong shock moving in argon with a small amount of hydrogen (0.4% by pressure). The resulting density and degree of ionization variations through the relaxation zone are given in Fig. 11, along with the experimental data (Ref. 15). The agreement between the predicted and measured results is good, confirming the choice of the theoretical model. From a comparison of the results of Figs. 9 and 11, it is readily seen that the total relaxation length of the pure argon shock transition is substantially reduced by a factor of four through the addition of the 0.4% hydrogen impurity. This result is quite different from the argon-xenon mixtures used by Kelly (Ref. 12). Kelly showed that the addition of 0.1% and 0.48% xenon to the test gas argon did not substantially change the relaxation length from that for pure argon. The reason is that the excitational cross-section for pure xenon is smaller than that for pure argon. In addition, the mass of atomic hydrogen is markedly smaller than that of the argon atom. These two characteristics of the hydrogen impurity in the argon test gas give rise to a significant reduction of the relaxation length or time.

3.6 Discussion

The following conclusions can be made from the present calculations and their comparison with the experimental results for the relaxation processes occurring behind a strong shock wave moving in pure argon or argon with a small hydrogen impurity:

1. The initial process of ionization behind a strong shock moving in pure argon is due to atom-atom collisions. As the number of electrons increases sufficiently, the process is controlled by atom-electron collisions, and subsequently by three-body recombination (ion-electron-electron).

2. The new value of the excitational cross-section constant for argon-argon atom collisions, $S^*_{Ar\text{-}Ar} = 3.5 \times 10^{-20}$ cm^2/eV, as determined from a comparison of predicted and measured data, is smaller than the value of 1.2×10^{-19} cm^2/eV determined by Kelly (Ref. 10) and slightly larger than the value 2.5×10^{-20} cm^2/eV given by McLaren and Hobson (Ref. 14).

3. Owing to the low mass of the hydrogen atom and the large excitational cross-section between hydrogen atom-atom and hydrogen atom-electron collisions, the impurity effect of hydrogen in the argon test gas is to markedly reduce the relaxation length or time of the ionization processes behind the shock wave, even when the impurity level of hydrogen is as low as 0.4%.

4. The effects of radiation losses and of the wall boundary layer are problems for further study.

4. LAMINAR BOUNDARY-LAYER FLOW OF PARTIALLY IONIZED ARGON BEHIND A STRONG SHOCK WAVE

4.1 Introduction

The nonlinear partial differential equations for most boundary-layer problems are difficult to solve. As a result, many researchers have resorted to using simplifying similarity transformations. In the similarity approach the system of partial differential equations is reduced to a system of ordinary differential equations, which can usually be solved by standard integration techniques. These so-called similarity solutions are, however, limited to certain types of flows. For this reason, and because of the mathematical difficulties encountered in obtaining exact solutions for general boundary layer cases, approximate methods have also been developed.

One approximate method of interest for this work is based on Karman's momentum integral, which has been extended by Pohlhausen. This approach is now known as the Karman-Pohlhausen integral method. For such integral methods certain assumptions are made as to the form of the unknown functions, which reduces the problem to solving a set of ordinary differential equations. By satisfying appropriate boundary conditions at the wall, the velocity profile normal to the wall through the boundary layer is reduced to a function of only one independent variable. Libby and Morduchow (Refs. 21 and 22) have extended the Karman-Pohlhausen method to a sixth-degree velocity profile and a seventh-degree stagnation-enthalpy profile. Chung and Anderson (Refs. 23, 24) have successfully applied this method to the boundary layer flow of a dissociated gas over a flat plate. Another method developed by Dorodnitsyn (Ref. 25) has been applied by Pallone (Ref. 26) to solve a mass-transfer problem, and also applied by Lo (Ref. 27) to solve a corner-flow problem. This latter method combines the Dorodnitsyn integration scheme and Karman-Pohlhausen integral method. Note also that this approach was used by Pallone, Moore and Erdos (Ref. 28) in solving the boundary layer equations for dissociation and ionizing air in a nonequilibrium flow.

Another powerful method of solving the boundary layer equations is the finite-difference approach. Blottner (Ref. 29) has applied this numerical method in solving nonequilibrium laminar boundary layer flows of an ionized gas. Kendall and Bartlett (Ref. 30) have combined the finite-difference approach and matrix-inversion techniques (so-called integral-matrix method) to obtain a nonsimilar solution of a multicomponent laminar boundary layer.

The laminar boundary layer behind a shock wave moving in a perfect gas has been studied quite extensively (Refs. 31 to 34). The correct boundary layer equations were used in Ref. 32. Values of skin friction and heat transfer coefficients were obtained. However, velocity and temperature profiles through the boundary layer were not given. Mirels (Refs. 33 and 34) solved the laminar and turbulent boundary layer equations for the flow behind a shock wave. The most extensive calculations for laminar boundary layers behind a strong shock wave for a dissociating gas can be found in Refs. 35 to 37. Knoos (Ref. 38) studied the Rayleigh and shock-tube end-wall boundary layers for partially ionized argon. In his analysis, the basic assumption is that of thermochemical equilibrium. Fay and Kemp (Ref. 39) considered the heat transfer to a shock-tube end wall from an ionized monatomic gas for both frozen and equilibrium flows.

For the steady laminar boundary layer in a partially ionized gas, many researchers (Refs. 40 to 42) have studied the effects of a nonequilibrium electron temperature. Back (Ref. 43) solved this problem based on a similarity-solution approach for a frozen low-speed flow. The effects of high temperature on transport properties and nonequilibrium flow remain unsolved.

For the present theoretical work the boundary layer is assumed to be laminar. Note also that the boundary layers in the actual experiments (Refs. 15 and 18) are assumed to be laminar.

4.2 Transport Properties of Partially-Ionized Argon

The kinetic theory of gases provides a means of estimating the transport coefficients of a partially-ionized gas. In this section, transport properties of partially-ionized argon gas are considered, as based on the mixture rule of Fay and Kemp (Ref. 39).

For the mixture of atoms, ions and electrons the thermal conductivity (κ) can be calculated by means of the approximate mixture rule:

$$\kappa = \sum_j \frac{x_j \kappa_j}{\sum_i x_i G_{ji}} \tag{4.1}$$

$$G_{ji} = \left[\frac{2m_i}{m_i + m_j} \right]^{1/2} \frac{Q_{ji}}{Q_{jj}} \tag{4.2}$$

The respective symbols κ_j and x_j are the thermal conductivity and mole fraction of the pure component j, and Q_{ji} is the effective hard-sphere cross-section for a collision pair j and i.

The thermal conductivities of argon atoms (κ_{Ar}) and of a completely singly-ionized gas (κ_s) are given by the following approximate expressions:

$$\kappa_{Ar} = 5.8 \times 10^{-7} \; T^{3/4} \qquad \text{cal/cm sec°K} \tag{4.3}$$

$$\kappa_s = 4.4 \times 10^{-13} \; T^{5/2} / \ell n \; \Lambda \qquad \text{cal/cm sec°K} \tag{4.4}$$

The ratio of the Debye distance to the impact parameter (for 90° deflection) is denoted by Λ, which is given by the following relation:

$$\Lambda = 1.24 \times 10^{4} \; T^{3/2} / n_e^{1/2}$$

where, T is in °K and n_e in cm^{-3}.

The thermal conductivities for the electron gas (κ_e) and argon ions (κ_{Ar^+}) can be related to (κ_s) as shown below:

$$\kappa_e = (1 + \sqrt{2}) \; \kappa_s \tag{4.5}$$

$$\kappa_{Ar^+} = \left[\frac{m_e}{m_{Ar}} \right]^{1/2} (1 + \sqrt{2}) \; \kappa_s \tag{4.6}$$

From Eqs. 4.1 to 4.6 the thermal conductivity (κ) for partially ionized argon is given below:

$$\kappa = \kappa_s \left[1 + \sqrt{2} \; \frac{m_e}{m_{Ar}} \; \frac{\kappa_s}{\kappa_{Ar}} \; \frac{Q_{ae}}{Q_{aa}} \; \frac{1-\alpha}{\alpha} \right]^{-1} + \kappa_{Ar} \left[1 + \frac{Q_{ai}}{Q_{aa}} \; \frac{\alpha}{1-\alpha} \right]^{-1} \tag{4.7}$$

The viscosity of partially ionized argon can be calculated from simple kinetic theory, and it is given below:

$$\mu = \frac{5\pi}{32} \; \frac{m_{Ar} \; U_{Ar}}{Q_{aa}} \; \frac{1 + \dfrac{\alpha}{1-\alpha} \; \dfrac{1 + \dfrac{\alpha}{1-\alpha} \; \dfrac{Q_{ai}}{Q_{aa}}}{\dfrac{Q_{ai}}{Q_{aa}} + \dfrac{\alpha}{1-\alpha} \; \dfrac{Q_{ii}}{Q_{aa}}}}{1 + \dfrac{\alpha}{1-\alpha} \; \dfrac{Q_{ai}}{Q_{aa}}} \tag{4.8}$$

where

$$U_{Ar} = \left[\frac{8kT}{\pi \; m_{Ar}} \right]^{1/2}$$

is the mean thermal speed of the argon atoms. The electrons make no contribution to the viscosity because of their extremely low mass.

The ambipolar diffusion coefficient D_{am} is defined in terms of the atom-ion diffusion coefficient D_{ai},

$$D_{am} \equiv \frac{2}{1+\alpha} \; D_{ai} \tag{4.9}$$

From kinetic theory D_{ai} is related to the ratio of the drive velocity V_d and the electric field E (Ref. 30),

$$D_{ai} = - \frac{V_d}{E} \frac{kT_I}{e} \tag{4.10}$$

The ion temperature T_I may be taken as that for which the mean thermal speed equals the drift velocity, $V_d = \left[\frac{8kT_I}{\pi \, m_{Ar}} \right]^{1/2}$. From experimental data, the effective hard-sphere collision momentum-exchange cross-sections for argon atom-atom collisions (Q_{ea}), and for argon ion-atom-collisions (Q_{ai}) can be expressed as functions of the gas temperature (Refs. 18 and 19),

$$Q_{aa} \simeq 17 \left(\frac{T}{10^4} \right)^{-0.26} \text{Å}^2$$

$$Q_{ai} \simeq 1.44 \; T^{0.16} \; Q_{aa} \tag{4.11}$$

The effective hard-sphere argon ion-ion collision cross-section Q_{ii} is quite large ($\sim 10^3$ to 10^4 Å^2); for example, see Fig. 7 of Ref. 38.

Finson and Kemp (Ref. 44) have assumed that the pure ion viscosity can be obtained from the ion's thermal conductivity by using monatomic perfect-gas relations, and they developed an expression for the Prandtl number,

$$Pr = \frac{2}{3} \; \frac{\kappa_{Ar}}{\kappa} \; (1 + \alpha) \; (A + B) \tag{4.12}$$

where

$$A = \frac{(1 + \sqrt{2}) \left(\frac{\kappa_s}{\kappa_{Ar}} \right) \left(\frac{m_e}{m_{Ar}} \right)^{1/2}}{\alpha + (1 - \alpha) \frac{Q_{ai}}{Q_{aa}} (1 + \sqrt{2}) \frac{\kappa_s}{\kappa_{Ar}} \left(\frac{m_e}{m_{Ar}} \right)^{1/2}}$$

and

$$B = \frac{1 - \alpha}{(1 + \alpha) + \alpha \left(\frac{Q_{ai}}{Q_{aa}} \right)}$$

The degree of ionization for an argon plasma with freestream and surface conditions given in Table 2 is plotted in Fig. 12 as a function of gas temperature (T) for an equilibrium flow. Predictions for the Prandtl number (Pr), Lewis number (Le) and the density-viscosity product ratio ($C = \rho\mu/\rho_e\mu_e$, where, "e" denotes the boundary layer edge), all obtained from the preceding equations, are shown in Fig. 13. These results for argon were specifically based on the initial conditions summarized in Table 3, and the temperature range of 300 to 14,000°K covers the surface wall to freestream temperature range for the boundary layer. At the wall where T is approximately 300°K, Pr, Le and C are equal to 2/3, 0.44 and I, respectively. At the other end of the temperature range (14,000°K and higher) the gas is significantly ionized, and these quantities become small. For a completely ionized gas (T > 20,000°K) the thermal conductivity is due almost entirely to electrons, and the electrical conductivity is strongly dependent on temperature. For these reasons the Prandtl and Lewis numbers are very small at high temperatures. Note that for a completely ionized gas or plasma, the viscosity given by Eq. 4.8 may be related to the electron thermal conductivity given by Eq. 4.5 (take the limit as $n_a \to 0$). Then,

$$Pr \simeq \left(\frac{m_e}{m_a}\right)^{1/2}$$

and the Prandtl number is of the order of 1/100 for a completely ionized plasma.

4.3 Karman-Pohlhausen Integral Method

Since the original work of Karman and Pohlhausen, their momentum-integral method for solving boundary-layer problems has been studied and used by many researchers. Libby, Morduchow and Bloom (Ref. 45) and Morduchow (Ref. 22) have made a critical study of the integral method for a compressible laminar boundary layer for a perfect gas. Chung and Anderson (Ref. 24) have applied this method to the boundary layer over a flat plate for a dissociating gas. The basic principle of the integral method is to reduce the set of non-linear partial differential equations for the boundary layer to a set of ordinary differential equations. Additionally, the profile through the boundary layer for each flow or dynamic variable is represented by a polynomial equation of appropriate degree.

In this section, the integral method is formulated in a general fashion for a steady, two-dimensional laminar, compressible, boundary-layer flow of a reacting-gas mixture. The freestream flow outside the boundary layer is assumed to be in equilibrium. It is also assumed that the electron and atom temperatures are equal in the boundary layer, or there is one characteristic temperature, T. If the wall velocity is zero, we have the usual boundary layer behind a moving shock wave, we let the wall velocity be equal to the negative value of the shock velocity or attach the coordinate system to the shock front, as a matter of mathematical convenience. By taking the x-axis along the wall surface and the y-axis perpendicular to the wall, the boundary-layer equations for a partially-ionized-argon flow of either type are given by Eqs. 2.19, 2.20, 2.30 and 2.31.

The boundary conditions for the boundary-layer flow behind a moving shock wave are listed below,

Wall surface (y = 0)

$$\begin{aligned} u &= u_w \\ v &= 0 \\ H &= H_w \\ \alpha &= \alpha_w \end{aligned} \tag{4.13}$$

Boundary-layer edge (y = 0)

$$\begin{aligned} u &= u_e \\ H &= H_e \\ \alpha &= \alpha_e \end{aligned} \tag{4.14}$$

Note that the boundary conditions for a steady flow over a flat-plate are the same as those above, except at the wall (y = 0) the condition $u = u_w$ is replaced by $u = 0$.

By using the boundary condition given in Eqs. 4.13 for v, the equation of continuity (Eq. 2.19) can be integrated with respect to y to yield the following expression:

$$\rho v = -\int_0^y \frac{\partial(\rho u)}{\partial x}\, dy \tag{4.15}$$

By taking into account that H_e and α_e are assumed constant, integrations of the boundary-layer equations with respect to y from y = 0 to y = δ result in the following expressions:

$$\frac{d}{dx}\int_0^\delta \rho u(u - u_e)dy + \frac{du_e}{dx}\int_0^\delta \rho u\, dy = -\delta \frac{dp_e}{dx} - \mu_w \left[\frac{\partial u}{\partial y}\right]_w \tag{4.16}$$

$$\frac{d}{dx}\int_0^\delta \rho u(H - H_e)dy = -\left[\frac{\mu}{Pr}\frac{\partial H}{\partial y} + \frac{\mu}{Pr}\frac{\partial H}{\partial y} + \frac{\mu}{Pr}\frac{\partial H}{\partial y} + \frac{\mu}{Pr}(Le - 1)(I + \frac{5}{2}RT)\frac{\partial \alpha}{\partial y}\right]_w \tag{4.17}$$

$$\frac{d}{dx}\int_0^\delta \rho u(\alpha - \alpha_e)dy = -\left[\frac{\mu}{Sc}\frac{\partial \alpha}{\partial y}\right]_w - \int_0^\delta \dot{\omega}\, dy \tag{4.18}$$

The Schmidt number (Sc) is given below,

$$Sc = \frac{\mu}{\rho D_{am}} = Pr/Le \tag{4.19}$$

We now apply the following transformation,

$$\xi = x/L$$

$$\eta = \frac{1}{\bar{\delta}} \int_0^y \frac{\rho}{\rho_e} \, dy \tag{4.20}$$

where, L is a suitable characteristic length and

$$\bar{\delta} = \int_0^{\delta} \frac{\rho}{\rho_e} \, dy \tag{4.21}$$

Under this transformation, $y = 0$ and $y = \delta$ correspond to $\eta = 0$ and $\eta = 1$, respectively. By introducing the following dimensionless variables,

$$\begin{aligned} f &= u/u_e \\ g &= H/H_e \\ Z &= \alpha/\alpha_e \end{aligned} \tag{4.22}$$

and the following notation,

$$F_1 = \int_0^1 f(1 - f)d\eta$$

$$F_2 = \int_0^1 f(1 - g)d\eta \tag{4.23}$$

$$F_3 = \int_0^1 f(1 - Z)d\eta$$

the following set of first-order ordinary differential equations are obtained from Eqs. 4.16 to 4.18,

$$\lambda \frac{dF_1}{d\xi} + \frac{1}{2} F_1 \frac{d\lambda}{d\xi} + \frac{\lambda}{u_e} \frac{du_e}{d\xi} \{(1 - M_e^2) F_1 - P_1 - S_1\} = \bar{R} \left[\frac{\partial f}{\partial \eta} \right]_w \tag{4.24}$$

$$\lambda \frac{dF_2}{d\xi} + \frac{1}{2} F_2 \frac{d\lambda}{d\xi} + \frac{\lambda}{u_e} \frac{du_e}{d\xi} (1 - M_e^2) F_2 = \bar{R} \left[\frac{1}{Pr} \frac{\partial g}{d\eta} \right]_w + \bar{R} \left[\frac{1}{Pr} (Le - 1) \frac{\alpha_e (I + \frac{5}{2} RT)}{H_e} \frac{\partial Z}{\partial \eta} \right]_w \tag{4.25}$$

$$\lambda \frac{dF_3}{d\xi} + \frac{1}{2} F_3 \frac{d\lambda}{d\xi} + \frac{\lambda}{u_e} \frac{du_e}{d\xi} (1 - M_e^2) F_3 = \bar{R} \left[\frac{1}{S_c} \frac{\partial Z}{\partial \eta} \right]_w - \frac{\lambda L}{\alpha_e u_e} \int_0^1 \frac{\dot{w}}{\rho} \, d\eta \tag{4.26}$$

In the above expressions the following conditions were used:

$$
\begin{aligned}
M_e^2 &= \frac{3}{5}\frac{u_e^2}{RT_e(1+\alpha_e)} \\
\lambda &= Re_\infty\left(\frac{\bar{\delta}}{L}\right)^2 \\
Re_\infty &= \frac{\rho_\infty u_\infty L}{\mu_\infty} \\
\bar{R} &= Re_\infty\frac{\rho_w\mu_w}{\rho_e^2 u_e L} \\
P_1 &= \int_0^1 f^2\, d\eta \\
S_1 &= \int_0^1 \frac{\rho_e}{\rho}\, d\eta
\end{aligned}
\qquad (4.27)
$$

Equations 4.24 to 4.26 are the basic integral-differential equations for the boundary-layer flow. Approximate solutions to these equations can be obtained by assuming f, g and α are functions of only η , which satisfy certain conditions at $\eta = 0$ and $\eta = 1$. These boundary conditions will be discussed later.

The general solution, based on the previous integral-differential equations, can be obtained for the special case of a flow without a pressure gradient. For this special case the simplified integral-differential equations for the flow over a flat plate are given below,

$$\lambda\frac{dF_1}{d\xi} + \frac{1}{2}F_1\frac{d\lambda}{d\xi} = \bar{R}\left[\frac{\partial f}{\partial\eta}\right]_w \qquad (4.28)$$

$$\lambda\frac{dF_2}{d\xi} + \frac{1}{2}F_2\frac{d\lambda}{d\xi} = \bar{R}\left[\frac{1}{P_r}\frac{\partial g}{\partial\eta} + \left(\frac{Le-1}{Pr}\right)\frac{(I+\frac{5}{2}RT)\alpha_e}{H_e}\frac{\partial Z}{\partial\eta}\right]_w \qquad (4.29)$$

$$\lambda\frac{dF_3}{d\xi} + \frac{1}{2}F_2\frac{d\lambda}{d\xi} = \bar{R}\left[\frac{1}{Sc}\frac{\partial Z}{\partial\eta}\right]_w - \frac{L\lambda}{\alpha_e u_e}\int_0^1\frac{\dot{w}}{\rho}\, d\eta \qquad (4.30)$$

The boundary conditions for velocity, enthalpy and degree of ionization are given below:

$$
\text{For } \eta = 0 \qquad
\begin{aligned}
f &= r \equiv u_w/u_e \\
g &= g_w \\
\frac{\partial Z}{\partial\eta} &= K\sqrt{\lambda}\, Z
\end{aligned}
\qquad (4.31a)
$$

This last relation will be developed subsequently.

$$\text{For } \eta = 1 \qquad \begin{array}{llllll} f = 1 & g = 1 & Z = 1 \\ f' = 0 & g' = 0 & Z' = 0 \\ f'' = 0 & g'' = 0 & Z'' = 0 \\ f''' = 0 & g''' = 0 \end{array} \tag{4.31b}$$

where, the prime denotes differentiation with respect to η. The edge of the sheath is now the boundary condition for the boundary layer. Consequently, K, the catalytic efficiency coefficient, is determined as follows: The wall is at a floating potential. The momentum equation, Eq. 4.32a, can be obtained (Ref. 41) from Langmuir-probe theory, if the electrons have a Maxwellian velocity distribution,

$$\frac{1}{4}\left[n_e < v_e > \right]_s \exp\left(\frac{-e\Delta\phi}{kT_s}\right) - n_{i,s}\, e\, V_i = 0 \tag{4.32a}$$

where

$$< V_e > = \left(\frac{8kT_s}{\pi M_e}\right)^{1/2}$$

$$V_i = \left(\frac{kT_s}{M_{Ar^+}}\right)^{1/2}$$

and $\Delta\phi$ is the potential between the wall and plasma, e denotes the electronic charge and s denotes the sheath edge. The second relation (Eq. 4.32b) is obtained from the continuity of mass flow of ions at the outer edge of the sheath.

$$\rho_s D_{am,s}\left(\frac{\partial\alpha}{\partial y}\right)_s = \rho_s \alpha_s V_i \tag{4.32b}$$

The final relation (Eq. 4.32c) is obtained (Refs. 41 and 42) from the continuity of electron-energy flux through the outer edge of the sheath,

$$\left[\kappa_e \frac{\partial T}{\partial y} - \rho \alpha V_{de} h_e\right]_s = (2kT_s + e\Delta\phi)\, n_{es} \frac{<V_e>}{4} \exp\left(\frac{e\Delta\phi}{kT_s}\right) \tag{4.32c}$$

where, κ_e is the thermal conductivity of electrons, V_{de} is the drift velocity of electrons, and h_e is the enthalpy of electrons.

As already mentioned in Section 2.4, the sheath is very thin compared with the boundary-layer thickness for the present problem, and the boundary conditions are taken to be those at the wall. From the above equations for the sheath, $z'(x,0)$ can be related to $z(x,0)$ and K are given by (Refs. 41 and 42),

$$K = \frac{Sc\, V_i}{u_\infty \theta_w (\bar{\delta}/L)} \tag{4.33}$$

where, $\theta_w = T_w/T_e$.

The dimensionless velocity, total enthalpy and the degree of ionization, defined by Eqs. 4.22, can be approximated by the following polynomial equations for their profiles,

$$f(\eta,\xi) = \sum_{n=0}^{6} a_n(\xi)\ \eta^n \tag{4.34}$$

$$g(\eta,\xi) = \sum_{n=0}^{7} b_n(\xi)\ \eta^n \tag{4.35}$$

$$\alpha(\eta,\xi) = \sum_{n=0}^{5} c_n(\xi)\ \eta^n \tag{4.36}$$

Morduchow (Ref. 22) has shown that sixth and seventh degree polynomial equations for the velocity and enthalpy profiles, respectively, appear to be the most promising approximation. Chung and Anderson (Ref. 24) have assumed a fifth-degree polynomial for the profile of the degree of dissociation in a reacting dissociative gas, and found this approximation to be reasonable, as did others.

The other supplementary boundary conditions for a_n, b_n and c_n can be found by estimating Eqs. 2.20, 2.30 and 2.31 and their derivatives with respect to coordinate y. The following supplementary boundary conditions for a boundary-layer flow without a pressure gradient and at $\eta = 0$ (or $y = 0$) yield,

$$\left[C \frac{\partial f}{\partial \eta} \right]'_w = 0 \tag{4.37a}$$

$$\left[C \frac{\partial f}{\partial \eta} \right]''_w = 0 \tag{4.37b}$$

$$\left[\frac{C}{Pr} \frac{\partial g}{\partial \eta} + \frac{C}{Pr} (Le - 1) \frac{(I + \frac{5}{2} kT)\alpha_e}{He} \frac{\partial z}{\partial \eta} \right]'_w = - \frac{u_e^2}{He} \left[C \left(\frac{1}{Pr} \right) \left(\frac{\partial f}{\partial \eta} \right)^2 \right]_w \tag{4.37c}$$

$$\left[\frac{C}{Pr} \frac{\partial g}{\partial \eta} + \frac{C}{Pr} (Le - 1) \frac{(I + \frac{5}{2} kT)\alpha_e}{He} \frac{\partial z}{\partial \eta} \right]''_w = - \frac{u_e^2}{He} \left[C \left(1 - \frac{1}{Pr} \right) \left(\frac{\partial f}{\partial \eta} \right)^2 \right]'_w \tag{4.37d}$$

$$\left[\frac{C}{Sc} \frac{\partial z}{\partial \eta} \right]'_w = \frac{1}{R} \left[- \frac{L\lambda}{u_e \alpha_e} \frac{\dot{\omega}}{\rho} \right]_w \tag{4.37e}$$

where, $C = \rho\mu/\rho_e\mu_e$ and the prime denotes differentiation with respect to η. Equations 4.31 and 4.37 produce seven, seven, and five boundary conditions for a_n, b_n and c_n, respectively.

An esti ate of the effect of C varying a ross the boundary layer was studied by Back and Witte (Ref. 46) from the stagr..cion-point heat-transfer predictions for a high-temperature un-ionized gas. Lees (Ref. 47) has set $\rho_w\mu_w = \rho_e\mu_e$ in the heat transfer calculation. This approximation might be reasonable for an accelerated ionized gas flow over a highly cooled wall. For simplicity, we adopt the method of Lees by assuming that C is constant.

From the given boundary conditions, a_n, b_n and c_n are listed below,

$$a_o = r \equiv \frac{\mu_w}{\mu_e}$$

$$a_1 = 2(1 - r)$$

$$a_2 = 0$$

$$a_3 = 0$$

$$a_4 = -5(1 - r)$$

$$a_5 = 6(1 - r)$$

$$a_6 = -2(1 - r)$$

$$b_o = g_w$$

$$b_2 = \frac{\alpha_e}{2}(Le - 1)\frac{(I + \frac{5}{2}RT_w)}{He}\left[\frac{\partial^2 z}{\partial \eta^2}\right]_w - \frac{u_e^2}{2He}\left(1 - \frac{1}{Pr}\right)\frac{Pr}{C}\left[\frac{\partial f}{\partial \eta}\right]_w^2 \qquad (4.38)$$

$$b_3 = \frac{\alpha_e}{6}(Le - 1)\frac{(I + \frac{5}{2}RT_w)}{He}\left[\frac{\partial^3 z}{\partial \eta^3}\right]_w$$

$$b_4 = 35(1 - b_o) - 20b_1 - 10b_2 - 4b_3$$

$$b_5 = -84(1 - b_o) + 45b_1 + 20b_2 + 6b_3$$

$$b_6 = 70(1 - b_o) - 36b_1 - 15b_2 - 4b_3$$

$$b_7 = -20(1 - b_o) + 10b_1 + 4b_2 + b_3$$

$$c_1 = K\sqrt{\lambda}\, c_o$$

$$c_2 = -\left(\frac{Sc}{2c}\right)_w \frac{1}{R}\frac{L\lambda}{u_e\alpha_e}\left[\frac{\dot{\omega}}{\rho}\right]_w$$

$$c_3 = 10(1 - c_o) - 6c_1 - 3c_2$$

$$c_4 = -15(1 - c_o) + 8c_1 + 3c_2$$

$$c_5 = 6(1 - c_o) - 3c_1 - c_2$$

The remaining two unknowns c_o and b_1 can be obtained by solving Eqs. 4.29 and 4.30.

By using the above results, the following relations can be obtained,

$$F_1 = (1 - r)\frac{985}{9009} + \frac{227}{1287} r(1 - r) \tag{4.39a}$$

$$F_2 = B_o - B_1 b_1 - B_2 b_2 - B_3 b_3 \tag{4.39b}$$

$$F_3 = C_o - C_1 c_1 - C_2 c_2 \tag{4.39c}$$

where,

$$B_o = \frac{31}{126}(1 - b_o)(1 - r) + \frac{1}{2} r(1 - b_o)$$

$$B_1 = \frac{821}{12012}(1 - r) + \frac{3}{28} r$$

$$B_2 = \frac{151}{9009}(1 - r) + \frac{r}{42}$$

$$B_3 = \frac{953}{36036}(1 - r) + \frac{r}{280}$$

$$C_o = \frac{1}{4}(1 - c_o)(1 - r) + \frac{r}{2}(1 - c_o)$$

$$C_1 = \frac{32}{495}(1 - r) + \frac{r}{10}$$

$$C_2 = \frac{47}{3960}(1 - r) + \frac{r}{60}$$

Substitution of F_1 into Eq. 4.28 yields the following expression for λ ,

$$\frac{d\lambda}{d\xi} = \lambda_o \tag{4.40}$$

$$\lambda_o = \frac{2\bar{R}a_1}{F_1} \tag{4.41}$$

where $a_1 = 2(1 - r)$.

The solution for λ can be obtained from Eq. 4.40 by using the initial conditions $\lambda = 0$ at $\xi = 0$, as shown below,

$$\lambda = \lambda_o \xi \tag{4.42}$$

This solution implies that the boundary layer thickness is proportional to the square root of ξ (or x).

The boundary layer displacement thickness δ^*, which is defined by the following expression,

$$\delta^* = \int_o^\infty \left[1 - \frac{\rho u}{\rho_e u_e} \right] dy \tag{4.43}$$

can be related to λ as follows:

$$\delta^* = \frac{\lambda^2 L}{Re_\infty^2} J$$

where, J is defined by the expression,

$$J = \int_0^1 \left[\frac{\rho_e}{\rho} - \frac{u}{u_e} \right] d\eta \tag{4.44}$$

When Eqs. 4.38 to 4.40 are used in conjunction with Eqs. 4.29 and 4.30, the following expressions for $b_1(\xi)$ and $c_o(\xi)$ are obtained,

$$B_1 \xi \frac{db_1}{d\xi} + \left[\frac{1}{2} B_1 + \frac{\bar{R}}{Pr\, \lambda_o} \right] b_1 = \frac{1}{2} B_o - \frac{1}{2} B_2 b_2 - \frac{1}{2} B_3 b_3$$

$$- B_2 \xi \frac{db_2}{d\xi} - B_3 \frac{db_3}{d\xi} - \frac{\bar{R}}{Pr\, \lambda_o} (Le - 1) \frac{(I + \frac{5}{2} RT_w)\alpha_e}{He} C_1 \tag{4.45}$$

$$\left[\frac{1}{4} (1 + r) + C_1 K \sqrt{\lambda_o \xi} \right] \xi \frac{dc_o}{d\xi} + \left[\frac{1}{8} (1 + r) + \frac{1}{2} C_1 K \sqrt{\lambda_o \xi} \right.$$

$$\left. + \frac{\bar{R}}{Sc \lambda_o} K \sqrt{\lambda_o \xi} \right] c_o = \frac{1}{8} (1 + r) - \frac{1}{2} C_2 c_2 - C_2 \xi \frac{dc_2}{d\xi} + \frac{L\lambda}{\alpha_e u_e \lambda_o} \int_0^1 \frac{\dot{\omega}}{\rho} d\eta \tag{4.46}$$

The derivatives of b_2, b_3 and c_2 with respect to ξ are found from Eqs. 4.38.

The initial conditions for Eqs. 4.45 and 4.46 are: b_1 is finite and $c_o = 1$ at $\xi = 0$. These conditions will be discussed later for the equilibrium, frozen and nonequilibrium flows.

The solutions for the velocity, total enthalpy and degree of ionization profiles can be obtained from Eqs. 4.34, 4.35 and 4.38 and from the results of Eqs. 4.45 and 4.46.

The use of the integral method to obtain a solution for the laminar boundary layer equations is widely accepted in aerodynamics. Generally, solutions are determined by integrating the appropriate equations in two ways: first, in the direction normal to the wall, using assumed polynomial distributions; and, second, in the flow direction, where new dependent variables arise as a result of the first integration. Such a method has proved to be of considerable value in assessing skin-friction and heat-transfer effects. However, such methods are of limited usefulness, since they give no indication of the detailed nature of the flow.

It can be seen from Eqs. 4.24 to 4.26 that the solutions are independent of the variations of the Prandtl and Lewis numbers inside the boundary layer, and they are dependent only on these numbers evaluated at the wall. As a result, the successful method of Pallone (Ref. 26), who included the Dorodnitsyn (Ref. 25) integration scheme with the Karman-Pohlhausen approach was used.

The method is formulated as follows. The viscous domain from the body surface to the outer edge of the boundary layer is divided into N curvilinear strips. The boundary layer equations can then be integrated along a coordinate normal to the body from the surface to the boundary of each strip. The essential difference between the Karman-Pohlhausen and Dorodnitsyn integral methods is that, in the former, the partial differential equations are satisfied only on the average over the entire boundary-layer thickness and in the latter the partial differential equations are satisfied on the average over each strip of the boundary layer. Note that for the laminar boundary-layer flow of a non-equilibrium ionized gas, the use of the Dorodnitsyn integration scheme makes the calculations very complicated.

4.4 Equilibrium Flow of Partially-Ionized Argon

The Rayleigh and shock-tube wall boundary layers for an equilibrium flow of ionized argon were studied quite extensively by Knöös (Ref. 38). He concluded that, for a freestream temperature of 12,000°K or greater and a freestream pressure of the order of 1 atm, the equilibrium assumption is typically correct for the region of the boundary layer where $T > 11{,}000°K$, but breaks down for $T < 9{,}000°K$, at times of the order of 10 μsec for a Rayleigh boundary layer, and at a distance (x) of about 5 cm for the shock-tube boundary layer. Hence, near the freestream edge of the boundary layer the flow is in equilibrium, and near the wall surface the flow is in nonequilibrium.

In the case of ionization equilibrium the degree of ionization (α) is normally considered as a function of temperature (T) and pressure (p), while the pressure is related to α, T and density ρ by the equation of state (Eq. 2.23). The equation for α for an equilibrium boundary layer is given below (Eq. 3.16), and is called the Saha equation (Ref. 3),

$$\alpha = \left[\frac{p}{R\rho_I T_I} \left(\frac{T_I}{T} \right)^{5/2} e^{(T_I/T)} + 1 \right]^{-1/2} \tag{4.47}$$

Note that $\rho_I = 150.27$ gm/cm^3 and $T_I = 182{,}850°K$ for argon (Table 3),

$$C_p = \frac{5}{2} R(1 + \alpha) + \frac{\alpha}{2} (1 - \alpha^2) R \left(\frac{5}{2} + \frac{T_I}{T} \right)^2 \tag{4.48}$$

The basic equations for an equilibrium boundary layer flow of partially ionized argon are given by Eqs. 2.19, 2.20 and 2.21, where α is related to T through the Saha equation (Eq. 4.47). Thus, $\partial\alpha/\partial y$ can be related to $\partial T/\partial y$.

$$\frac{\partial \alpha}{\partial y} = \frac{\partial \alpha}{\partial T} \frac{\partial T}{\partial y} \tag{4.49}$$

The supplementary boundary conditions given by Eqs. 4.37c and 4.37d are now given as follows:

$$\left[\frac{C}{Pr} g' + \frac{C}{Pr} (Le - 1) \beta g' \right]_w^{\mu} = - \frac{u_e^2}{He} \left[C \left(1 - \frac{1}{Pr} \right) a_1^2 \right]_w \tag{4.50a}$$

$$\left[\frac{C}{Pr} g' \frac{C}{Pr} (Le - 1) \beta g' \right]_w'' = - \frac{u_e^2}{He} \left[C \left(1 - \frac{1}{Pr} \right) a_1^2 \right]_w' \tag{4.50b}$$

$$\beta = \left[1 + \frac{4}{5} \left(\frac{\epsilon}{1+\epsilon} \right)^2 \frac{1}{\alpha(1-\alpha)} \right]^{-1} \tag{4.50c}$$

$$\epsilon = \frac{5}{2} RT/I \tag{4.50d}$$

The variations of ϵ and β with T are shown in Fig. 14. For a wall temperature of 300°K ϵ and β are approximately zero. Also, $\beta_w \simeq 0$ and $\beta_w' \simeq 0$. If Pr, Le and C are assumed constant at the wall surface, Eq. 4.50a reduces to,

$$b_2 = \frac{2 \frac{u_e^2}{He} (Pr - 1) (1 - r)^2}{1 + (Le - 1) \beta_w} \tag{4.51}$$

and Eq. 4.50b becomes,

$$b_3 \simeq 0 \tag{4.52}$$

The differential equation for b_1 (Eq. 4.45) can be expressed as shown below,

$$\xi B_1 \frac{db_1}{d\xi} + \left[\frac{1}{2} B_1 + \frac{\bar{R}}{Pr\lambda_o} \right] b_1 = \frac{1}{2} B_o - \frac{1}{2} B_2 b_2 \tag{4.53}$$

The initial condition for b_1 is that b_1 must be finite at $\xi = 0$. Equation 4.53 then yields the following solution,

$$b_1 = \frac{\frac{1}{2} B_o - \frac{1}{2} B_2 b_2}{\frac{1}{2} B_1 + \frac{\bar{R}}{Pr\lambda_o}} \tag{4.54}$$

In Refs. 22, 23 and 24 it was shown that in an equilibrium boundary layer a similar solution can exist, as the solution for f, g and α are independent of ξ. However, if C is not assumed constant, then a similar solution does not exist in the general case.

4.5 Frozen Flow of Partially-Ionized Argon

In the case of a frozen flow of partially-ionized argon it is assumed that α remains constant. Then, the temperature derivative of α (i.e., $2\alpha/2T$) is zero. The specific heat at constant pressure for a frozen flow is given by,

$$C_p = \frac{5}{2} R(1 + \alpha) \tag{4.55}$$

If the degree of ionization is constant, there is no net production of ions or atoms and $\dot{\omega}$ is zero. Hence, the electron conservation of energy equation (Eq. 2.30) reduces to,

$$\rho u \frac{\partial \alpha}{\partial x} + \rho v \frac{\partial \alpha}{\partial y} = \frac{\partial}{\partial y}\left[\rho D_{am} \frac{\partial \alpha}{\partial y} \right] \tag{4.56}$$

Note that although α is a constant with temperature T, it varies with distance x and y.

The differential equations for $b_1(\xi)$ and $c_o(\xi)$ (Eqs. 4.45 and 4.46) now reduce to,

$$B_1 \xi \frac{db_1}{d\xi} + \left[\frac{1}{2} B_1 + \frac{\bar{R}}{Pr\lambda_o} \right] b_1 = \frac{1}{2} B_o - \frac{1}{2} B_2 b_2$$

$$- \frac{1}{2} B_3 b_3 - B_3 \frac{db_3}{d\xi} - \frac{\bar{R}}{Pr\lambda_o} (Le - 1) \frac{(I + \frac{5}{2} RT_w)\alpha_e}{He} c_1 \tag{4.57}$$

$$\left[\frac{1}{4} (1 + r) + C_1 K \sqrt{\lambda_o \xi} \right] \xi \frac{dc_o}{d\xi} + \left[\frac{1}{8} (1 + r) + \frac{1}{2} C K \sqrt{\lambda_o \xi} \right.$$

$$\left. + \frac{\bar{R}}{Sc\lambda_o} K \sqrt{\lambda_o \xi} \right] c_o = \frac{1}{8} (1 + r) \tag{4.58}$$

Equation 4.38 for c_2 is given by reduced expression,

$$c_2 = C \tag{4.59}$$

The degree of ionization for the frozen boundary-layer flow can be found using Eq. 4.58 and 4.36. The initial condition required is that $c_o = 1$ at $\xi = 0$, since the degree of ionization has its freestream value at the leading edge ($\xi = 0$). After the degree of ionization α has been found, b_1 can be obtained from Eq. 4.57 by using the initial condition that b_1 should be finite at $\xi = 0$,

$$b_1 = \frac{\frac{1}{2} B_o - \frac{1}{2} B_2 b_2 - \frac{1}{2} B_3 b_3 - B_3 \frac{db_3}{d\xi} - \frac{\bar{R}}{Pr\lambda_o} (Le - 1) \frac{(I + \frac{5}{2} RT_w)\alpha_e}{He} c_1}{\frac{1}{2} B_1 + \frac{\bar{R}}{Pr\lambda_o}} \tag{4.60}$$

One can see from Eq. 4.58 that the degree of ionization is dependent on ξ, and therefore the profile for the degree of ionization in the frozen boundary layer is not similar, that is, a similar solution does not exist. The profile of the total enthalpy (g) is still a function of ξ and it is also not similar, in contrast to the equilibrium results. However, the velocity distribution for the frozen boundary layer is similar in the present work. If the value C was not assumed to be constant, then a nonsimilar velocity profile would also exist.

4.6 Nonequilibrium Flow of Partially-Ionized Argon

In the nonequilibrium boundary layer the mass-production rate for electrons (or ions) is not zero, but it is a function of temperature and

density. In order to solve Eqs. 4.45 and 4.46, the term $\dot{\omega}/\rho$ must be evaluated. The collisional ionization rates for a partially-ionized argon flow have been discussed in Chapter 3. The relationship between $\dot{\omega}/\rho$ and the reaction rate $d\alpha/dt$ given by Eq. 3.14 is,

$$\frac{\dot{\omega}}{\rho} = \frac{d\alpha}{dt} = \dot{\alpha}_a + \dot{\alpha}_e \tag{4.61}$$

where $\dot{\alpha}_a$ and $\dot{\alpha}_e$ are the atom-catalyzed and electron-catalyzed reaction rates, respectively, as described in Chapter 3.

In the present theory it is assumed that the electron and atom temperatures are equal in the boundary layer, or one temperature exists. Consequently, $\dot{\alpha}_a$ and $\dot{\alpha}_e$ are functions only of this gas temperature. The gas temperature in the boundary layer is expected to be less than 16,000°K for a freestream temperature (T_∞) of 13,000°K. For this temperature range the significant contribution to the mass-production rate $\dot{\omega}/\rho$ is due to ion-electron-electron recombination, and the contributions due to atom-atom and atom-electron collisions should be small.

The initial conditions imposed for b_1 and c_o at $\xi = 0$ are the same as for the case of a frozen boundary-layer flow. Thus, b_1 is given by Eq. 4.60 and $c_o = 1$.

4.7 Comparison of Theoretical and Experimental Results

4.7.1 Shock-Tube Side-Wall Boundary Layer

For the case of a laminar boundary layer induced behind a moving shock wave, the boundary conditions for the freestream flow and the wall are listed in Table 4. These initial conditions used for the boundary layer calculations correspond to the experimental conditions for Brimelow's experiments (Ref. 15), facilitating the comparison of theoretical and experimental results. Note that appropriate constants for argon used in the calculations are listed in Table 4.

The predicted equilibrium, frozen and nonequilibrium density (ρ_e/ρ) and degree of ionization (α) profiles for an assumed laminar boundary layer behind a shock wave are shown in Fig. 15. The initial conditions are for Case I, Table 4. The experimental results from Ref. 15 for 3.75 cm behind the wave are also shown. The three predicted density profiles are very similar, and they are in good agreement with the experimental data. For the three predicted degree of ionization profiles, the equilibrium profile differs markedly from the very similar frozen and nonequilibrium profiles, which are in good agreement with the experimental data.

For the equilibrium boundary layer the degree of ionization attains its equilibrium value instantaneously at the local temperature and pressure. Since the wall temperature is very low α equals zero at the wall ($y = 0$). However, it can be shown by using Eq. 4.47 that $(\partial\alpha/\partial y)_w$ is almost zero, or $(\partial y/\partial\alpha)_w$ is almost infinite. Consequently, the equilibrium solution for the degree of ionization differs markedly near the wall from the frozen and nonequilibrium solutions. Note that at the freestream edge of the boundary layer the equilibrium solution for the degree of ionization is in good agreement with the experimental results, as expected. This behaviour is in agreement with the conclusions of Knöös (Ref. 38).

For the frozen solution, the ionization reaction does not occur and the degree of ionization is controlled by diffusion. It is also affected by the surface recombination catalycity, as described in Section 4.3. From the initial conditions for c_o, the degree of ionization profile at x = 0 should be constant, as $\alpha(y) = \alpha_\alpha$. For x greater than zero the profile changes due to diffusion. As x increases from zero the value of α_w decreases from α_∞ and approaches zero as x tends to infinity. The degree of ionization at the edge of the sheath layer is not zero. It can be determined by using Eqs. 4.33 and 4.31a for z'(0). In Fig. 15, the degree of ionization at the edge of the thin sheath layer is seen to be very small, but it is nonzero.

The nonequilibrium solution for the degree of ionization is very similar to the frozen solution. The reason for this behaviour is that the gas temperature within the boundary layer is below 15,000°K and the mass production rate of electrons therefore has a minor effect on the degree of ionization.

For Case II of Tables 2 and 4, the predicted equilibrium, frozen and nonequilibrium solutions for the density and degree of ionization profiles are shown in Figs. 16 and 17, along with the experimental results. The same comments made for the previous case apply to these results. Additionally, by comparing theoretical and experimental results it can be seen that near the edge of the boundary layer the flow is in quasi-equilibrium due to radiation losses that become increasingly important with distance (20 cm). Nonequilibrium effects are important near the wall region.

For Case III of Tables 2 and 4, the equilibrium, frozen and nonequilibrium solutions for the density and degree of ionization profiles are shown in Figs. 18 and 19. For this weaker shock wave and lower ionization case, the predicted and measured results are in good agreement. At 12 cm and lower temperatures radiation does not appear to be too significant.

For the case of a steady boundary layer in a partially-ionized-gas flow over a flat plate, the integral method described in Section 4.3 can be applied by setting r equal to zero. The significant difference between this quasi-steady boundary layer and the boundary layer behind a shock wave is in the velocity profile. In the latter case the velocity of the wall equals zero.

4.7.2 Quasi-Steady Flat-Plate Boundary Layer

The freestream and wall conditions assumed for the steady laminar boundary layer over a flat plate in the UTIAS hypersonic shock tube are summarized in Table 3.

For the case of an equilibrium boundary layer, the predicted degree of ionization and temperature profiles as a function of η (η_B is defined in Section 4.8) for two particular Prandtl numbers of 1 and 0.7 are shown in Fig. 20. It can be readily seen that the effect of the Prandtl number (in the energy equation) on the degree of ionization and temperature is significant.

Equilibrium and frozen solutions for the temperature and degree of ionization profiles for a flat-plate boundary layer are compared in Fig. 21, and the associated density profiles are compared in Fig. 22. For both

solutions the Prandtl and Lewis numbers were set equal to unity. The equilibrium and frozen solutions exhibit sizeable differences. Note that the frozen solutions displayed in both Fig. 21 and 22 were calculated for the case when x approaches infinity, or when $\alpha_w = 0$. Then, an exact numerical solution can be obtained easily by using the similarity assumption.

For a flat-plate boundary layer having the boundary conditions given in Table 3, equilibrium, frozen and nonequilibrium solutions for the density profile are compared in Fig. 23a, and those for the degree of ionization profile are given in Fig. 23b. For these calculations the Prandtl number, Lewis number and the density-viscosity product, C, were taken as 0.67, 0.44 and 1.0, respectively. The three predicted profiles for the density are all similar, but their agreement with Whitten's experimental data (Ref. 18) is not good. Note that the minimum value of the density is at the edge of the boundary layer for the predicted profile, while it occurs at y equal to 0.7 mm in the experimental profile. This disagreement is presently being investigated.

The predicted profiles for the degree of ionization are quite different (Fig. 23b). Also, a significant discrepancy exists between the theoretical and experimental results. The overshoot of the degree of ionization beyond its freestream value is not understood at present. Some of the disagreement between the predicted and experimental results could be due to errors in the integral method. As described in Section 4.3, the present Kaman-Pohlhausen integral method uses flow quantities that are averaged over the entire boundary layer thickness.

4.8 Comparison of Integral Method and Exact Numerical Calculations

Similar solutions and exact numerical calculations were made for identical boundary-layer problems for comparison purposes. By an exact solution it is meant that the Blasius-type solution is obtained by using the Howarth transformation (Ref. 48) specified below.

$$\xi_B = \int_0^x f_e \, \mu_e \, \mu_e \, dx \tag{4.62a}$$

$$\eta_B = \frac{u_e}{\sqrt{2\xi_B}} \int_0^y \rho \, dy \tag{4.62b}$$

The subscript B refers to the Blasius type of variable. In order to distinguish between the notation of the dimensionless velocity in this section and in Section 4.3, we define

$$f'_B = \frac{u}{u_e}$$

For a steady laminar boundary layer of a partially-ionized gas, Back (Ref. 47) has discussed the similarity solution approach for a low-speed flow. The basic equations for the boundary layer (Eqs. 2.19, 2.20, 2.30 and 2.31) can be transformed to yield the following expressions.

$$\left[C \, f''_B \right]' + f_B f''_B + \gamma \left[\frac{\rho_e}{\rho} - (f'_B)^2 \right] = 0 \tag{4.63}$$

$$\left[\frac{C}{Pr} g' + \frac{C}{Pr} (b_e - 1) \frac{\alpha_e I}{He} (1 + \epsilon) z' \right]' + f_B g' + \frac{u_e^2}{He} \left[C(1 - \frac{1}{Pr}) f_B' f_B'' \right]' = 0 \tag{4.64}$$

$$\left[C \frac{Le}{Pr} z' \right]' + f_B z' - \Gamma f_B' z + \frac{2\xi}{u_e \alpha_e} \frac{d\xi}{dx} \left(\frac{\dot{\omega}}{\rho} \right) = 0 \tag{4.65}$$

$$\epsilon = \frac{\frac{5}{2} RT}{I}$$

$$\gamma = \frac{2\xi}{u_e} \frac{du_e}{d\xi}$$

$$\Gamma = \frac{2\xi}{\alpha_e} \frac{d\alpha_e}{d\xi}$$

The prime denotes differentiation with respect to η_B.

The flow over a flat plate is considered, with Pr, Le and C held constant for simplicity. For the equilibrium case the ion concentration gradient is expressed in terms of the enthalpy gradient. The basic equations (Eqs. 4.63 and 4.64) reduce to,

$$C f_B''' + f_B f_B'' = 0 \tag{4.66}$$

$$\frac{C}{Pr} \left\{ \left[1 + (Le - 1) \beta \right] g' \right\} + f_B g' + \frac{u_e^2}{He} C \left(1 - \frac{1}{Pr} \right) \left[f_B' f_B'' \right]' = 0 \tag{4.67}$$

The symbol β is defined by Eq. 4.50c. The boundary conditions for the equilibrium, similar boundary-layer equations are as follows:

$$\begin{aligned} f_B(0) &= f_B'(0) = 0 \\ f_B'(\eta) &\to 1 \text{ as } \eta \to \infty \\ g(0) &= g_w \\ g(\eta) &\to 1 \text{ as } \eta \to \infty \end{aligned} \tag{4.68}$$

For the case of a frozen boundary-layer flow, Eqs. 4.63 to 4.65 take the following forms,

$$C f_B''' + f_B f_B'' = 0 \tag{4.69}$$

$$\frac{C}{Pr} g'' + \frac{C}{Pr} (Le - 1) \frac{\alpha_e I}{He} [(1 + \epsilon)z']' + f_B g' + \frac{u_e^2}{He} C \left(1 - \frac{1}{Pr}\right) [f'_B f''_B]' = 0 \tag{4.70}$$

$$C \frac{Le}{Pr} z'' + f_B z' = 0 \tag{4.71}$$

The boundary conditions are as given in Eqs. 4.68 with the following additional ones,

$$\begin{aligned} z(0) &= \text{constant} \\ z(\eta) &\to 1 \text{ as } \eta \to \infty \end{aligned} \tag{4.72}$$

In order to compare results of both the integral method and the exact similar solutions, a common coordinate must be used. From Eq. 4.21 we have the following expression:

$$y = \bar{\delta} \int_0^{\eta} \frac{\rho_e}{\rho} d\bar{\eta} \tag{4.73}$$

Define η^* as the common coordinate,

$$\eta^* = \sqrt{\frac{\rho_\infty u_\infty}{\mu_\infty x}}\ y = \sqrt{\lambda_o} \int_0^{\eta} \frac{\rho_e}{\rho} d\eta \tag{4.74}$$

On the other hand, η^* can be related to η_B by,

$$\eta^* = \sqrt{2} \int_0^{\eta_B} \frac{\rho_e}{\rho} d\eta_B \tag{4.75}$$

From Eqs. 4.74 and 4.75 the relations between the derivatives are,

$$\frac{\partial \phi}{\partial \eta^*} = \frac{1}{\sqrt{\lambda_o}} \frac{\rho}{\rho_e} \frac{\partial \phi}{\partial \eta} = \sqrt{\frac{1}{2}} \frac{\rho}{\rho_e} \frac{\partial \phi}{\partial \eta_B} \tag{4.76}$$

where, ϕ represents an arbitrary parameter.

For a steady boundary layer over a flat plate with the freestream and wall conditions as given in Table 2, the exact numerical profiles of velocity, enthalpy, degree of ionization and temperature are displayed in Fig. 24. The corresponding density profile is shown in Fig. 25. Also, the effects of a different Prandtl number on the density are illustrated in this figure. The exact numerical temperature profile has also been plotted in Fig. 26, where it is compared with the integral method profile. The results obtained by the two different methods are in excellent agreement.

For an equilibrium boundary-layer flow over a flat plate, exact numerical and integral method results for the degree of ionization and temperature profiles were computed. These results are shown in Fig. 27, and it can be seen that both sets are in excellent agreement.

The comparison of the exact numerical and integral method results serves the particular purpose in showing the accuracy of using polynomial expressions in the integral method. From the comparisons shown in Figs. 26 and 27, it can be concluded that the present integral method is in good agreement with the exact numerical one.

4.9 Discussion

The integral method has been used to study both the laminar wall boundary layer induced by a moving shock wave and the quasi-steady flat-plate laminar boundary layer. The following concluding remarks can be made.

1. The integral method is in good agreement with experimental data for the laminar wall boundary layer behind a shock wave. Near the edge of the boundary layer the flow is expected to be in equilibrium, and near the wall, the flow is expected to be in a nonequilibrium or in a frozen state.

2. The fifth, sixth and seventh order polynomial equations for the degree of ionization, velocity and enthalpy profiles, respectively, are sufficiently accurate for the present method.

3. A comparison between some predicted and experimental results for the quasi-steady flat-plate boundary layer indicates that there are discrepancies. Part of the disagreement may be due to the fact that actual variations of Prandtl number, Lewis number and the density viscosity product were not included in the analysis. A more satisfactory method might be to combine the Karman-Pohlhausen integral method and the Dorodnitsyn integration scheme (Ref. 25).

It is possible that the analysis and experiment may agree for the side-wall boundary layer where radiation effects close to the shock front are not yet significant. However, in the case of the flat plate quasi-steady boundary layer, where measurements are made far from the shock front (20-30 cm), radiation losses are important. For example, at shock Mach numbers of about 17, the free-stream ionization has dropped from 16% to 5%. It will therefore be necessary, as a first step, to include the new initial conditions in the numerical analysis. As a second step, it appears that the boundary layer equations would have to be solved by including the effects of the radiation terms. Ultimately, a finite-difference scheme would have to be developed that would permit the inclusion of variable Prandtl and Lewis numbers through the boundary layer. Perhaps, when these major modifications are made in the analysis, better agreement with the interferometric results might be expected.

Nevertheless, when one looks at the results obtained by Brimelow (Ref. 15) for the side-wall boundary layer it is clear that the agreement of experiment with analysis is as good close (3.75 cm) to the shock front ($M_s \simeq 17$) as for large distances (20 cm). This points to some basic differences between the two sets of data and the analyses. This problem is being investigated.

5. INTERACTION OF A LAMINAR BOUNDARY-LAYER FLOW AND A CORNER-EXPANSION WAVE IN PARTIALLY-IONIZED ARGON

5.1 Introduction

For an ideal and inviscid flow at supersonic speed, the flow around a sharp corner takes place through a stationary expansion wave. Such a flow

is completely described by the well-known Prandtl-Meyer relations (Ref. 49). The steady, inviscid flow of a partially-ionized gas around a sharp, convex corner is much more complex to describe analytically, and it has been studied in detail by Glass and Takano (Ref. 3). For a real gas flow a boundary layer is produced on the wall surface. Its presence can lead to a considerable modification of the results predicted by inviscid flow theory near the surface. The interaction of a laminar supersonic or hypersonic boundary layer with a steady corner-expansion wave for a partially-ionized gas is an important problem for aerospace control surfaces and entry into planetary atmospheres. This problem is still not well understood both theoretically and experimentally.

The interaction of a laminar boundary layer and a corner-expansion wave for a perfect gas has been investigated extensively (Refs. 27, 50 and 51). A comprehensive solution to this problem has been given by Lo (Ref. 27) who used Dorodnitsyn's integral method to solve the Navier-Stokes equations. To solve the same problem Sullivan (Ref. 51) suggested a simpler approach called the cold-wall similarity method. This method predicts successfully the major features of the flow at the edge of the boundary layer. The main advantages of Sullivan's method are that the calculations are simple to perform and the results are in good agreement with Lo's for the pressure distribution and boundary-layer thickness. Additionally, the results of Sullivan's analysis are in good agreement with experimental data (Ref. 52).

For an inviscid flow, Glass and Takano (Ref. 3) made a detailed study of nonequilibrium, frozen and equilibrium expansion flows of ionized argon around a sharp corner. The numerical calculation procedure was based on the method of characteristics, and it is similar to that for dissociating oxygen (Ref. 53). Furthermore, Glass and Igra (Refs. 54, 55) showed that the experimental results substantiate the analysis of Glass and Takano for a nonequilibrium supersonic corner-expansion flow of partially ionized argon.

In this chapter, Sullivan's method is applied to solve the interaction of a laminar boundary layer and a corner-expansion wave for a partially-ionized gas. For simplicity the assumption of a frozen flow in the boundary layer is made from the onset. A complete solution for the corner-expansion problem would be based on the coupled solutions for inviscid flow (Ref. 3) and the Navier-Stokes equations, which makes the analysis complex.

5.2 Cold-Wall Similarity Method for a Supersonic Ionized Argon Flow

The assumptions of hypersonic flow and a simple expansion wave used in Sullivan's analysis (Ref. 51) are removed, in order to apply the cold-wall similarity method to the case of a supersonic flow.

The boundary layer displacement thickness δ^*, defined by Eq. 4.43, can be expressed as,

$$\delta^* = \frac{\sqrt{2C_\infty}}{\sqrt{Re_{x\infty}}}\, I(x)\, \frac{\left[x \int \frac{p_e}{p_\infty}\, dx \right]^{1/2}}{p_e/p_\infty} \qquad (5.1)$$

$$I(x) = \int_0^\infty \left[\frac{\rho_e}{\rho} - \frac{u}{u_e} \right] d\eta_B \tag{5.2a}$$

$$C_\infty = \frac{\mu_w T_\infty (1 + \alpha_\infty)}{\mu_\infty T_w (1 + \alpha_w)} \tag{5.2b}$$

The coordinate η_B is given by Eq. 4.62b. A function G(x) is defined as,

$$G(x) = \frac{C_{P_\infty} T_\infty}{u_\infty^2/2} \tag{5.3}$$

$$C_{P_\infty} = \frac{5}{2} R(1 + \alpha_\infty)$$

The basic relationship between δ^* and p_e/p_∞ is,

$$\delta^* = \frac{\sqrt{2}}{5} \sqrt{\frac{\mu_w}{T_w R}}\, u_\infty^{3/2}\, G(x)\, \frac{\left[x \int \frac{p_e}{p_\infty} dx \right]^{1/2}}{p_e/p_\infty} \tag{5.4}$$

Equation 5.1 can be written in an alternate way in terms of the freestream variables M_∞, p_∞ and μ_∞.

$$\delta^* = \frac{x}{M_\infty} \frac{\sqrt{2}}{5} \gamma^* \frac{G(x)}{z} \frac{\left[\int P\, dz \right]^{1/2}}{P} \tag{5.5}$$

where

$$P = \frac{p_e}{p_\infty}$$

$$z = \frac{Re_{x,\infty}}{M_\infty^6 C_\infty}$$

$$Re_{x,\infty} = \frac{c u_\infty x}{\mu_\infty}$$

$$a_\infty = \sqrt{\gamma^* R T_\infty (1 + \alpha_\infty)}$$

Note that z is proportional to x, and that γ^* equals 5/3 for the frozen flow.

From the cold-wall similarity assumption, G is independent of x, but it is of constant value. Differentiating Eq. 5.5 with respect to z, then,

$$M_\infty = \frac{d\delta^*}{dz} = \frac{\sqrt{2}}{5} \gamma^* \frac{G}{z^0} \sqrt{R} \left[\frac{1}{2R} - \frac{P'}{P^2} \right] \tag{5.6}$$

$$z^{o} = z/x$$

$$P' = dP/dZ$$

$$P = p_e/p_\infty$$

$$R = \int P\, dZ$$

For a frozen flow α_e is constant and the following relations are applicable,

$$P = \left[\frac{Te}{T_{t_\infty}} \right]^{\frac{\gamma^*}{\gamma^*-1}} \tag{5.8}$$

$$\frac{Te}{T_\infty} = \frac{2 + (\gamma^*-1)M_\infty^2}{2 + (\gamma^*-1)M_e^2} \tag{5.9}$$

$$\frac{\rho_e}{\rho_\infty} = \left(\frac{Te}{T_\infty} \right)^{\frac{1}{\gamma^*-1}} \tag{5.10}$$

$$\frac{\alpha_e}{\alpha_\infty} = 1 \tag{5.11}$$

The rate of growth of the boundary layer displacement thickness immediately downstream of the corner is,

$$\left[\frac{d\delta^*}{dx} \right]_d = \left[\frac{d\delta^*}{dx} \right]_c + \alpha_w = \alpha_T \tag{5.12}$$

Note that α_w is the corner turning angle. The rate of growth of the boundary-layer displacement thickness downstream of the corner can be related to the deflection angle $\nu(P)$.

$$\frac{d\delta^*}{dx} = \alpha_T - \nu(P) \tag{5.13}$$

$$\nu(P) = \nu(M_e) - \nu(M_\infty) \tag{5.14}$$

The Prandtl-Meyer function for a frozen flow $\nu(M)$ is given below.

$$\nu(M) = \sqrt{\frac{\gamma^* + 1}{\gamma^* - 1}}\, \tan^{-1} \sqrt{\frac{\gamma^* - 1}{\gamma^* + 1}(M^2 - 1)} - \tan^{-1} \sqrt{M^2 - 1} \tag{5.15}$$

Substituting Eq. 5.13 into Eq. 5.6 leads to the following equations for the boundary-layer and expansion-wave interaction problem,

$$\frac{dP}{dz} = \frac{P^2}{2R}\left[\, 1 - 5\sqrt{2}\,\frac{\sqrt{R\,M_\infty}}{\gamma^* G}\,[\alpha_T - \nu(P)]\,\right] \tag{5.16}$$

$$\frac{dR}{dz} = P \tag{5.17}$$

Solutions to these two ordinary differential equations using a Runge-Kutta technique gives the pressure distribution p_e/p_∞. The initial conditions for P and R are obtained from the values immediately upstream of the corner ($x = x_c$); that is, $P = 1$ and $R = R_c$ (see Fig. 28). Note that the equation for the skin friction is,

$$C_{f\infty} = \frac{\sqrt{2\,f''(0)}}{M_\infty^3}\,\frac{P}{\sqrt{R}} \tag{5.18}$$

5.3 Model Calculations

The freestream and wall conditions for the following calculations of a laminar boundary layer interacting with an expansion wave are given in Table 2. Note that x_c (Fig. 28) has been set at 13.5 cm. The value of G (Eq. 5.3) is obtained by solving Eqs. 4.69 to 4.71 (see Appendix A), giving $G = 0.274(12)$.

Calculated results of pressure, temperature and density distribution at the edge of the boundary layer as a function of distance are shown in Figs. 29 to 31, respectively. In each case the results for four different turning angles of 5, 10, 15 and 20 degrees are presented. Similar results for Mach number, boundary layer, displacement thickness and skin friction are given in Figs. 32, 33 and 34, respectively. It can be seen that as the turning angle for the corner increases, the surface pressure, temperature, density, and skin friction decrease, whereas the displacement thickness and Mach number increase.

Some experimental data on the interaction of a boundary layer and a corner-expansion wave are given in Ref. 18. Profiles for the degree of ionization and density have been measured. As in the flat-plate quasi-steady boundary layer (Figs. 23a, b), the post-corner boundary-layer profiles of these quantities are in disagreement with the present analysis. In this case as well, the reasons are being investigated.

5.4 Discussion

The cold-wall similarity method can be used to predict the flow quantities at the boundary layer edge downstream of the corner. It is believed that these predictions are quite reliable. However, it is doubtful that the method can predict accurately the heat-transfer and skin-friction coefficients, owing to the assumption of similarity. For the cold-wall similarity method $f''(0)$ is assumed constant downstream of the corner. Actually, $f''(0)$ is a function of $d(p_e/p_\infty)/dx$. Near the corner this distance derivative

of pressure is a maximum and decreases to zero only as x increases to infinity. Since the skin-friction coefficient is proportional to $f''(0)$, the predicted coefficient is therefore only as accurate as the underlying assumption, which is believed to be inaccurate. Similarly, the heat-transfer coefficient would not be predicted accurately.

A new method, based on an iterative procedure, is suggested below.

1. Calculate p_e/p_∞ and $d(p_e/p_\infty)/dx$ by the cold-wall similarity method.
2. Calculate du_e/dx from the results of step 1.
3. Substitute du_e/dx into Eqs. 4.63 to 4.65 and solve them.
4. From the new results for f'_B, g and g' calculate G(x).
5. By using the cold-wall similarity method recalculate p_e/p_∞ and $d(p_e/p_\infty)/dx$.
6. Repeat steps 2, 3, 4, 5 and 6 until the resulting error is satisfactorily small.

This new method should enable the flow quantities at the boundary-layer edge and on the wall surface to be predicted as accurately as with the finite difference method. Similarly, the velocity, enthalpy, and degree of ionization profiles for the boundary layer downstream of the corner would be predicted accurately. However, the advantage is that the new method should provide a means of predicting accurately the heat-transfer and skin-friction coefficients.

A complete solution for the flow field around a corner can be obtained by combining the boundary-layer solution described in Chapter 4 with the solution of Glass and Takano (Ref. 3) for the expansion wave. However, the difficulty of defining a common coordinate for both parts of the flow field - viscous and inviscid - would first have to be overcome.

6. CONCLUSIONS

A study was made of shock-wave structure, laminar boundary layers in nonequilibrium flows of partially-ionized argon induced by a shock wave on shock tube side walls and over a flat plate, and of the interaction of a laminar boundary layer with a corner-expansion wave.

A new value of the ionizational cross-section constant for argon atom-atom collisions, was determined as, $S^*_{Ar\text{-}Ar} = 3.5 \times 10^{-20}$ cm^2/eV, by comparing results from a theoretical two-step collision model with experimental data of shock structure and its relaxation processes. It was confirmed that the ionization rate is controlled by atom-atom collisions initially and then by the more efficient electron-atom collisions. When the electron number density increases to a certain level, the electron-production rate due to atom and electron collisions drops quickly and the process reaches equilibrium. Owing to the extremely low mass of a hydrogen atom and the large excitational cross-sections for hydrogen atom-atom and electron-atom collisions, even a low level of hydrogen impurity can reduce the total relaxation length of the shock wave in argon.

The integral method of Karman and Pohlhausen was applied to study the shock-induced laminar wall boundary layer and the quasi-steady flat-plate laminar boundary layer in an ionized argon flow. Equilibrium, frozen and nonequilibrium solutions were obtained, compared with each other, and with available experimental results. The experimental data show that the flow near the edge of the shock-induced boundary layer on a wall is in equilibrium but in the wall region the flow is in nonequilibrium. This conclusion is in agreement with Knoos' results.

For the quasi-steady boundary-layer flow over a flat plate, there is disagreement between the analytical and experimental results. It is not understood why the analysis should agree with the wall boundary layer experimental data and not with the flat-plate data. This discrepancy may be due to the error in using the integral method for the analysis. The solutions based on the integral method are independent of variations of the transport properties with gas temperature and degree of ionization, which is a serious deficiency of the present analysis. The present method also suffers from the fact that the results are averaged over the entire boundary layer, rather than reflecting rapidly varying local properties. However, if these were the reasons then they should be applicable to both boundary layers. This is not the case. Perhaps the major difficulty arises from radiation losses as discussed at the end of Section 4.9.

The cold-wall similarity method developed by Sullivan was extended and applied to the interaction of a laminar boundary layer and a corner-expansion flow for partially-ionized argon. The entire flow was assumed frozen both upstream and downstream of the corner. The hypersonic flow and simple expansion-wave assumptions were removed for the present case of supersonic flow. The cold-wall similarity method predicts the pressure, temperature and Mach number at the edge of the boundary layer, and the displacement thickness, but breaks down for predicting flow profiles inside the boundary layer. To overcome this difficulty a new method of solution was proposed. Available post-corner, boundary-layer experimental data are also in disagreement with the present analysis. The reasons why disagreements occur in the case of the quasi-steady boundary layers on a flat plate and after a corner-expansion interaction are presently under study, as discussed at the end of Section 4.9.

REFERENCES

1. J. P. Appleton, K. N. C. Bray — J. Fluid Mech. 20, 659 (1964).
2. L. Talbot, Y. S. Chou, F. Robben — "Expansion of a Partially Ionized Gas through a Supersonic Nozzle", AFOAR Rep. No. AS-65-14 (1965).
3. I. I. Glass, A. Takano — UTIAS Rep. No. 95 (1963).
4. O. Igra — UTIAS Review No. 38 (1974).
5. H. Petschek, S. Byron — Ann. Phys. 1, 270 (1957).
6. P. E. Oettinger, D. Bershader — AIAA 5, 1625 (1967).
7. C. E. Chapin — Ph.D. Thesis, Purdue University (1967).
8. H. F. Nelson, R. Goulard — Phys. of Fluids 12, 1605 (1969).
9. G. Kamimoto, K. Teshima, M. Nishimura — CP 36, Dept. of Aero. Eng., Kyoto University, Japan (1972).
10. K. E. Harwell, R. D. Jahn — Phys. of Fluids 7, 214 (1964).
11. E. J. Morgan, R. D. Morrison — Phys. of Fluids 8, 1608 (1965).
12. A. J. Kelly — J. Chem. Phys. 45, 1723 (1966).
13. M. I. Hoffert, H. Lien — Phys. of Fluids 10, 1769 (1967).
14. T. I. McLaren, R. M. Hobson — Phys. of Fluids 11, 2162 (1968).
15. P. I. Brimelow — UTIAS Technical Report No. 187 (1974).
16. D. J. Hollenbach, E. E. Salpeter — J. Chem. Phys. 50, 4157 (1969).
17. D. R. Bates, A. E. Kingston, R. W. P. McWeirter — Proc. Roy. Soc. (London) A267, 297 (1962).
18. B. T. Whitten — University of Toronto, UTIAS, Ph.D. Thesis (to be published).

19. A. N. Belozerov, R. M. Measures — J. Fluid Mech. 36, 695 (1969).

20. C. T. Chang — Riso Report No. 27, Denmark (1961).

21. P. A. Libby, M. Morduchow — NACA TN No. 3157 (1954).

22. M. Morduchow — NACA Report No. 1245 (1955).

23. P. M. Chung, A. D. Anderson — NASA TN No. 140 (1960).

24. P. A. Chung, A. D. Anderson — NASA TND-350 (1961).

25. A. A. Dorodnitsyn — Advances in Aero. Sci. (Macmillan Co., New York), Vol. 3, p. 207 (1962).

26. A. J. Pallone — J. Aero. Sci. 28, 449 (1961).

27. A. Lo — UTIAS Report No. 157 (1970).

28. A. J. Pallone, J. A. Moore, J. I. Erdos — AIAA 2, 1706 (1964).

29. F. G. Blottner — AIAA 2, 1921 (1964).

30. R. M. Kendall, E. P. Bartlett — AIAA 6, 1089 (1968).

31. C. duP. Donaldson, R. C. Sullivan — NACA TN No. 1942 (1949).

32. R. N. Hollyer, Jr. — Eng. Res. Inst., University of Michigan (July 1, 1953).

33. H. Mirels — NACA TN No. 3401 (1955).

34. H. Mirels — NACA TN No. 3712 (1956).

35. H. Mirels — NASA TN D-291 (1961).

36. R. A. Hartunian, P. V. Marrone — Cornell Aero. Lab. Rep. No. AD-1118-A-7 (1959).

37. J. A. Fay, W. H. Kemp — AIAA 1, 2741 (1963).

38. S. Knöös — J. Plasma Phys. 2, 207 (1968).

39. J. A. Fay, W. H. Kemp — J. Fluid Mech. 21, 659 (1965).

40. P. M. Chung, J. F. Mullen — AIAA Summer Meeting Paper No. 63-161 (1963).

41. K. Matsuoka, M. Nishida — AIAA 9, 2457 (1971).

42. M. Nishida — Ph.D. Thesis, Kyoto University, Japan (1969).

43. L. H. Back — Phys. of Fluids 10, 807 (1967).

44. M. L. Finson, H. Kemp — Phys. of Fluids 8, 201 (1965).

45. P. A. Libby, M. Morduchow, M. Bloom — NACA TN No. 2655 (1952).

46. L. H. Back, A. B. Witte — J. Heat Transfer 88, 249 (1966).

47 L. Lees — Jet Propulsion 26, 259 (1956).

48. H. Schlichting — "Boundary Layer Theory", McGraw-Hill (1955).

49. H. W. Liepmann, A. Roshko — "Elements of Gasdynamics", John Wiley & Sons, Inc., New York (1957).

50. V. Zakkay, K. Toba, T. Ku — AIAA 2, 1389 (1964).

51. P. A. Sullivan — UTIAS TN No. 129 (1968).

52. J. L. Stollery — ARL 70-0126 (July, 1970).

53. I. I. Glass, A. Takano — UTIAS Report No. 91 (1963).

54. I. I. Glass, O. Igra — Proc. Int. Sym. on Dynamics of Ionized Gases, Int. Union of Theo. & Appl. Mech., Tokyo, Japan (1971).

55. O. Igra — Progress in Aerospace Sciences, 16, 3, 299 (1975).

56. D.M. Dix — AIAA 2, 2081 (1964).

TABLE 1

NUMERICAL CONSTANTS USED IN THE CALCULATIONS

UNIVERSAL CONSTANTS	
Boltzmann constant	1.3803×10^{-16} erg/°K
Avogadro constant	6.023×10^{23} per mole
Mass of an electron (m_e)	9.1066×10^{-28} g
Partition function for electrons	2
CONSTANTS FOR ARGON	
Molecular weight of an argon atom (m_{Ar})	39.944 g/mole
Gas constant ($R_{Ar} = k/m_{Ar}$)	0.20813×10^{7} erg/g°K
Partition function for atoms	1
Partition function for ions	6
Ionization temperature (T_I)	182,850°K
First excitational temperature (T*)	135,000°K
Characteristic density of ionization (ρ_I)	150.27 g/cm^3
CONSTANTS FOR HYDROGEN	
Molecular weight of a hydrogen molecule (m_{H_2})	2.016 g/mole
Molecular weight of a hydrogen atom (m_H)	1.008 g/mole
Gas constant for a hydrogen atom (R_H)	8.3135×10^{7} erg/g°K
Partition function for atoms	2
Partition function for ions	1
Ionization temperature (T_I)	157,000°K
First excitational temperature (T*)	118,380°K

TABLE 2

INITIAL CONDITIONS FOR A STRONG SHOCK WAVE

MOVING IN A QUIESCENT GAS

Case	Gas	P_1(torr)	M_s	T_1(°K)
I	pure argon	5.6	16.5	298.7
II	pure argon	5.12	16.53	296.6
III	pure argon	5.09	13.59	296.7
IV	argon + 0.4% hydrogen (by pressure)	5.17	16.68	297.4

TABLE 3

FREESTREAM AND WALL CONDITIONS FOR A LAMINAR BOUNDARY LAYER

OVER A FLAT PLATE IN PURE ARGON

u_∞	4778 m/sec
M_∞	2.4
P_∞	2238.4 torr
T_∞	13,393°K
T_w	298.2°K
M_s	16.98
x	13.5 cm

TABLE 4

FREESTREAM AND WALL CONDITIONS FOR A LAMINAR BOUNDARY LAYER BEHIND A STRONG SHOCK WAVE IN PURE ARGON

Case	u_s (m/sec)	M_s	u_1 (m/sec)	$u_\infty = u_s - u_1$ (m/sec)	M_1	p_∞ (torr)	T_∞ (°K)	T_w (°K)	x (cm)
I	5303	16.53	4614.6	688.4	2.4	2231	13,221	297.9	3.75
II	5303	16.53	4614.6	688.4	2.4	2231	13,221	297.9	20
III	4369	13.59	3650.8	517.7	1.9	1331	11,758	299	12

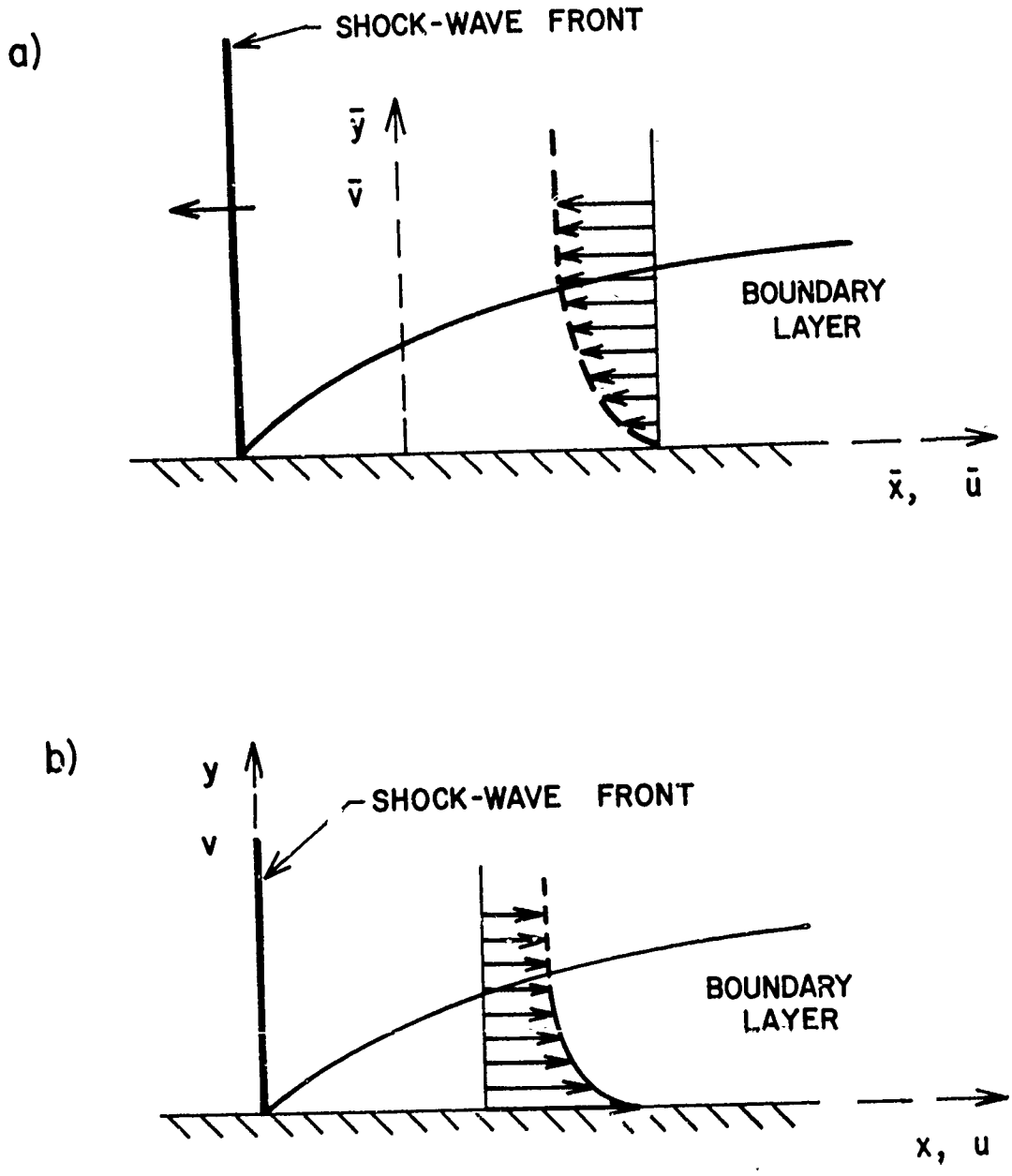

FIG. 1 TWO DIFFERENT COORDINATE SYSTEMS FOR A BOUNDARY LAYER INDUCED BEHIND A MOVING SHOCK WAVE, a) COORDINATE SYSTEM FIXED TO THE WALL, b) COORDINATE SYSTEM FIXED TC THE SHOCK-WAVE FRONT.

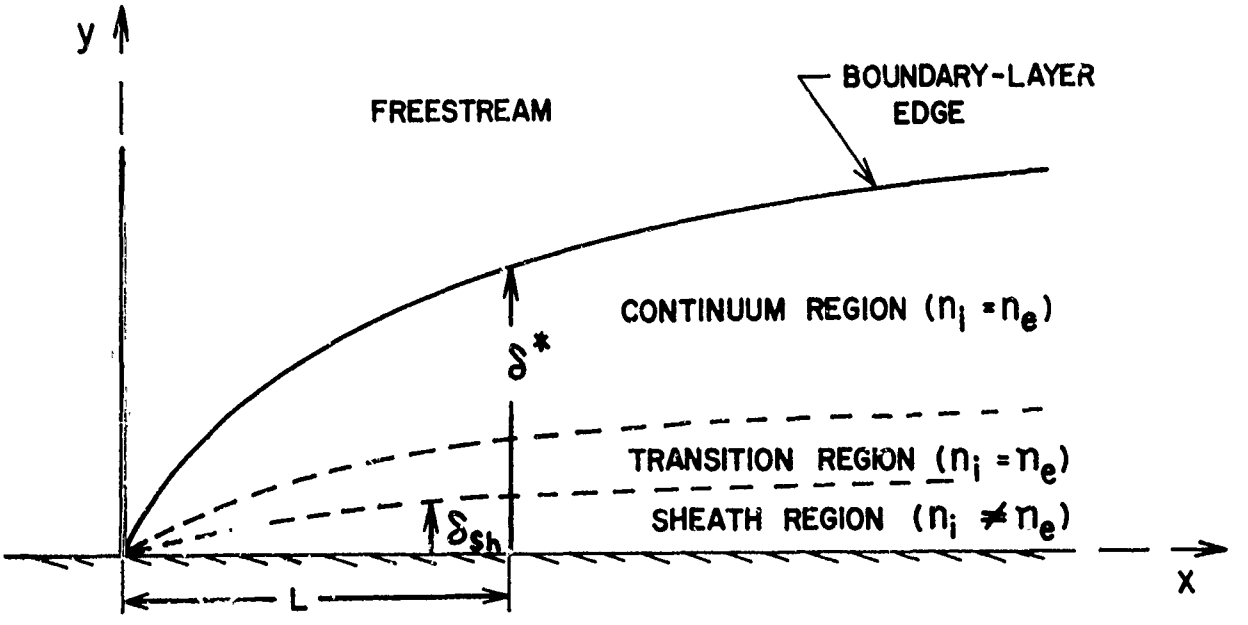

$$\delta^* \approx 0\,[L\,R_e^{-\frac{1}{2}}] \qquad \text{(Ref. 56)}$$

$$\delta_{Sh} \approx 0\,[L\,R_e^{-1/6}\,\beta^{2/3}] \qquad \text{(Ref. 56)}$$

$$\beta = \delta_d / L$$

$$\delta_d = \left(\frac{k\,T_e}{4\pi\,n_e\,e^2} \right)^{\frac{1}{2}} \qquad \text{(Debye length, Ref. 56)}$$

$\delta^* \gg \delta_{Sh}$ for a high freestream ion density

$\delta^* \sim \delta_{Sh}$ for a low freestream ion density

$\delta^* \gg \delta_{Sh}$ for a sufficiently low freestream ion density

FIG. 2 SHEATH, TRANSITION, CONTINUUM AND FREESTREAM REGIONS FOR A WALL BOUNDARY LAYER.

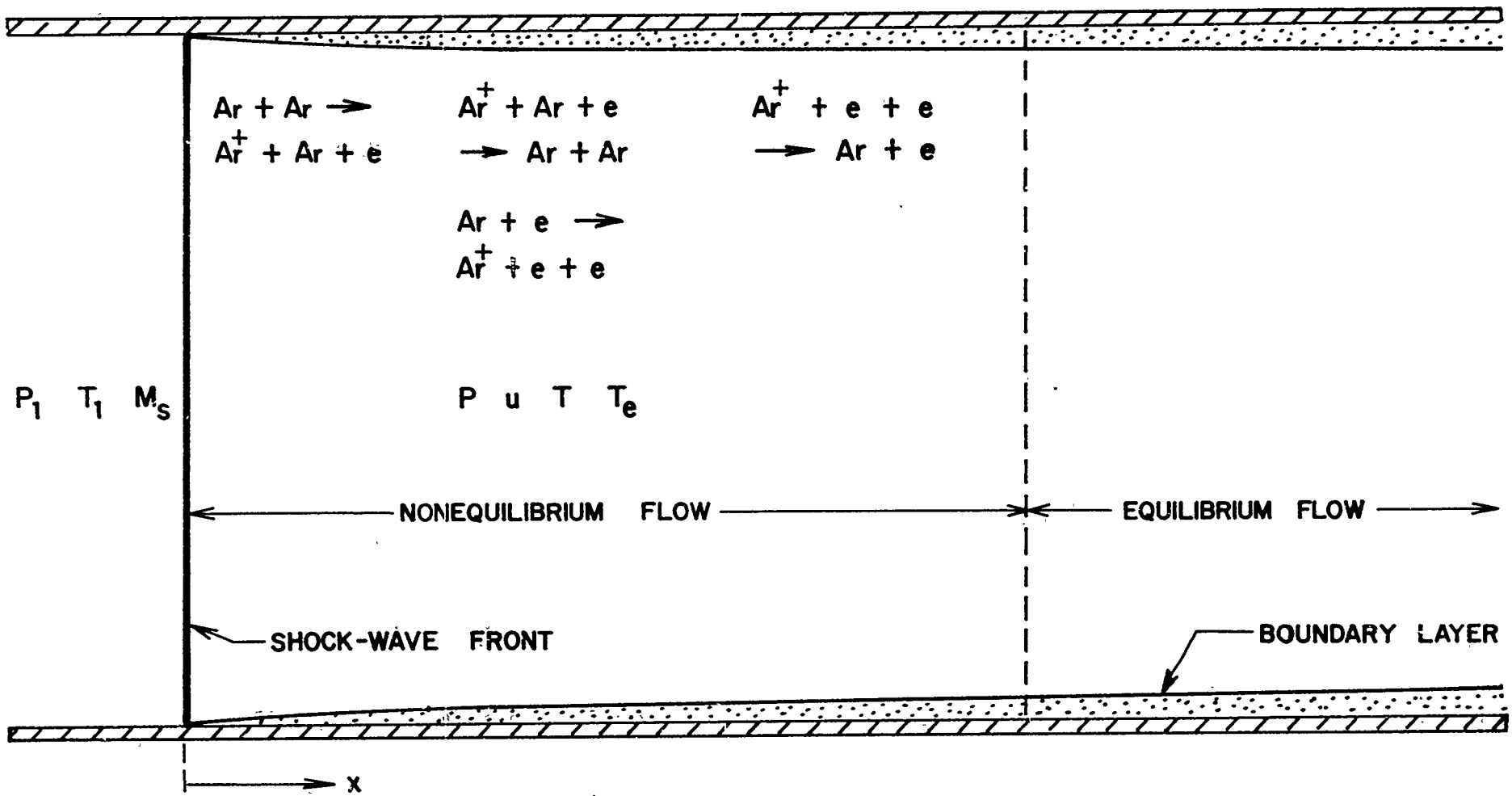

FIG. 3 SHOCK STRUCTURE IN A NONEQUILIBRIUM ARGON FLOW.

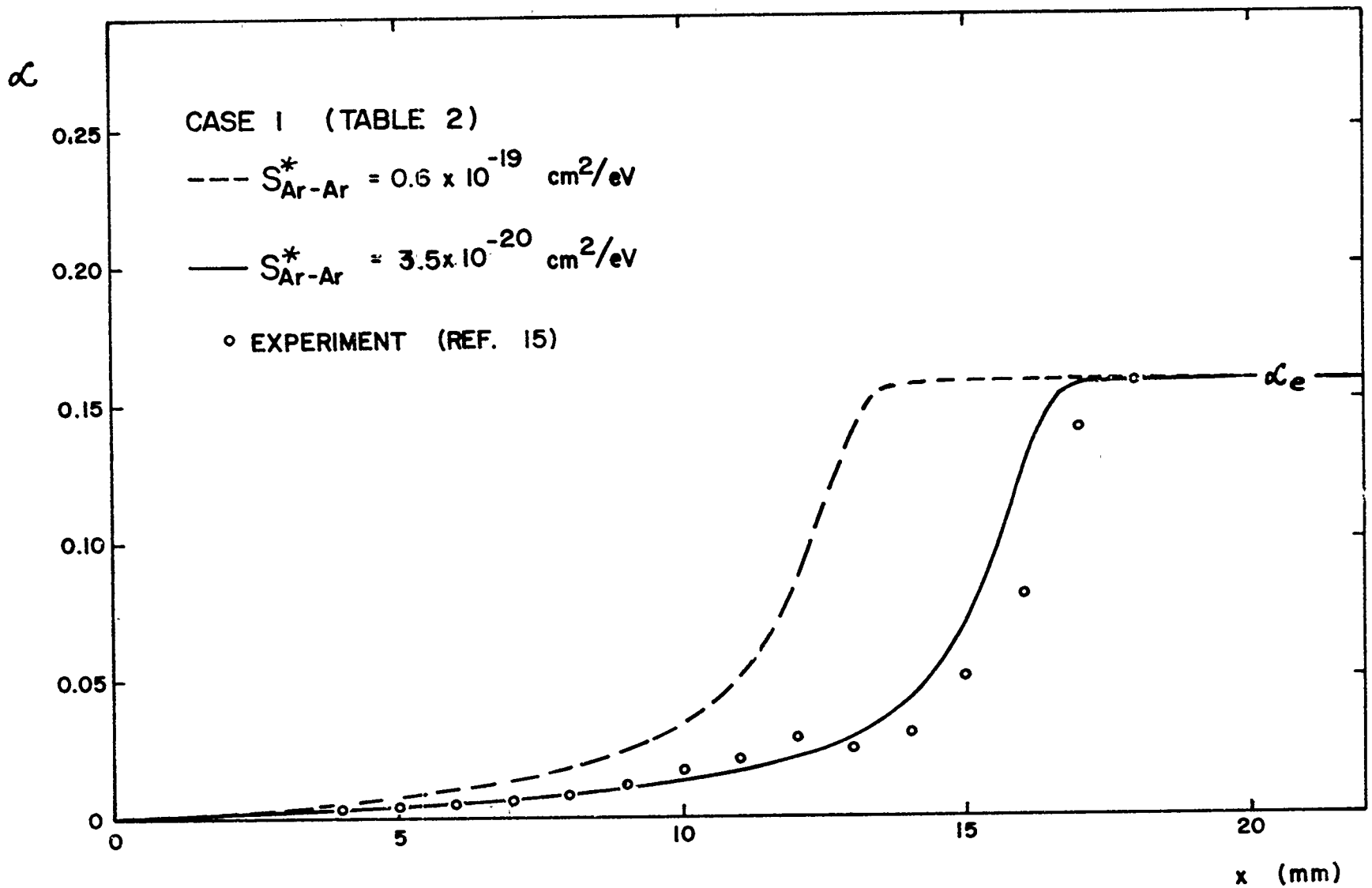

FIG. 4 VARIATION OF DEGREE OF IONIZATION (α) WITH DISTANCE (x) THROUGH RELAXATION REGION BEHIND A STRONG SHOCK WAVE IN PURE ARGON WITH p_1 = 5.6 TORR, M_s = 16.5 AND T_1 = 298.7°K.

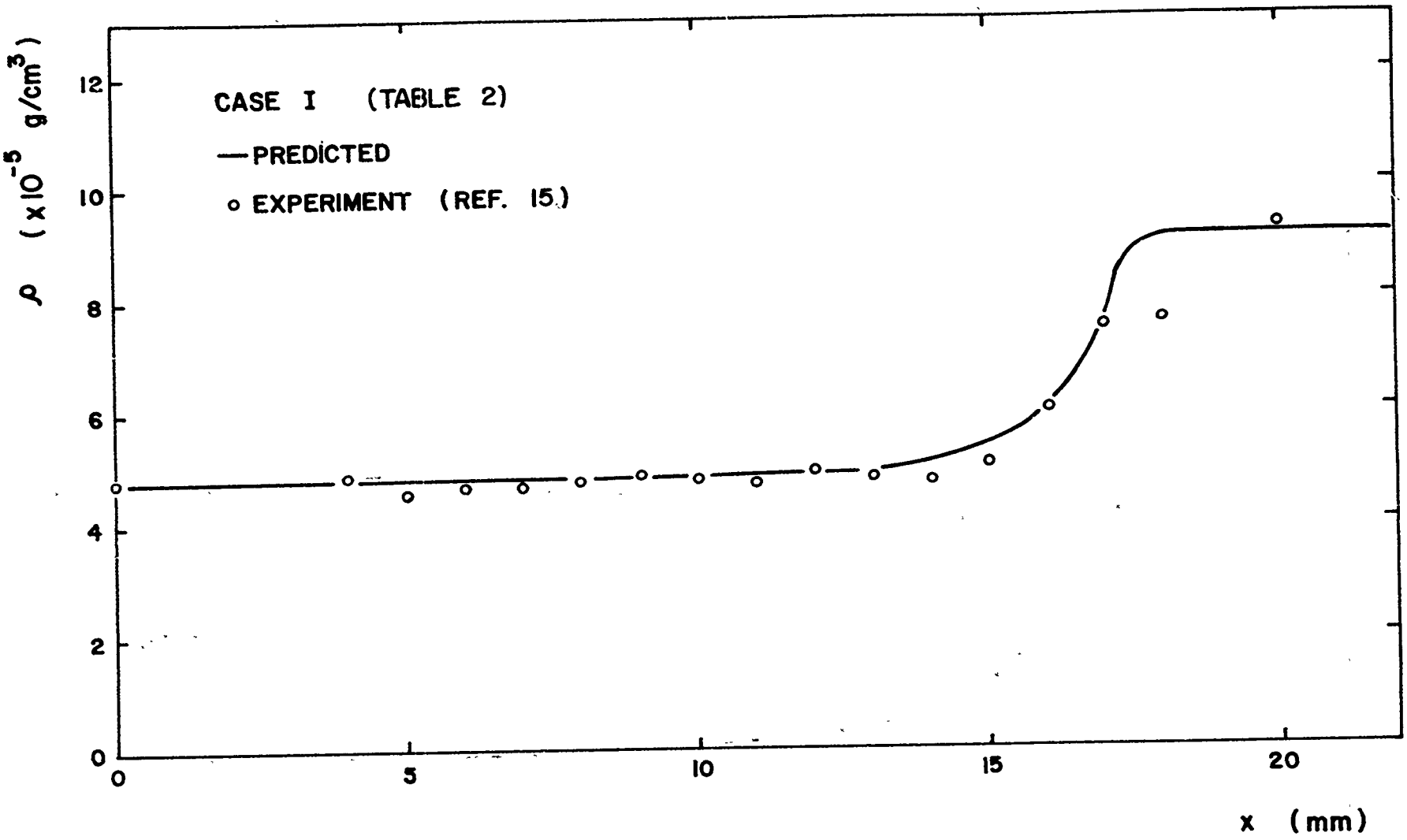

FIG. 5 DENSITY (ρ) VARIATION WITH DISTANCE (x) THROUGH THE RELAXATION REGION WITH p_1 = 5.6 TORR, M_s = 16.5 AND T_1 = 298.7°K IN PURE ARGON.

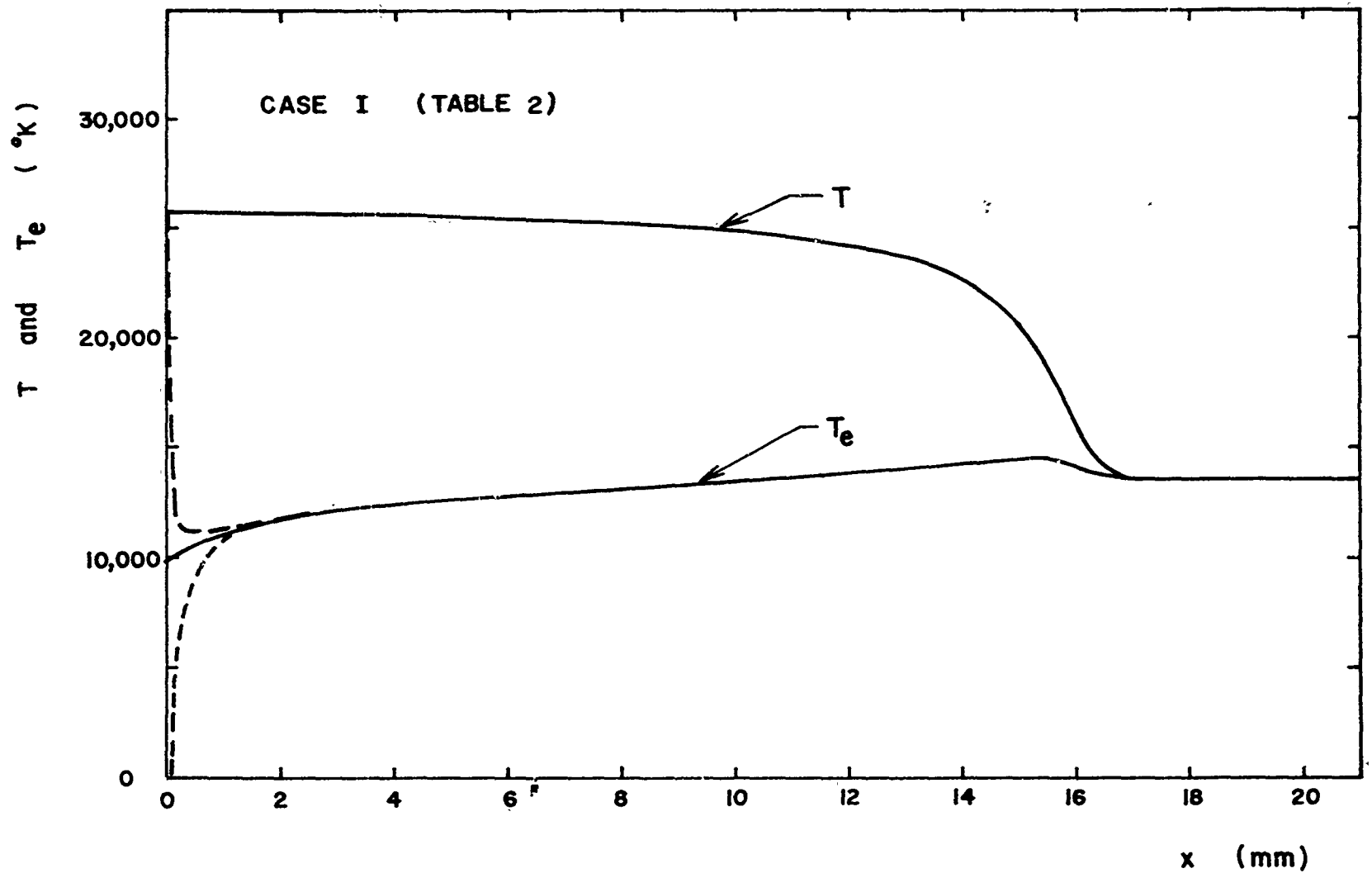

FIG. 6 ATOM TEMPERATURE (T) AND ELECTRON TEMPERATURE (T_e) VARIATIONS WITH DISTANCE (x) THROUGH THE RELAXATION REGION FOR p_1 = 5.6 TORR, M_s = 16.5 AND T_1 = 298.7°K IN PURE ARGON.

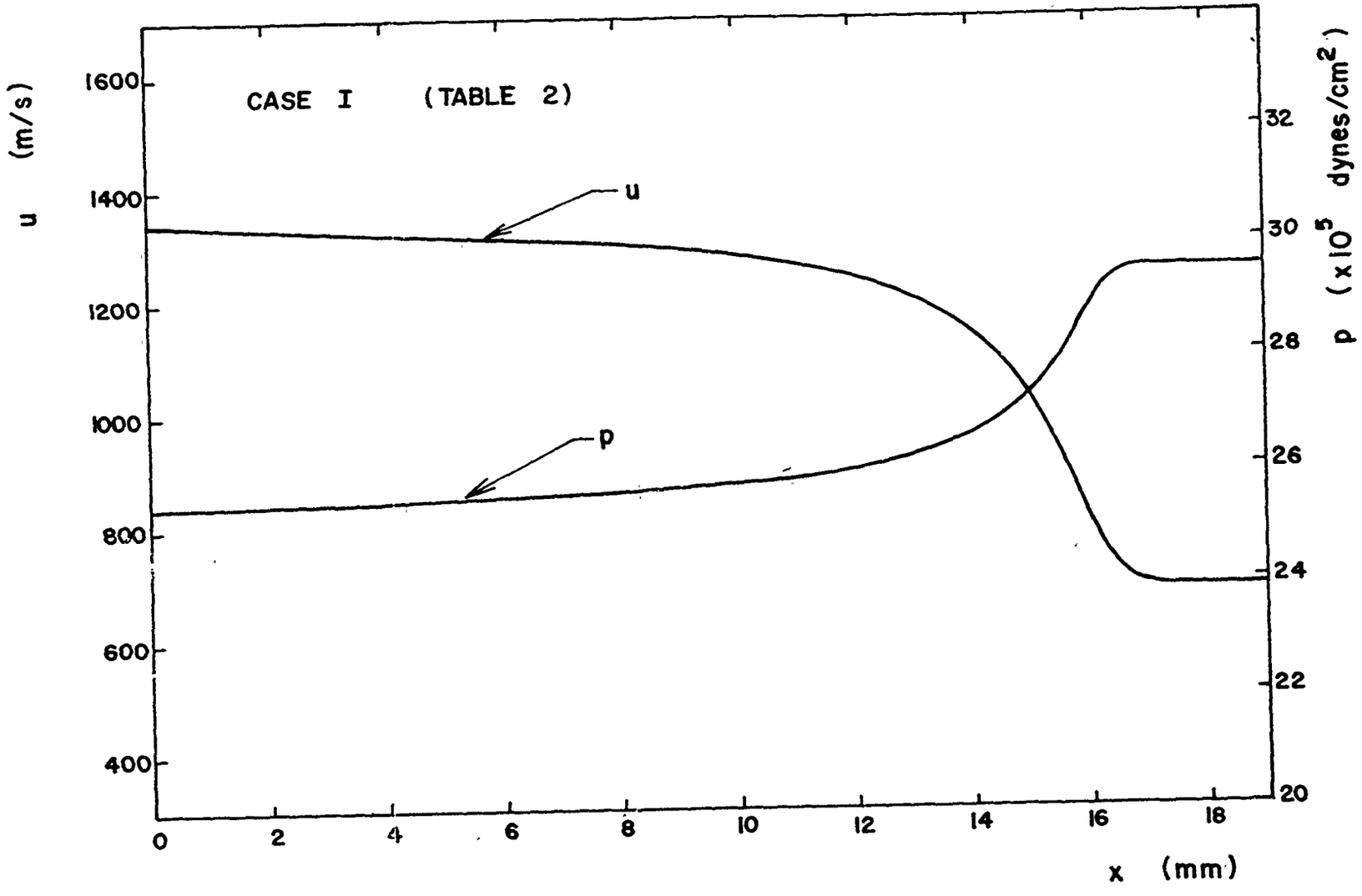

FIG. 7 FLOW VELOCITY (u) AND PRESSURE (p) VARIATIONS WITH DISTANCE (x) THROUGH THE RELAXATION REGION FOR p_1 = 5.6 TORR, M_s = 16.5 AND T_1 = 298.7°K IN PURE ARGON.

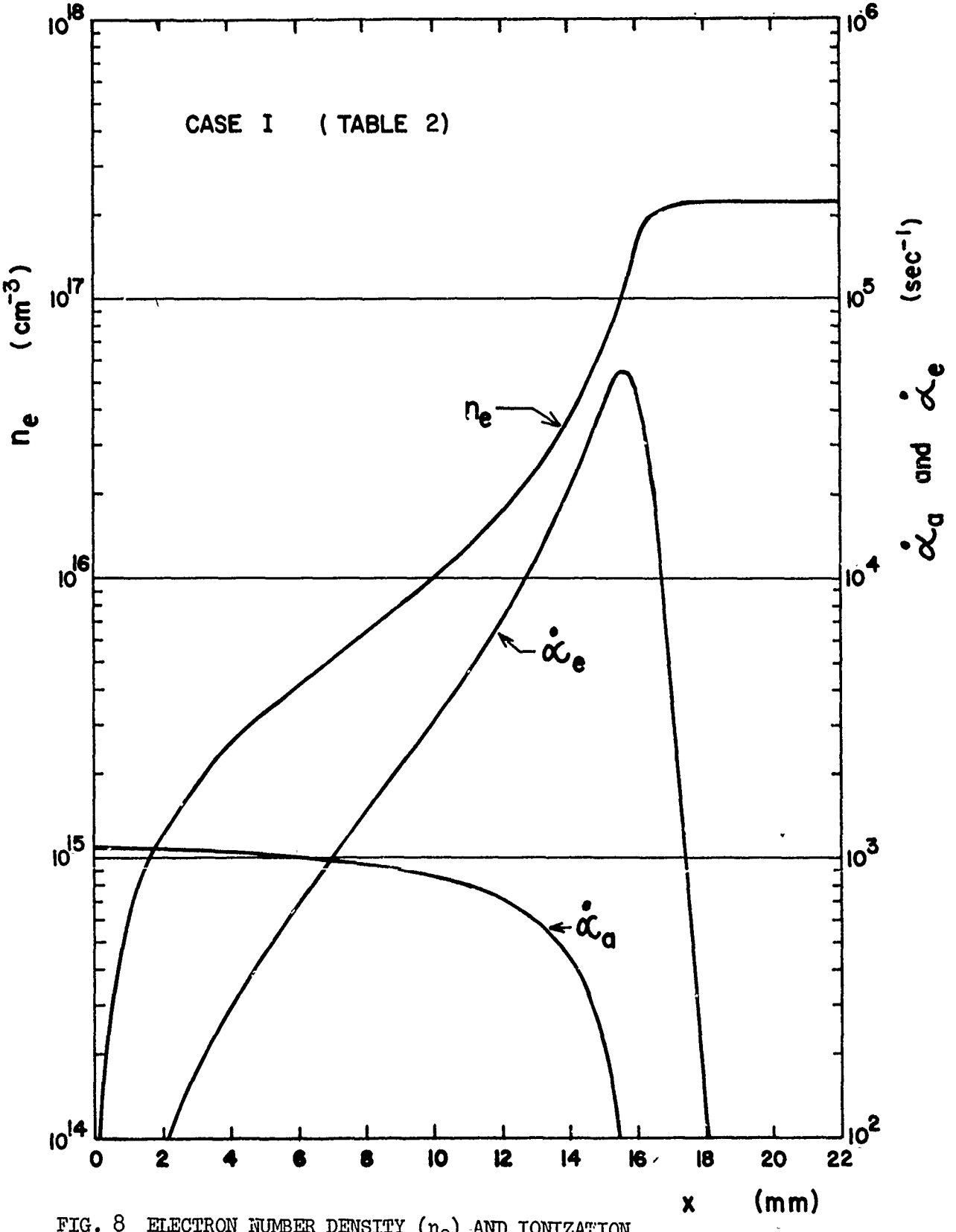

FIG. 8 ELECTRON NUMBER DENSITY (n_e) AND IONIZATION PRODUCTION RATES $\dot{\alpha}_a$ AND $\dot{\alpha}_e$ WITH DISTANCE (x) THROUGH THE RELAXATION REGION FOR p_1 = 5.6 TORR, M_s = 16.5 AND T_1 = 298.7°K IN PURE ARGON.

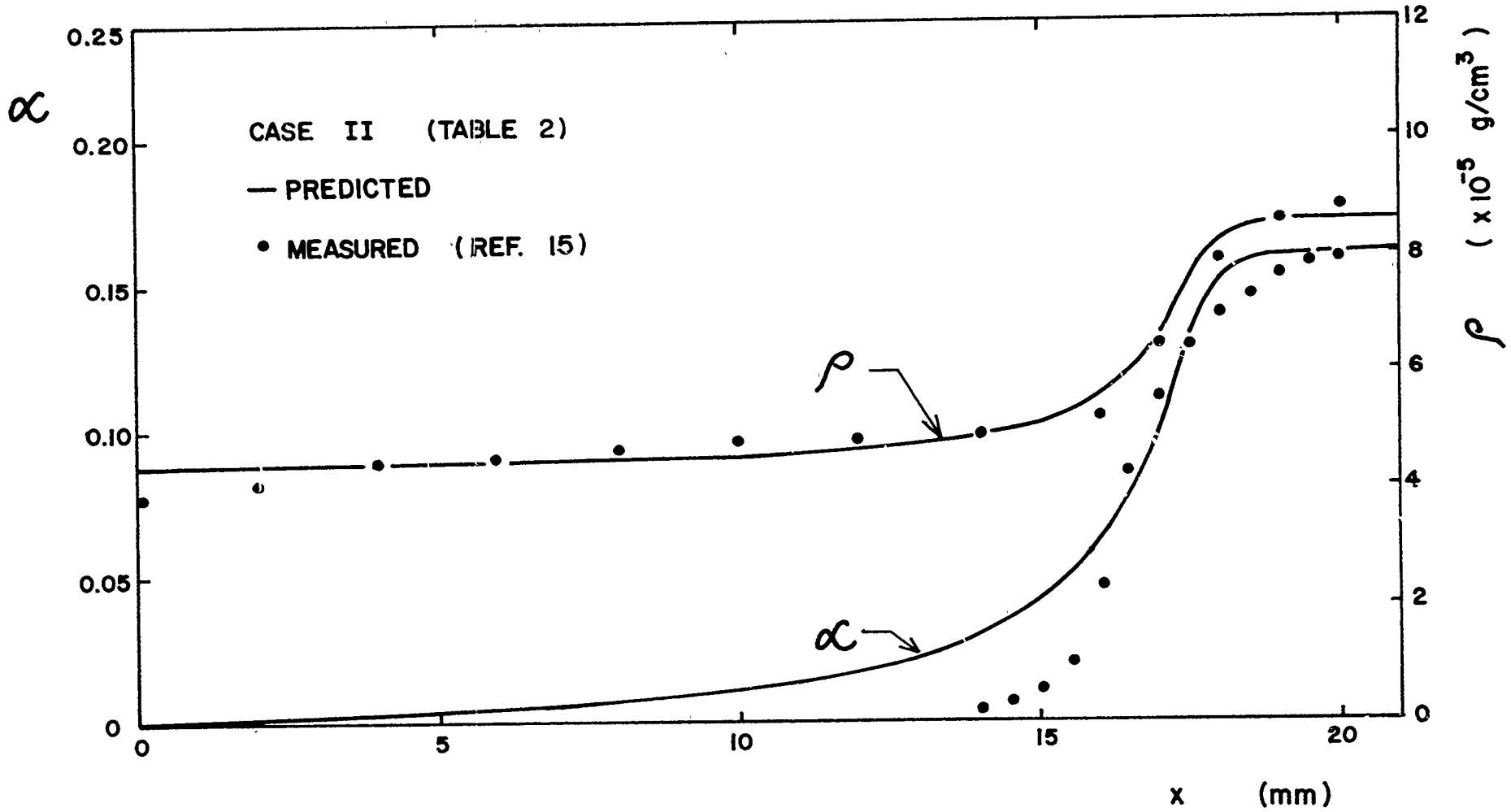

FIG. 9 DENSITY (ρ) AND DEGREE OF IONIZATION (α) WITH DISTANCE FOR p_1 = 5.12 TORR, M_s = 16.53 AND T_1 = 296.6°K IN PURE ARGON.

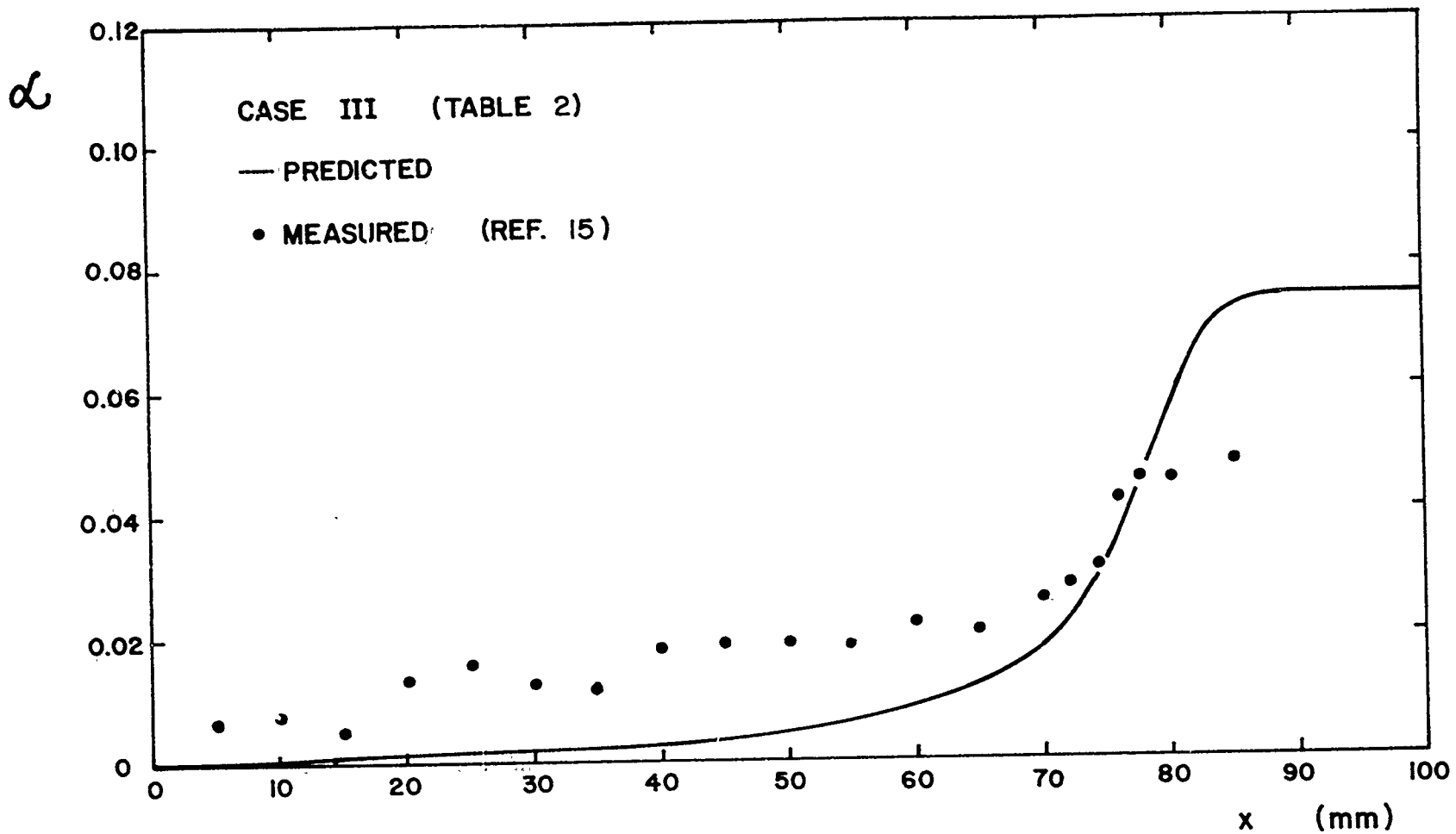

FIG. 10 DEGREE OF IONIZATION (α) WITH DISTANCE (x) THROUGH THE RELAXATION REGION FOR p_1 = 5.09 TORR, M_s = 13.59 AND T_1 = 296.7°K IN PURE ARGON.

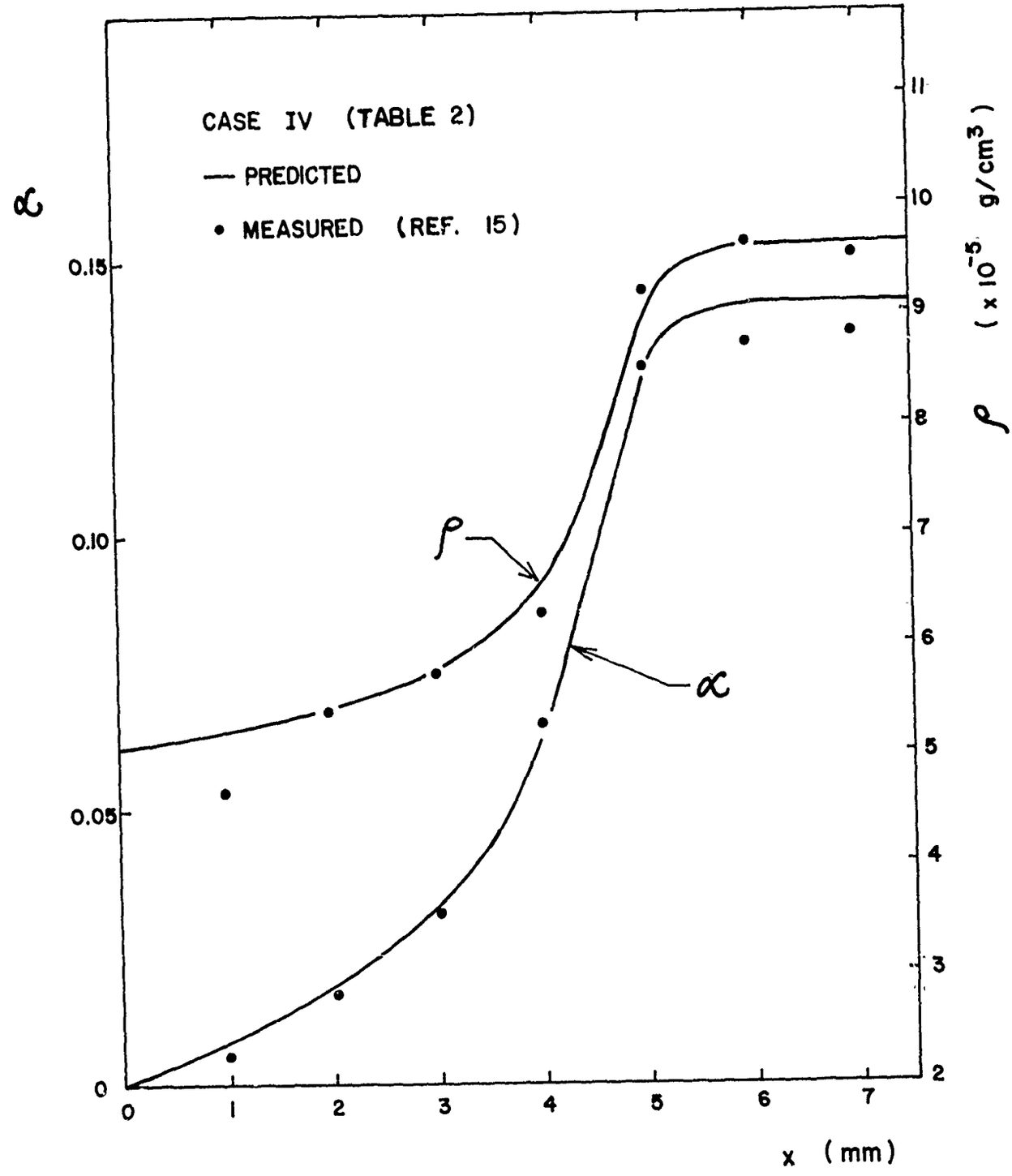

FIG. 11 DENSITY (ρ) AND DEGREE OF IONIZATION (α) WITH DISTANCE (x) THROUGH THE RELAXATION REGION FOR ARGON + 0.4% HYDROGEN (BY PRESSURE) WITH p_1 = 5.17 TORR, M_S = 16.88 and T_1 = 297.4°K.

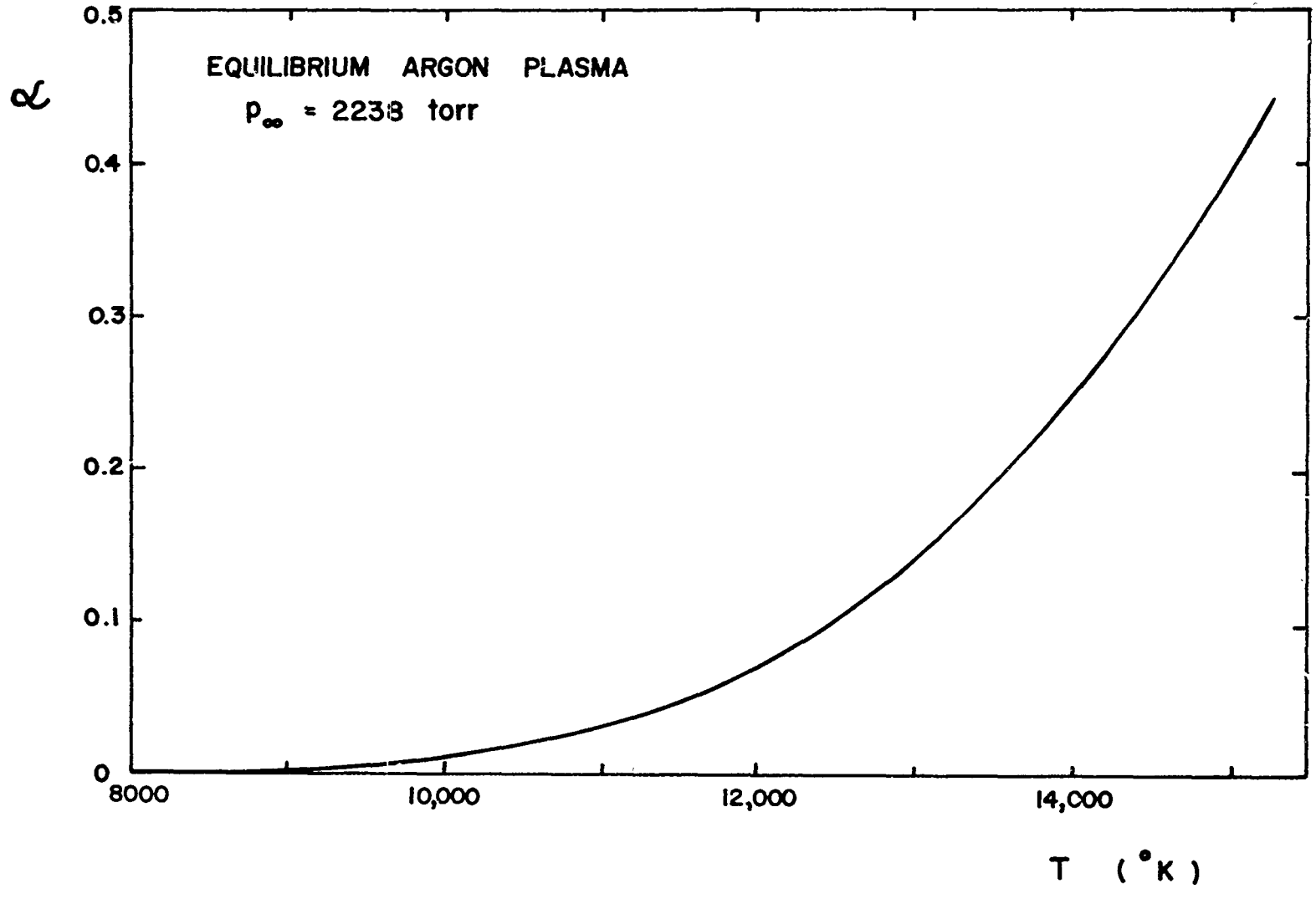

FIG. 12 DEGREE OF IONIZATION (α) AS A FUNCTION OF TEMPERATURE (T) FOR AN EQUILIBRIUM ARGON PLASMA.

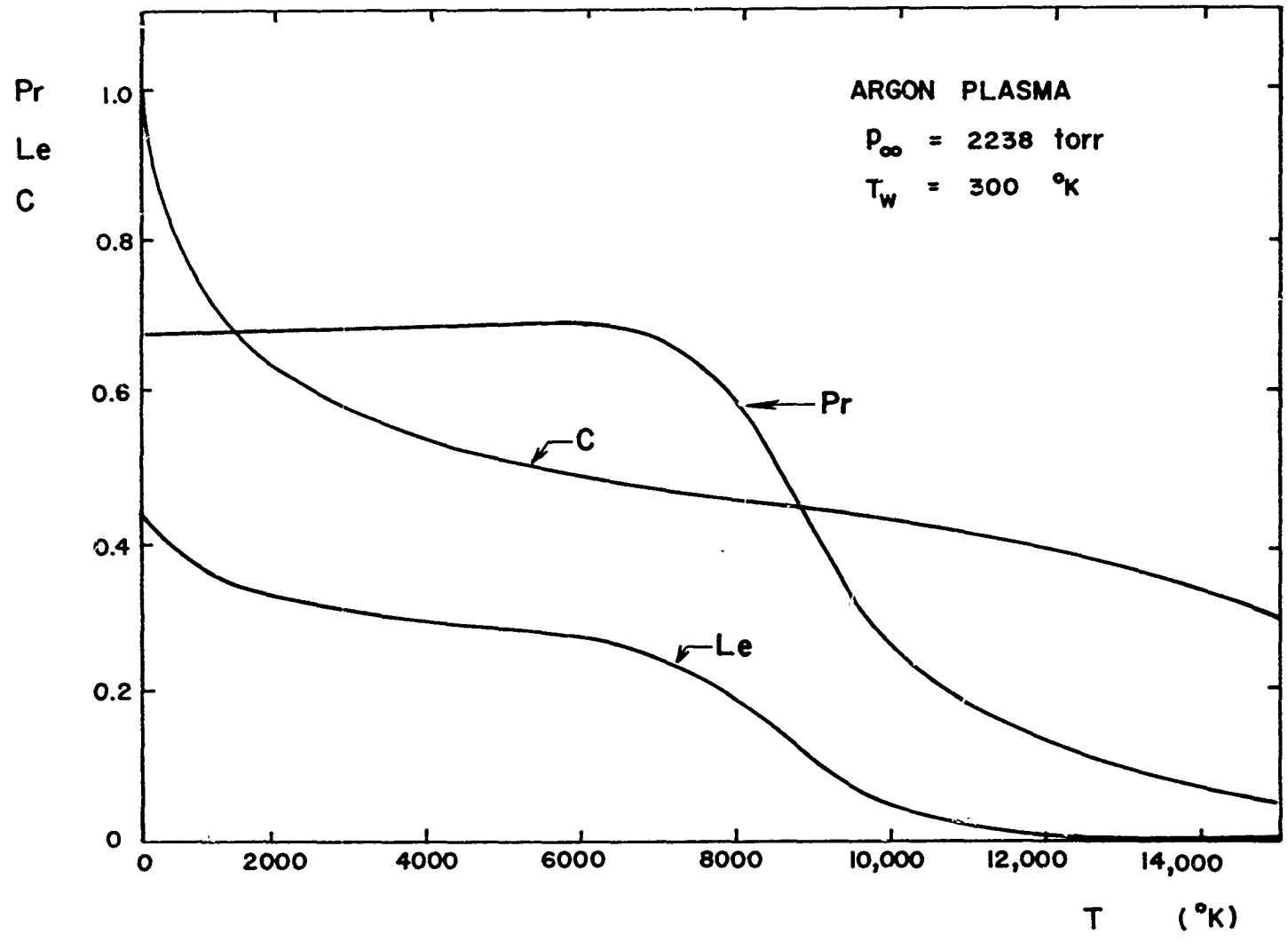

FIG. 13 PRANDTL NUMBER (Pr), LEWIS NUMBER (Le) AND DENSITY-VISCOSITY PRODUCT (C) VERSUS TEMPERATURE (T) FOR AN EQUILIBRIUM ARGON PLASMA.

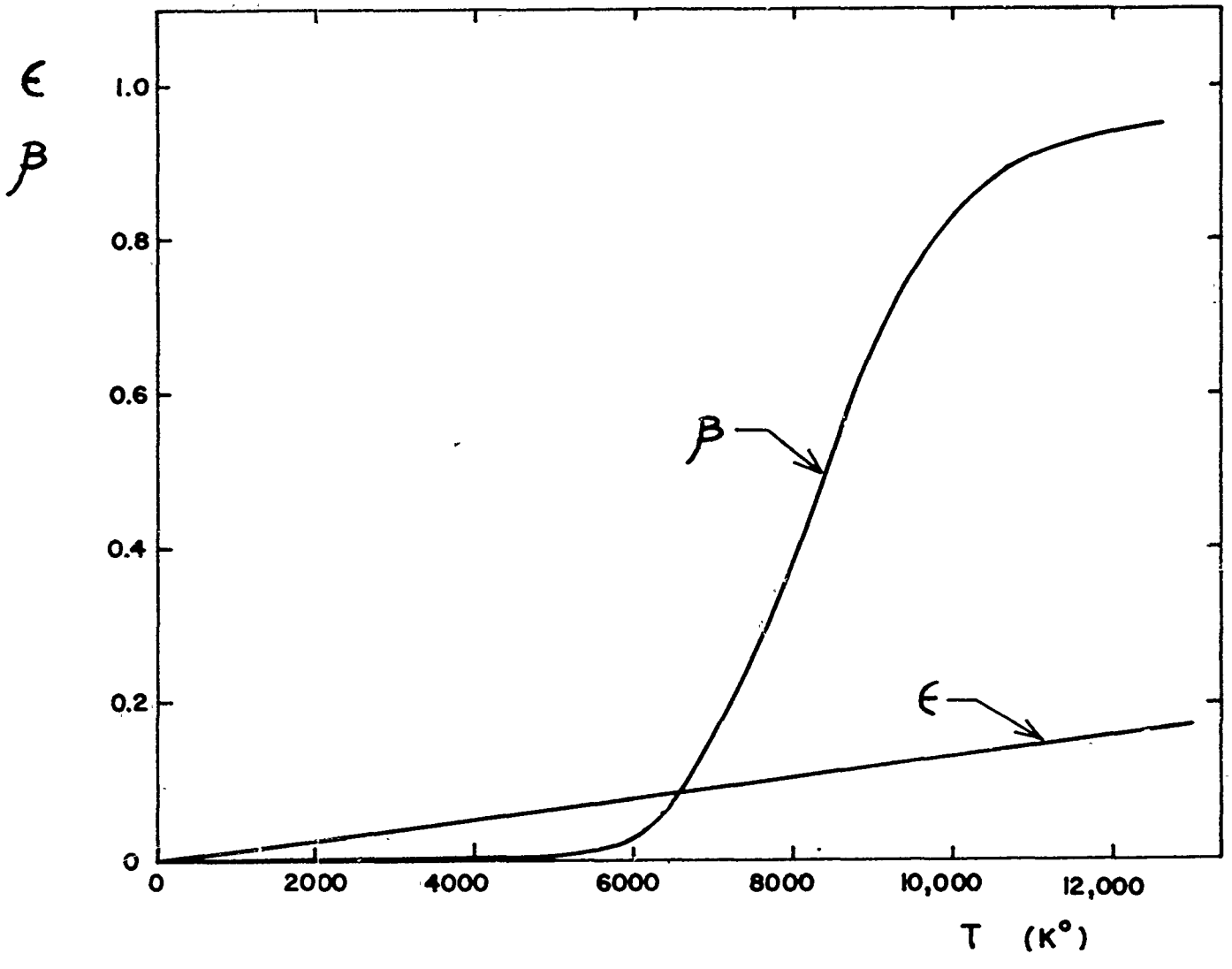

FIG. 14 VARIATION OF ϵ AND p AS A FUNCTION OF TEMPERATURE (INITIAL CONDITIONS GIVEN IN TABLE 3).

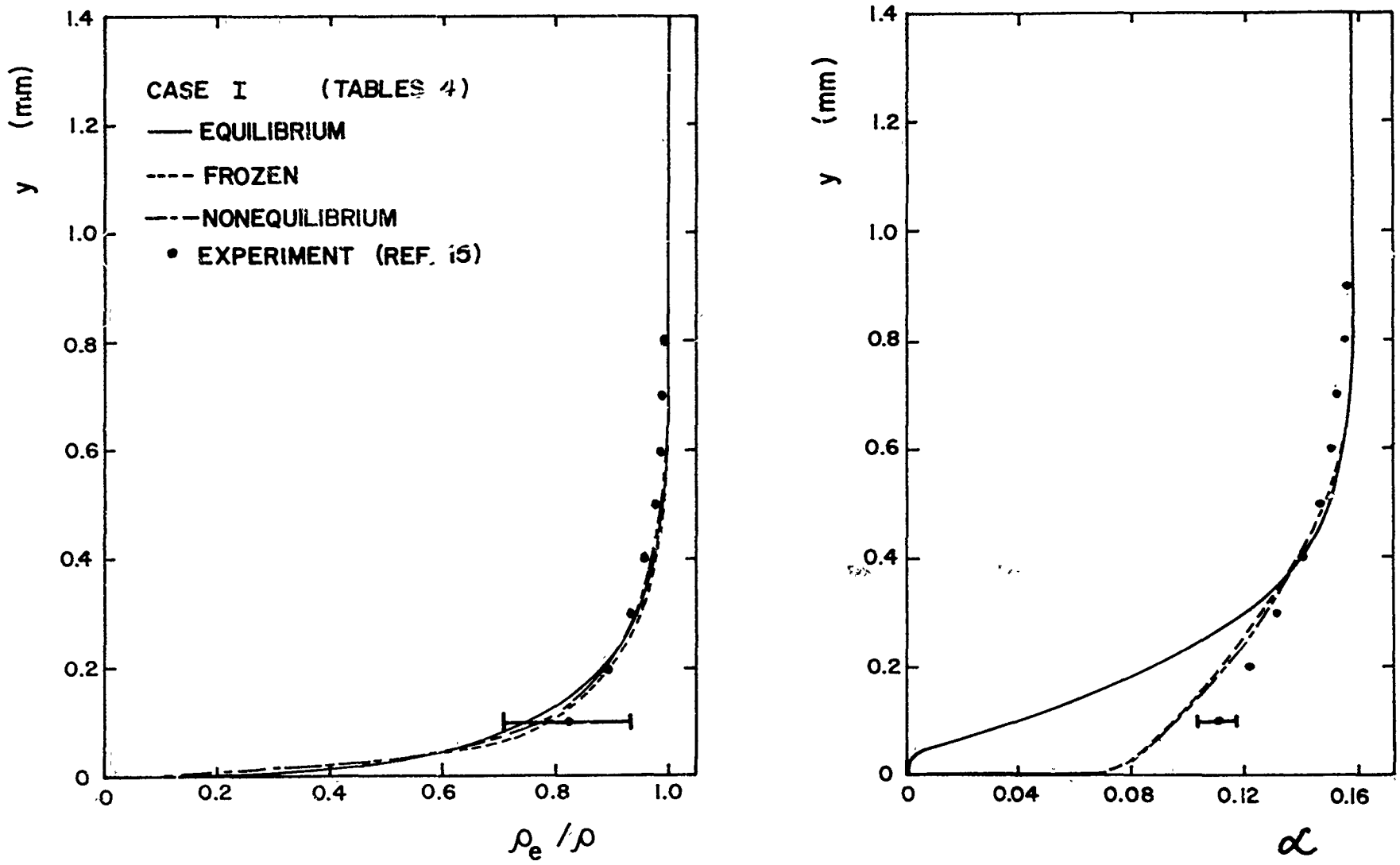

FIG. 15 DENSITY RATIO (ρ_e/ρ) VARIATION THROUGH A LAMINAR WALL BOUNDARY LAYER BEHIND A SHOCK WAVE IN PURE ARGON. THE INITIAL CONDITIONS ARE GIVEN IN FIG. 15, EXCEPT x = 20 CM. THE ERROR BAR SHOWS THE UNCERTAINTY IN THE QUANTITIES DUE TO THE ERROR IN THE EXACT WALL POSITION NEAR THE WALL.

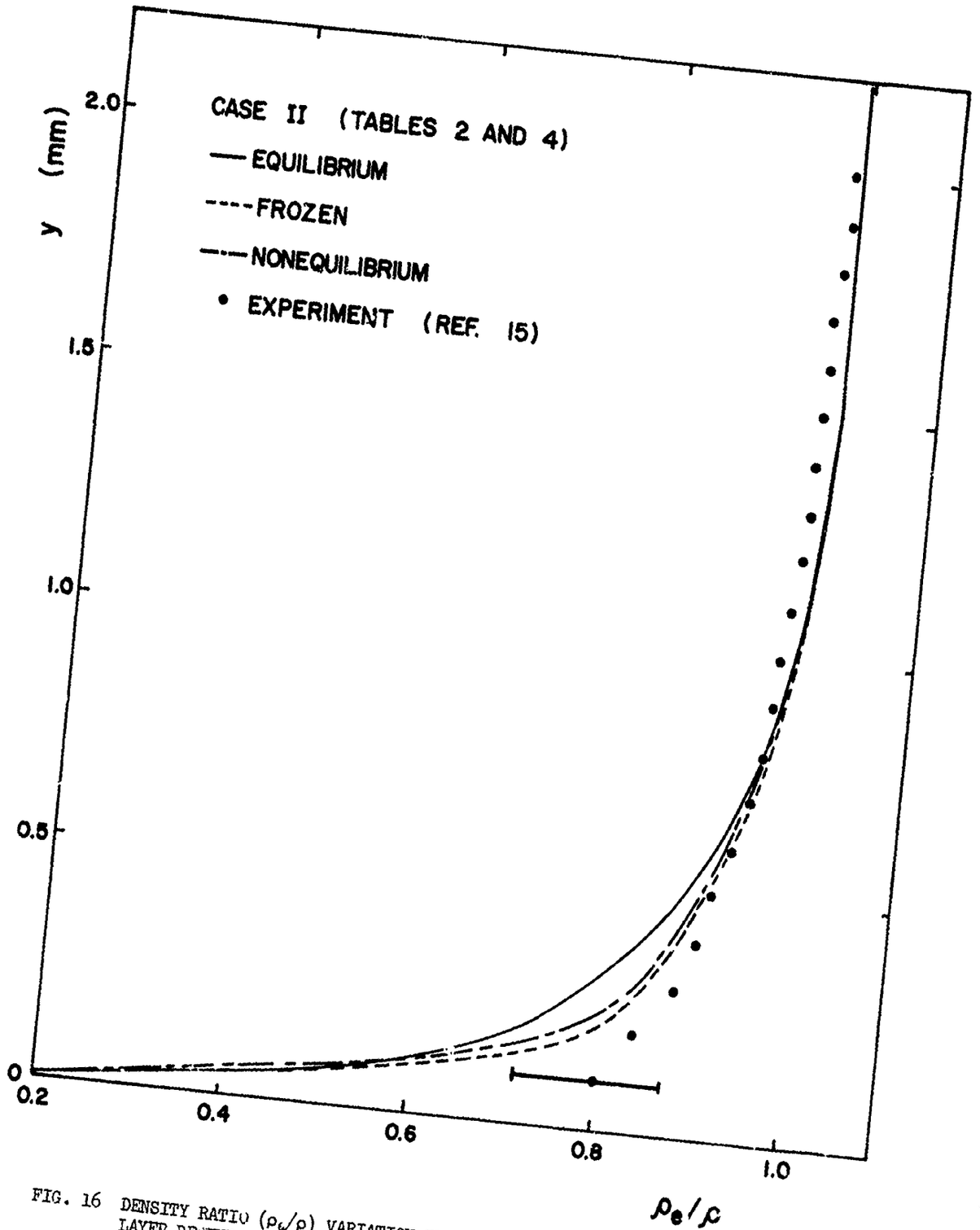

FIG. 16 DENSITY RATIO (ρ_e/ρ) VARIATION THROUGH A LAMINAR WALL BOUNDARY LAYER BEHIND A SHOCK WAVE IN PURE ARGON. THE INITIAL CONDITIONS ARE GIVEN IN FIG. 15, EXCEPT λ = 20 CM.

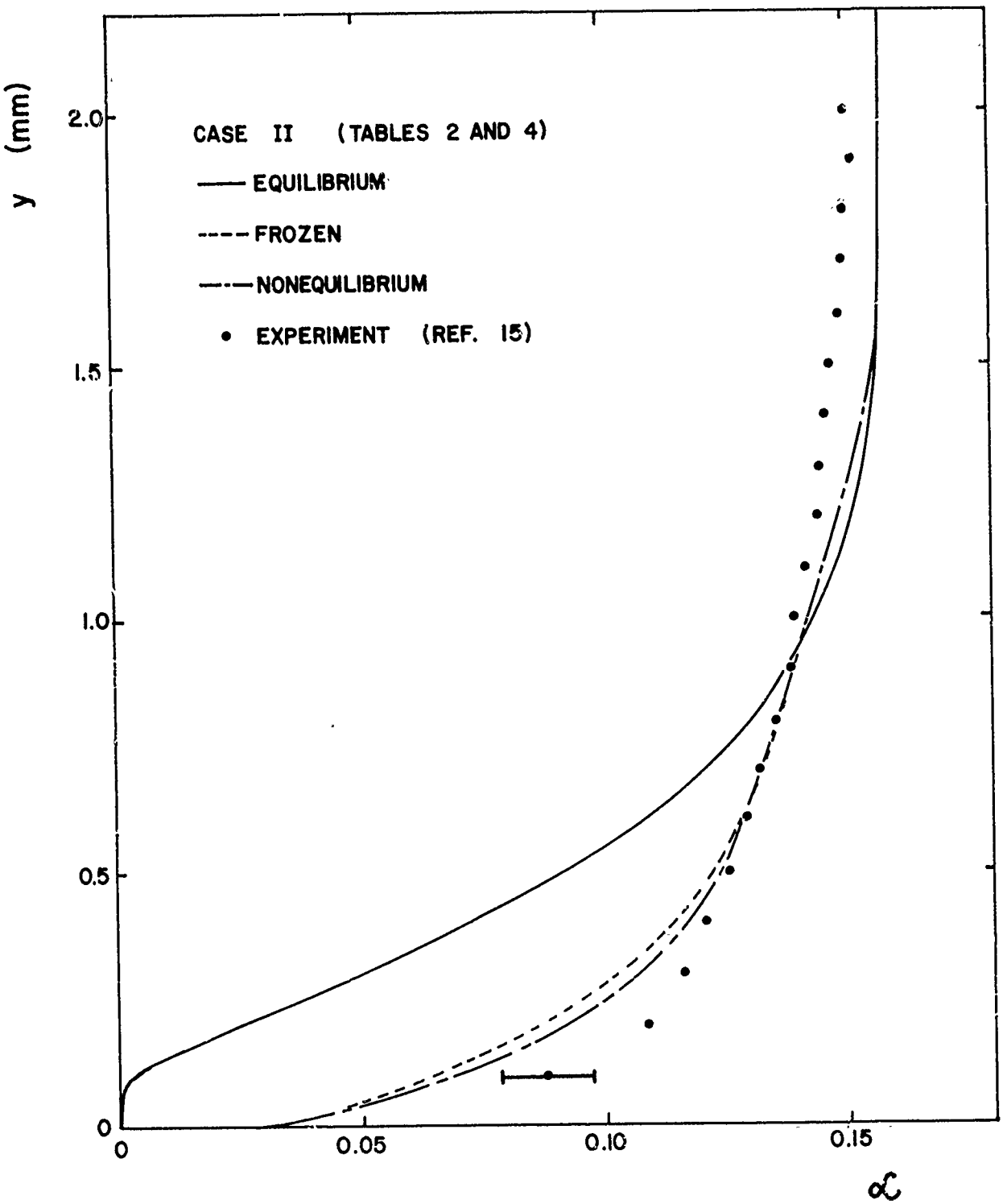

FIG. 17 DEGREE OF IONIZATION VARIATION (α) THROUGH A LAMINAR WALL BOUNDARY LAYER BEHIND A SHOCK WAVE. INITIAL CONDITIONS AS FOR FIG. 16.

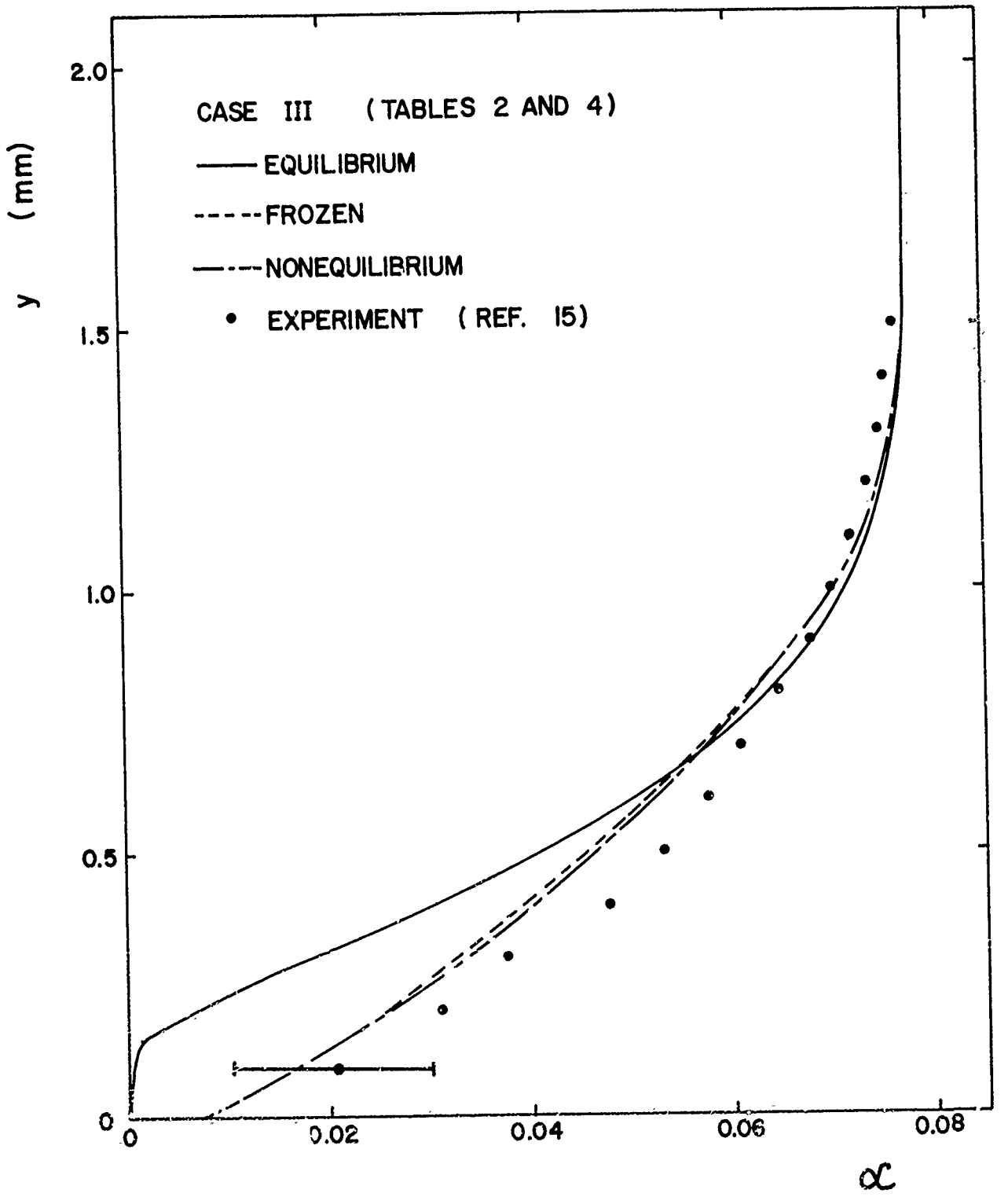

FIG. 16 DEGREE OF IONIZATION (α) WITH NORMAL DISTANCE (y) FOR p_∞ = 1331 TORR, M_s = 13.59, u_∞ = 517.7 M/SEC, T_∞ = 11,758°K, T_w = 299°K AND x = 12 CM IN PURE ARGON.

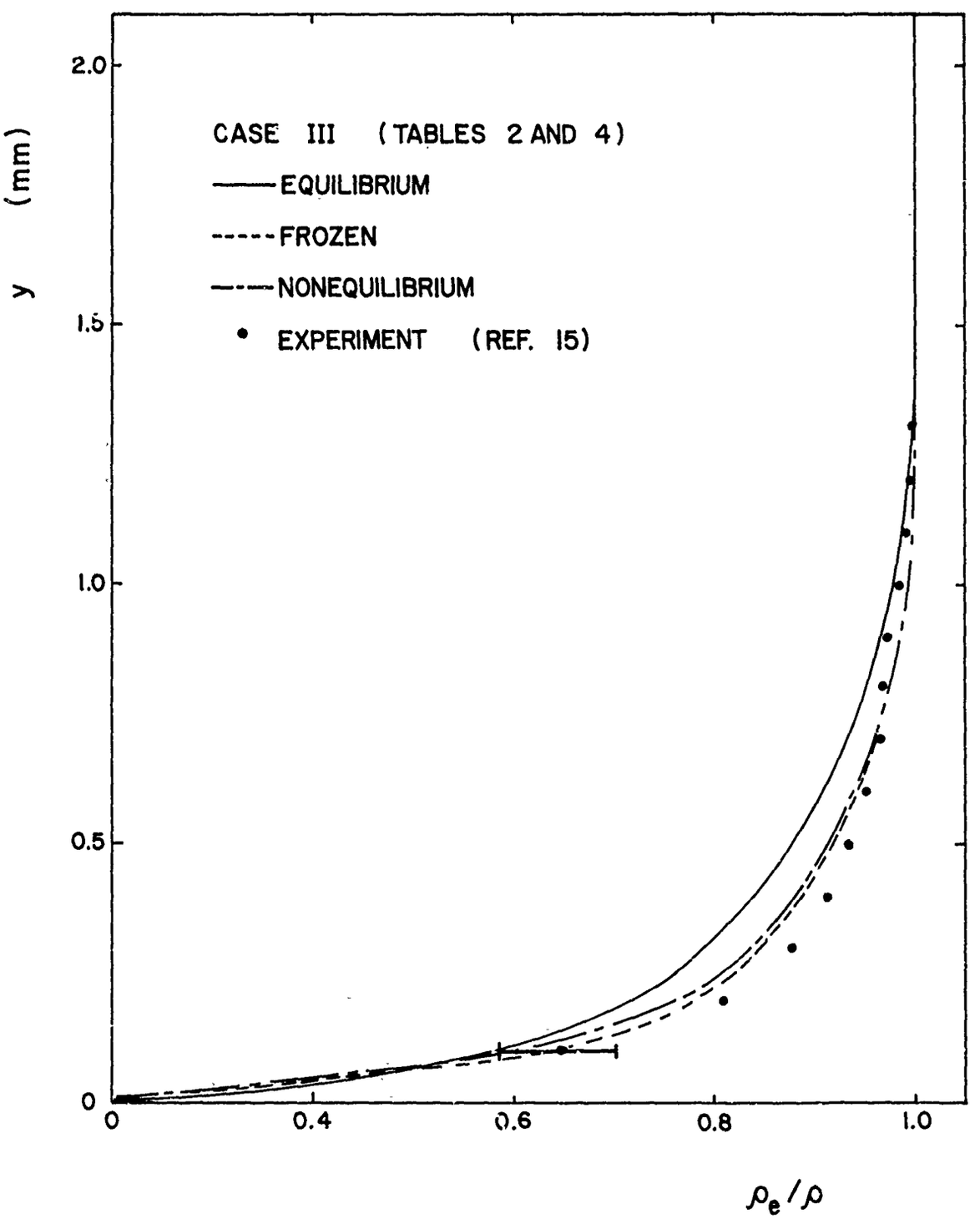

FIG. 19. DENSITY VARIATION (ρ_e/ρ) THROUGH A LAMINAR WALL BOUNDARY LAYER BEHIND A SHOCK WAVE. INITIAL CONDITIONS AS IN FIG. 18.

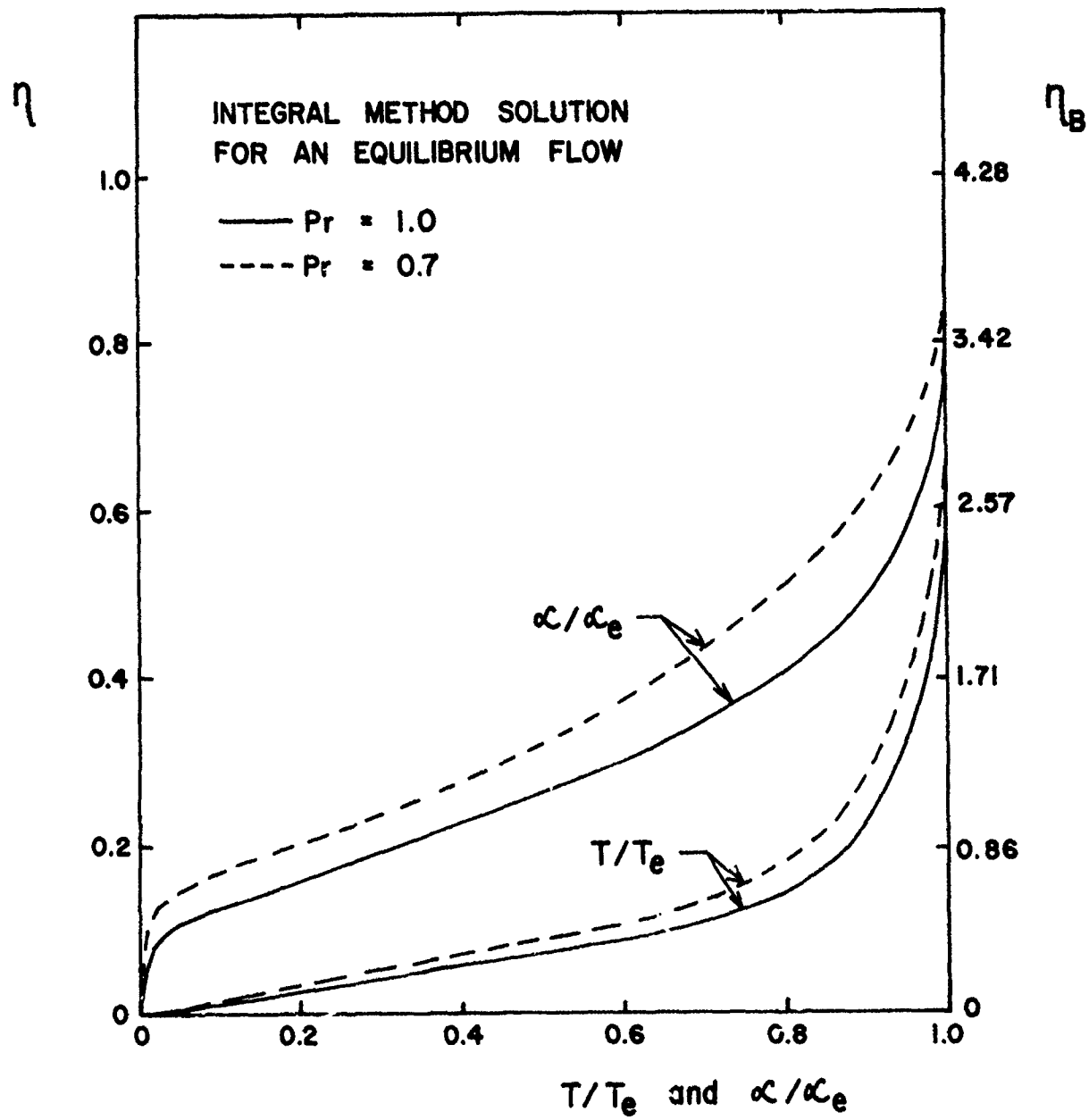

FIG. 20 TEMPERATURE (T/T_e) AND DEGREE OF IONIZATION (α/α_e) VARIATIONS THROUGH A QUASI-STEADY FLAT-PLATE BOUNDARY LAYER.

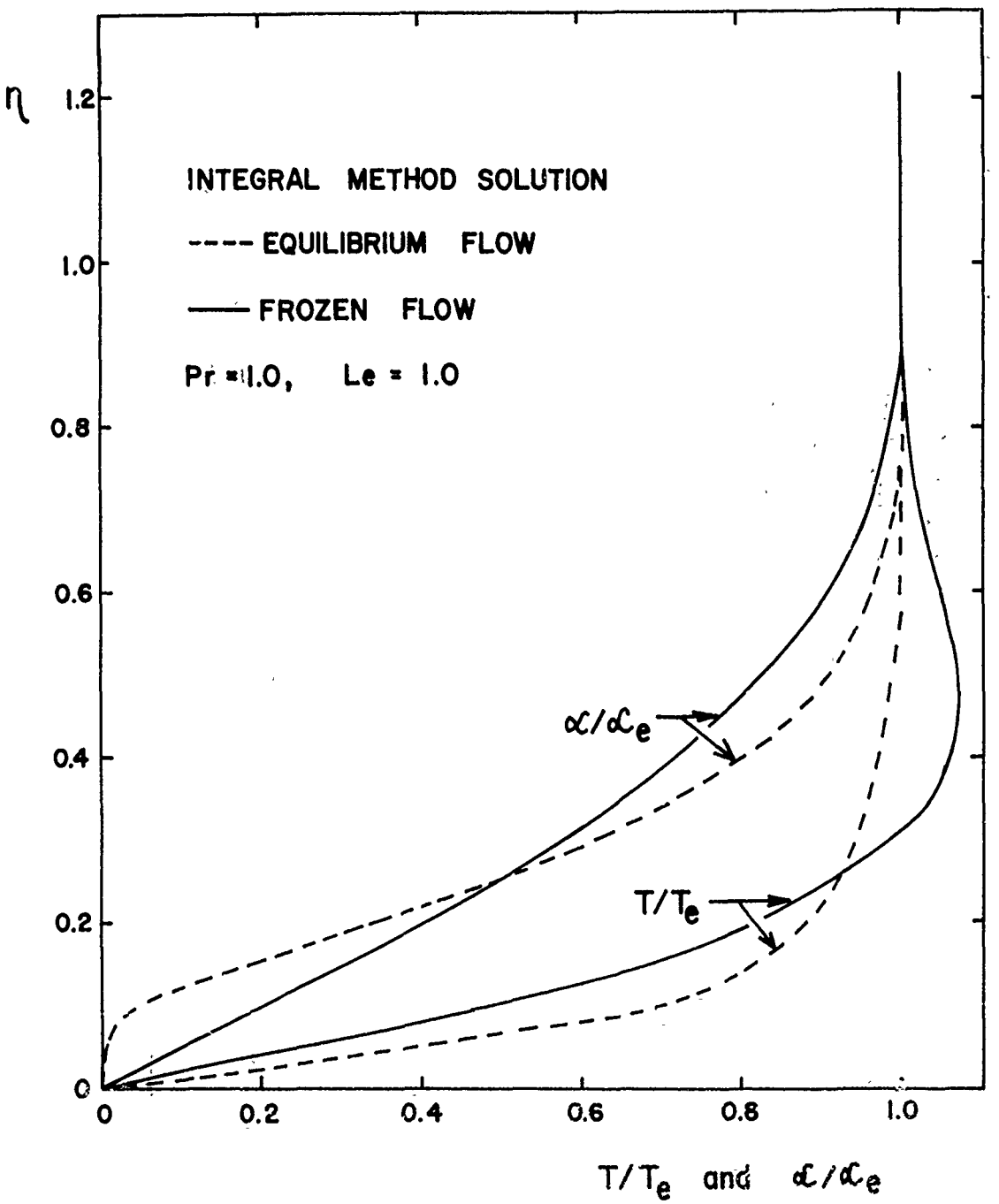

FIG. 21 TEMPERATURE (T/T_e) AND DEGREE OF IONIZATION (α/α_e) VARIATIONS THROUGH A QUASI-STEADY FLAT-PLATE BOUNDARY LAYER.

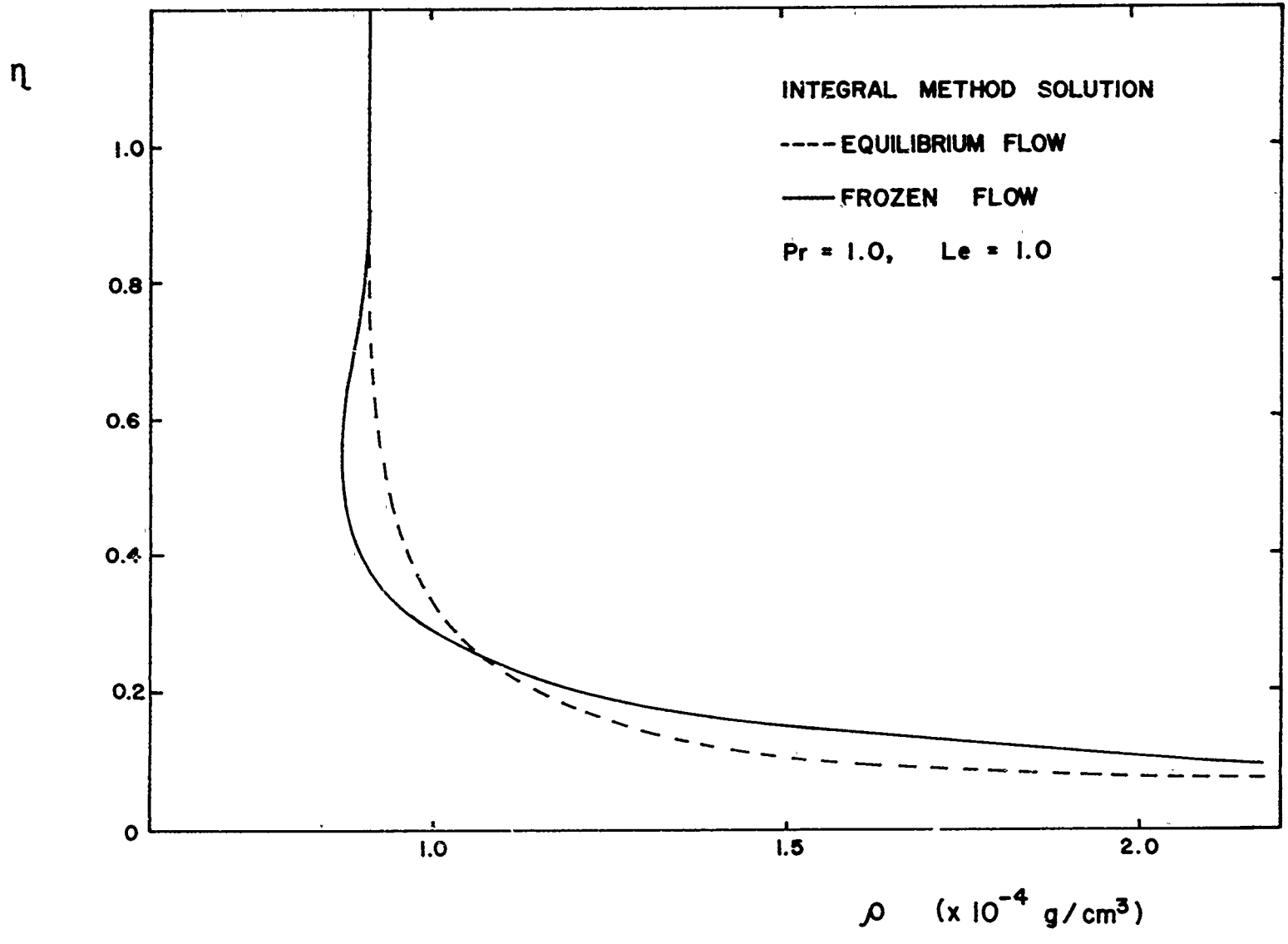

FIG. 22 DENSITY VARIATION (ρ) THROUGH A QUASI-STEADY FLAT-PLATE BOUNDARY LAYER.

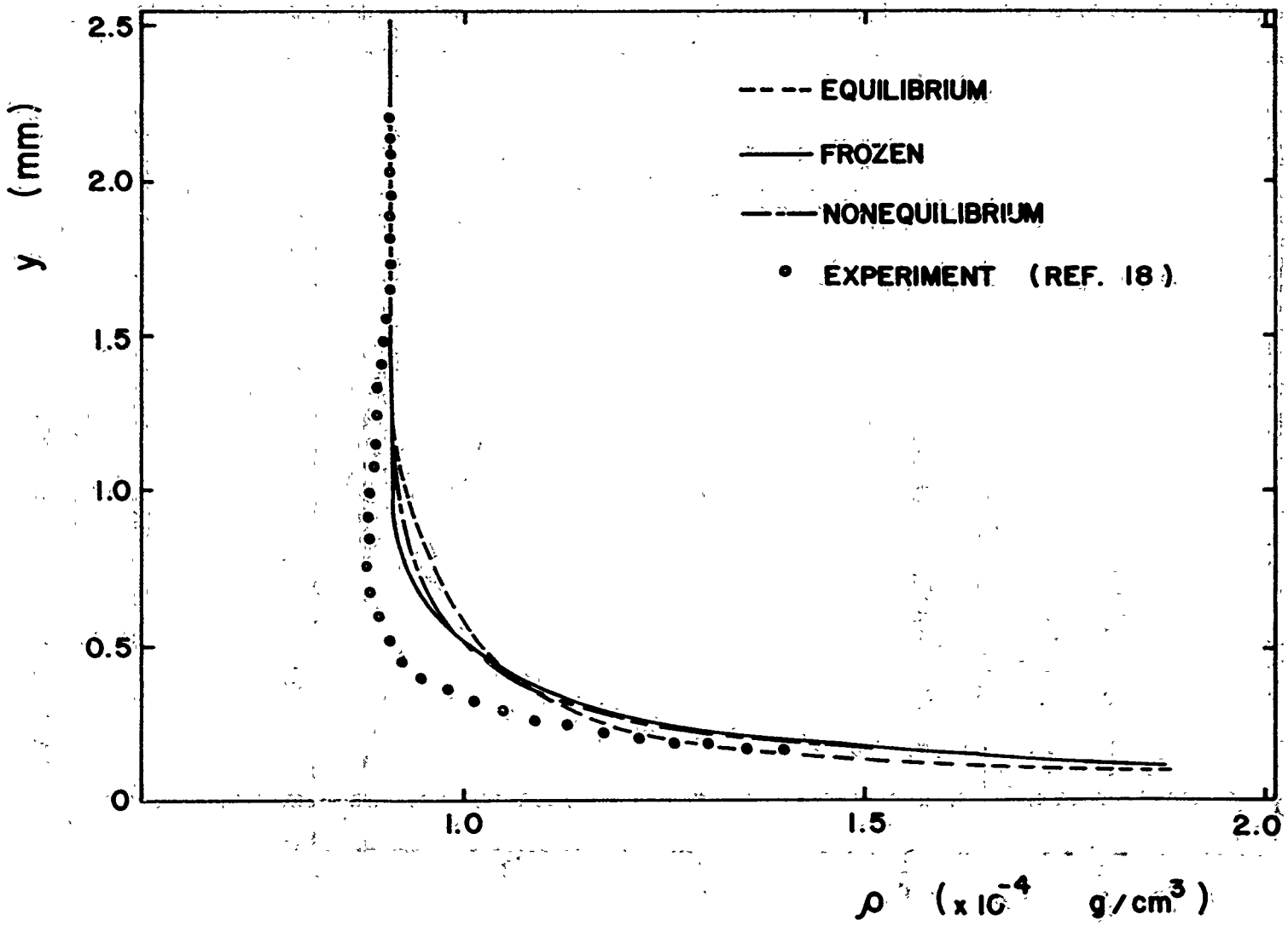

FIG. 23a PREDICTED AND MEASURED DENSITY VARIATIONS THROUGH A QUASI-STEADY FLAT-PLATE BOUNDARY LAYER.

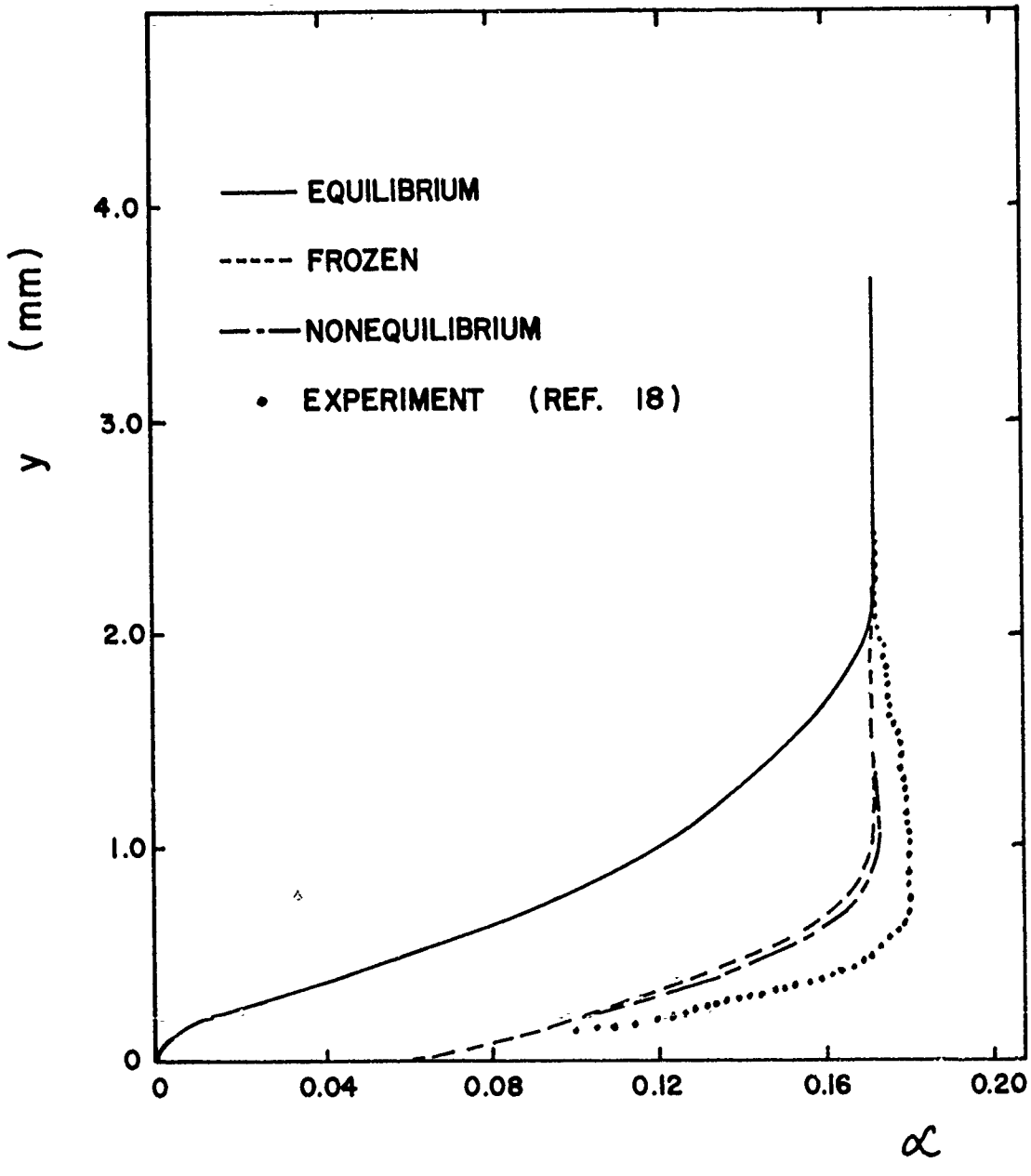

FIG. 23b PREDICTED AND MEASURED DEGREE OF IONIZATION PROFILES THROUGH A QUASI-STEADY FLAT-PLATE BOUNDARY LAYER.

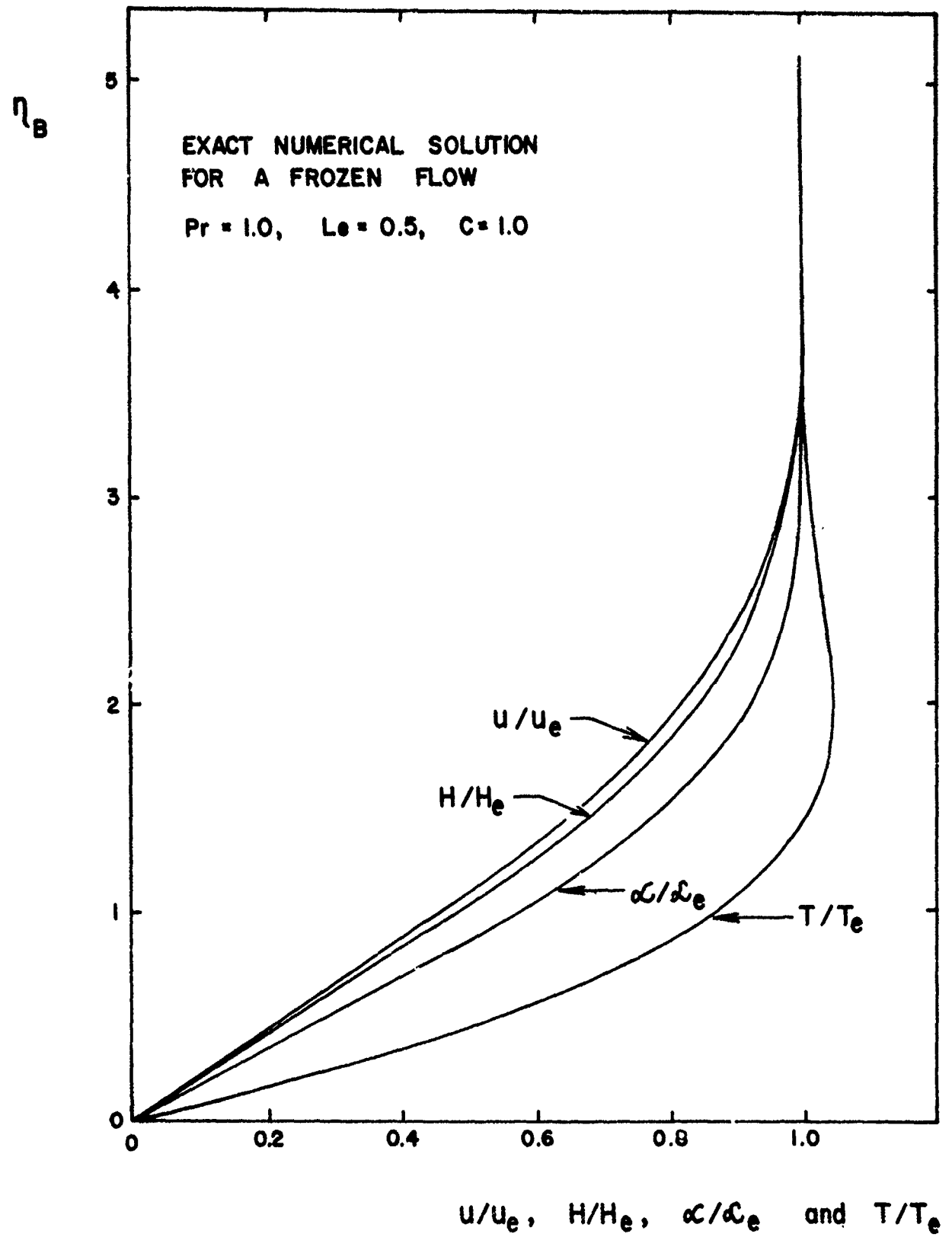

FIG. 24 PREDICTED PROFILES OF FLOW VELOCITY, TOTAL ENTHALPY, DEGREE OF IONIZATION AND TEMPERATURE FOR A QUASI-STEADY FLAT-PLATE BOUNDARY LAYER.

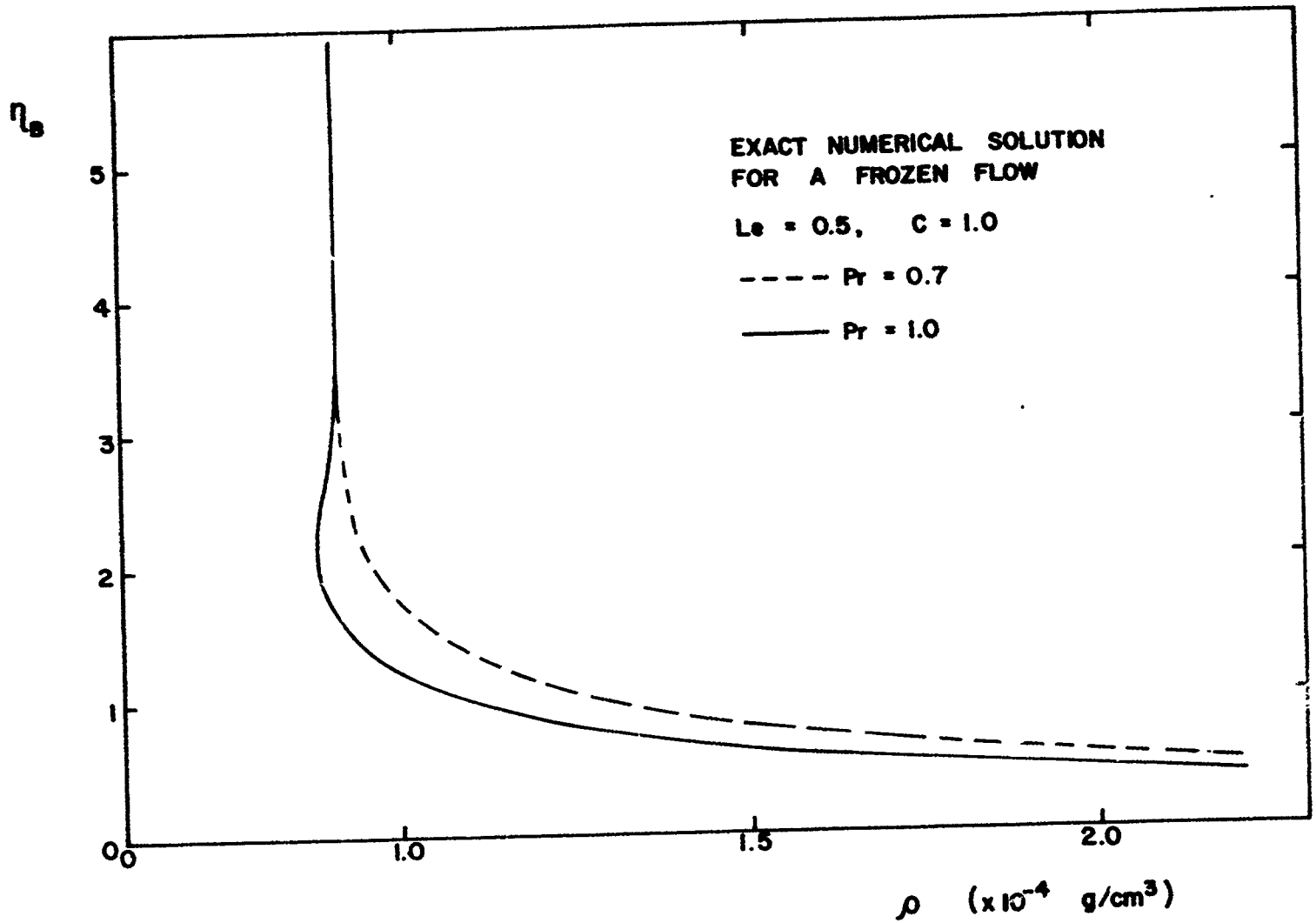

FIG. 25 DENSITY VARIATION THROUGH A QUASI-STEADY FLAT-PLATE BOUNDARY LAYER, FOR TWO DIFFERENT PRANDTL NUMBERS.

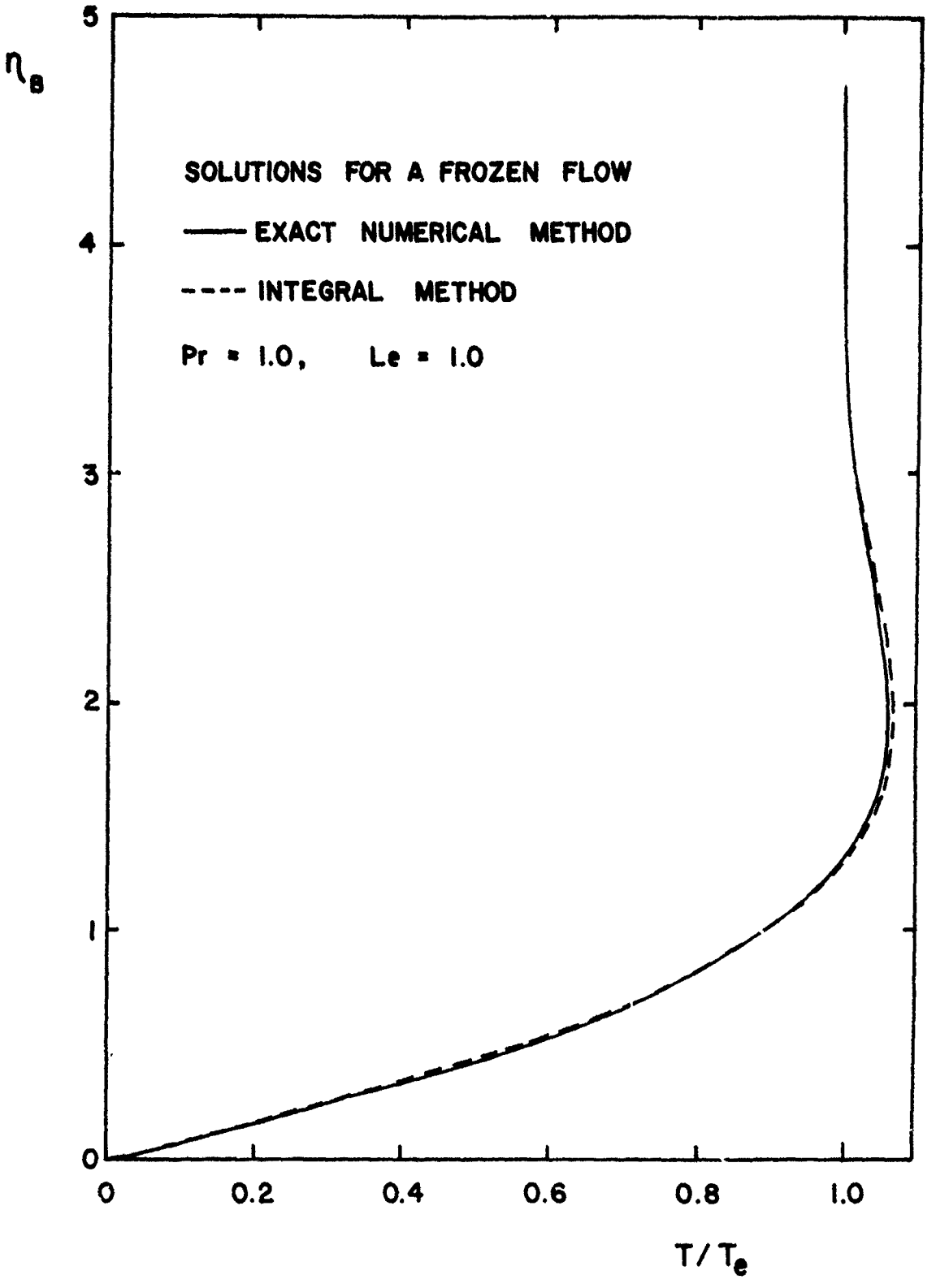

FIG. 26 COMPARISON FO EXACT NUMERICAL AND INTEGRAL METNOD SOLUTIONS OF TH TEMPERATURE PROFILE FOR A QUASI-STEADY FLAT-PLATE BOUNDARY LAYER.

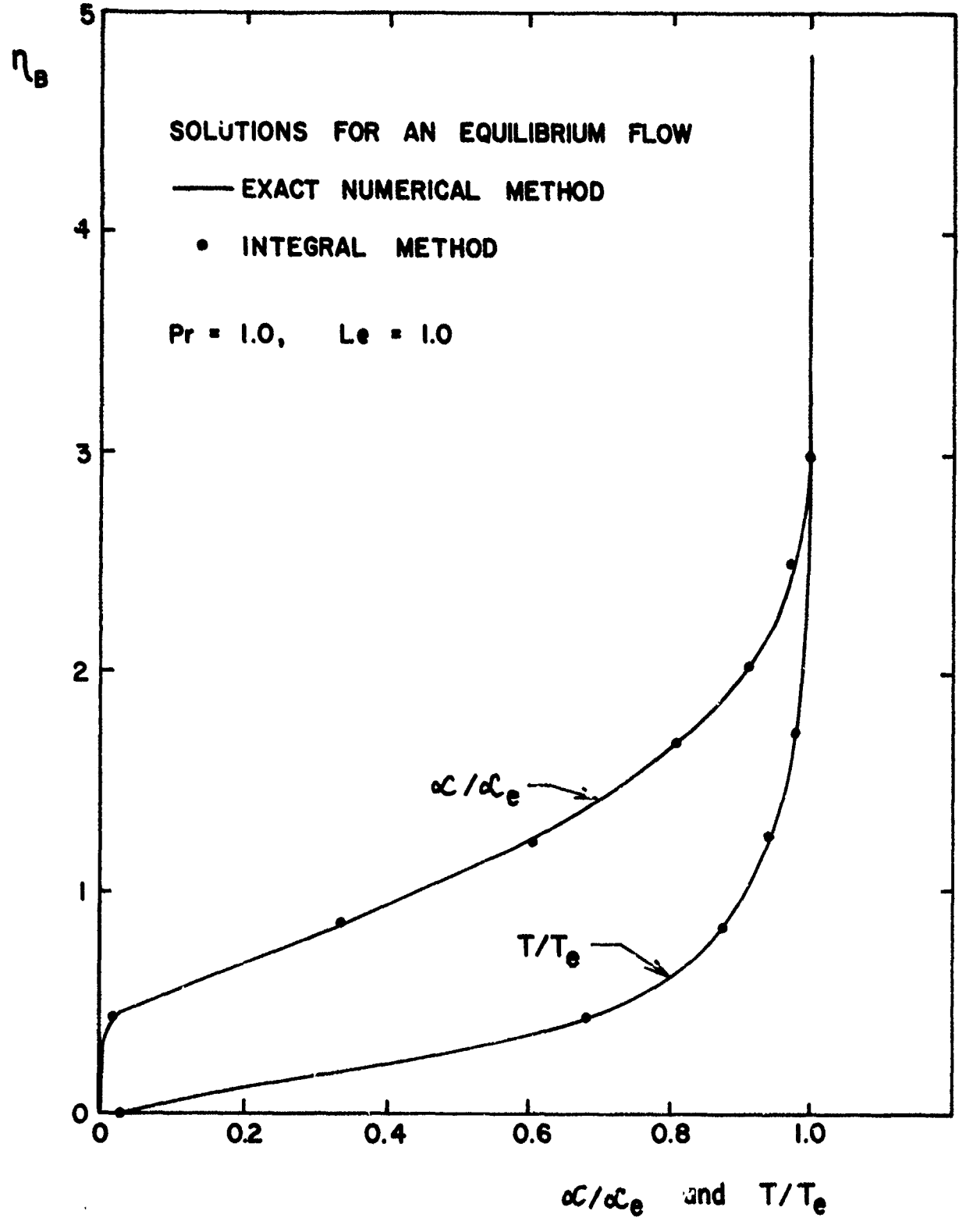

FIG. 27 COMPARISON OF EXACT NUMERICAL AND INTEGRAL METHOD SOLUTIONS FOR BOTH THE TEMPERATURE AND DEGREE OF IONIZATION PROFILES FOR A QUASI-STEADY FLAT-PLATE BOUNDARY LAYER.

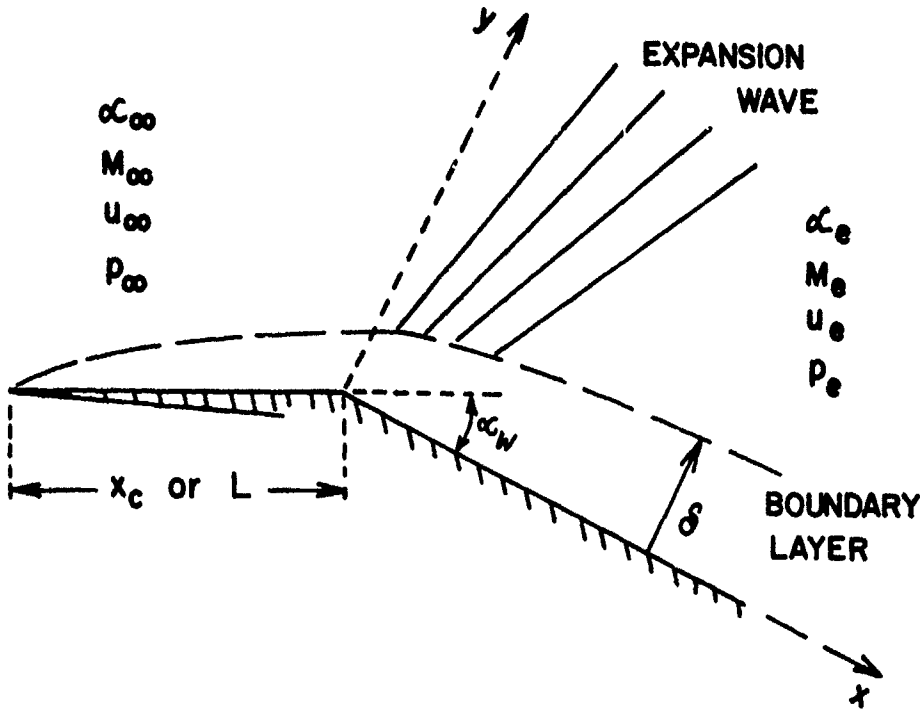

FIG. 28 FLOW PATTERN OF THE BOUNDARY LAYER INTERACTION WITH A CORNER-EXPANSION WAVE.

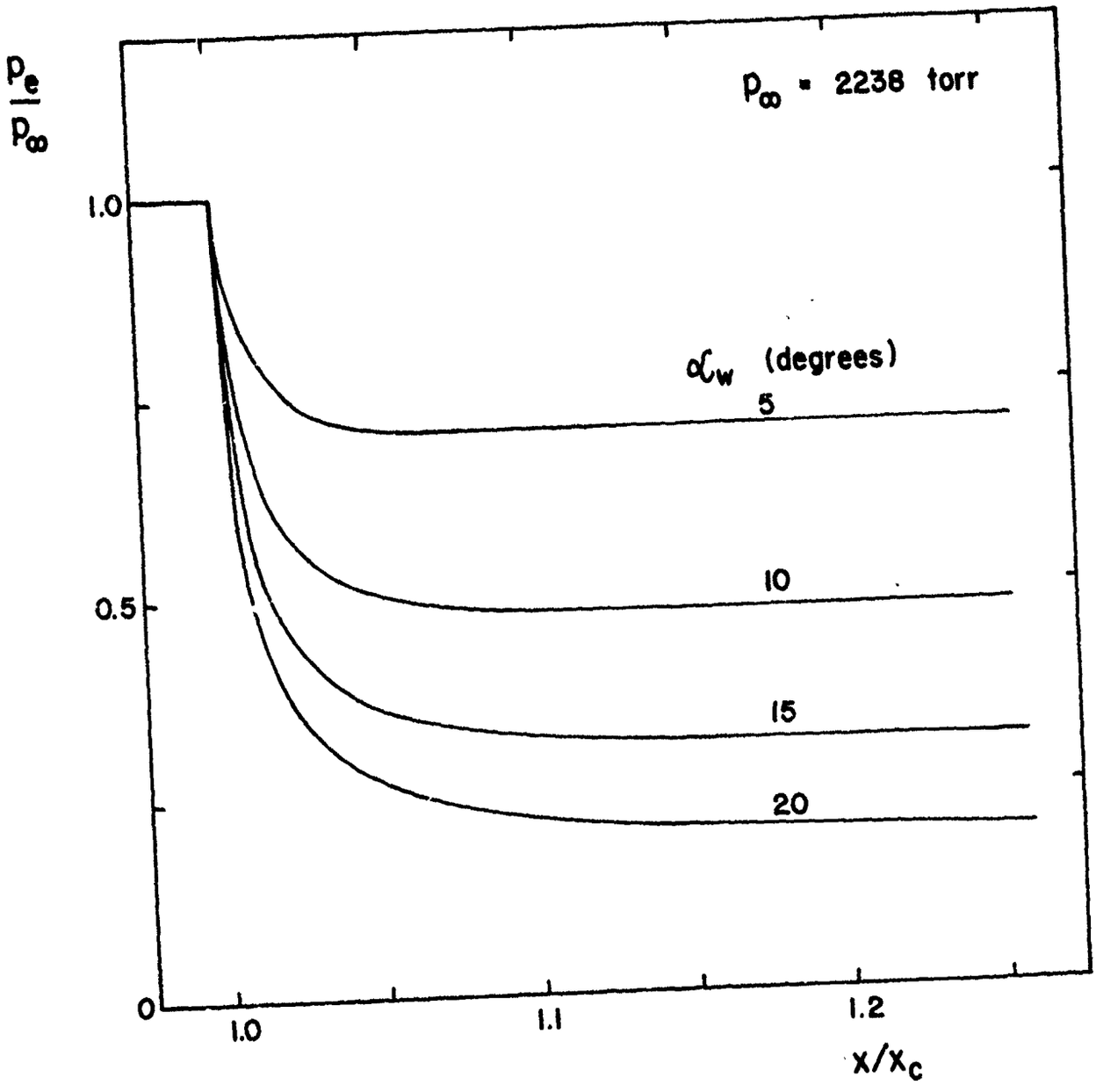

FIG. 29 PRESSURE VARIATION WITH DISTANCE FOR A BOUNDARY LAYER-CORNER EXPANSION FLOW.

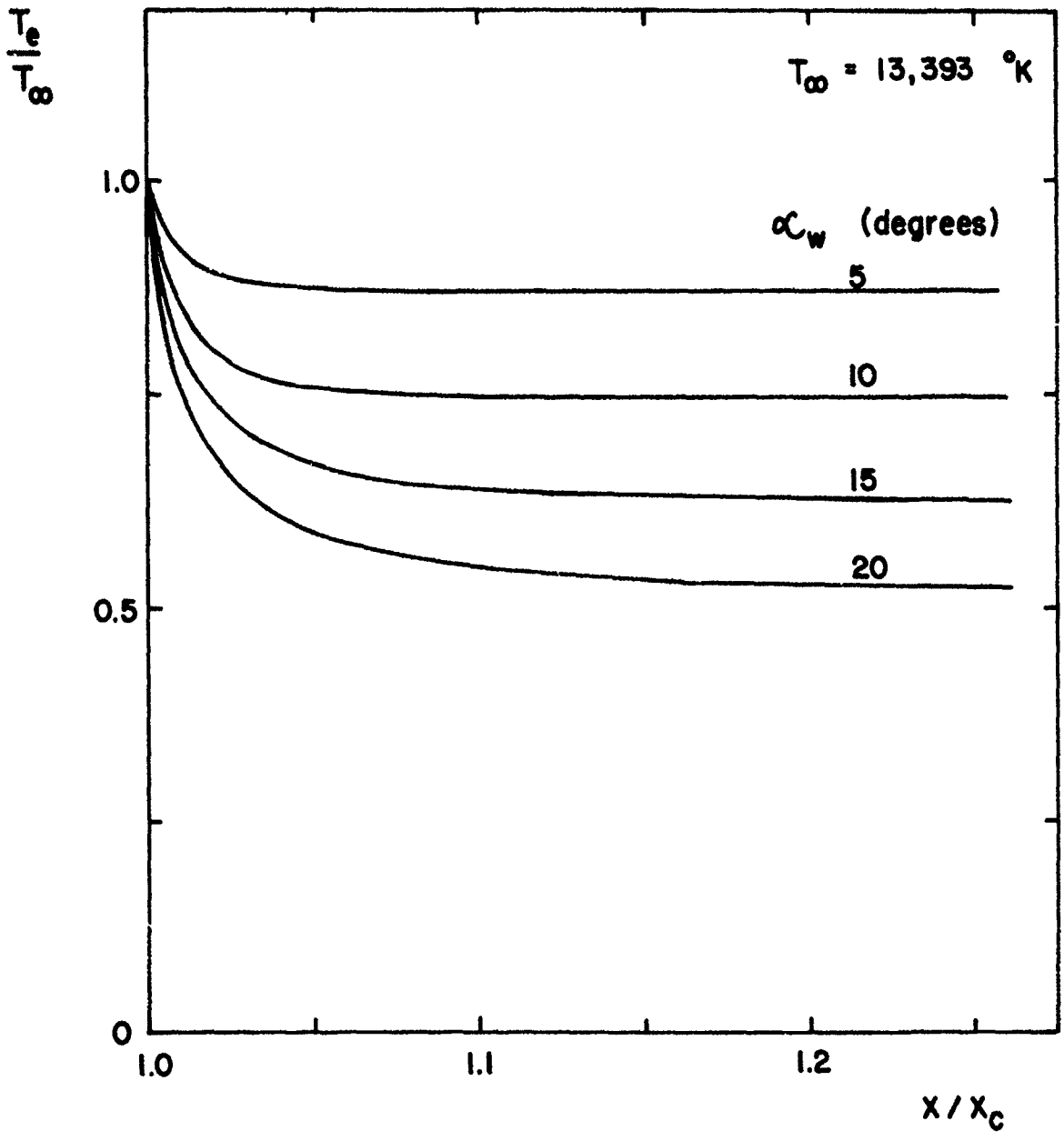

FIG. 30 TEMPERATURE VARIATION WITH DISTANCE FOR A BOUNDARY LAYER-CORNER EXPANSION FLOW.

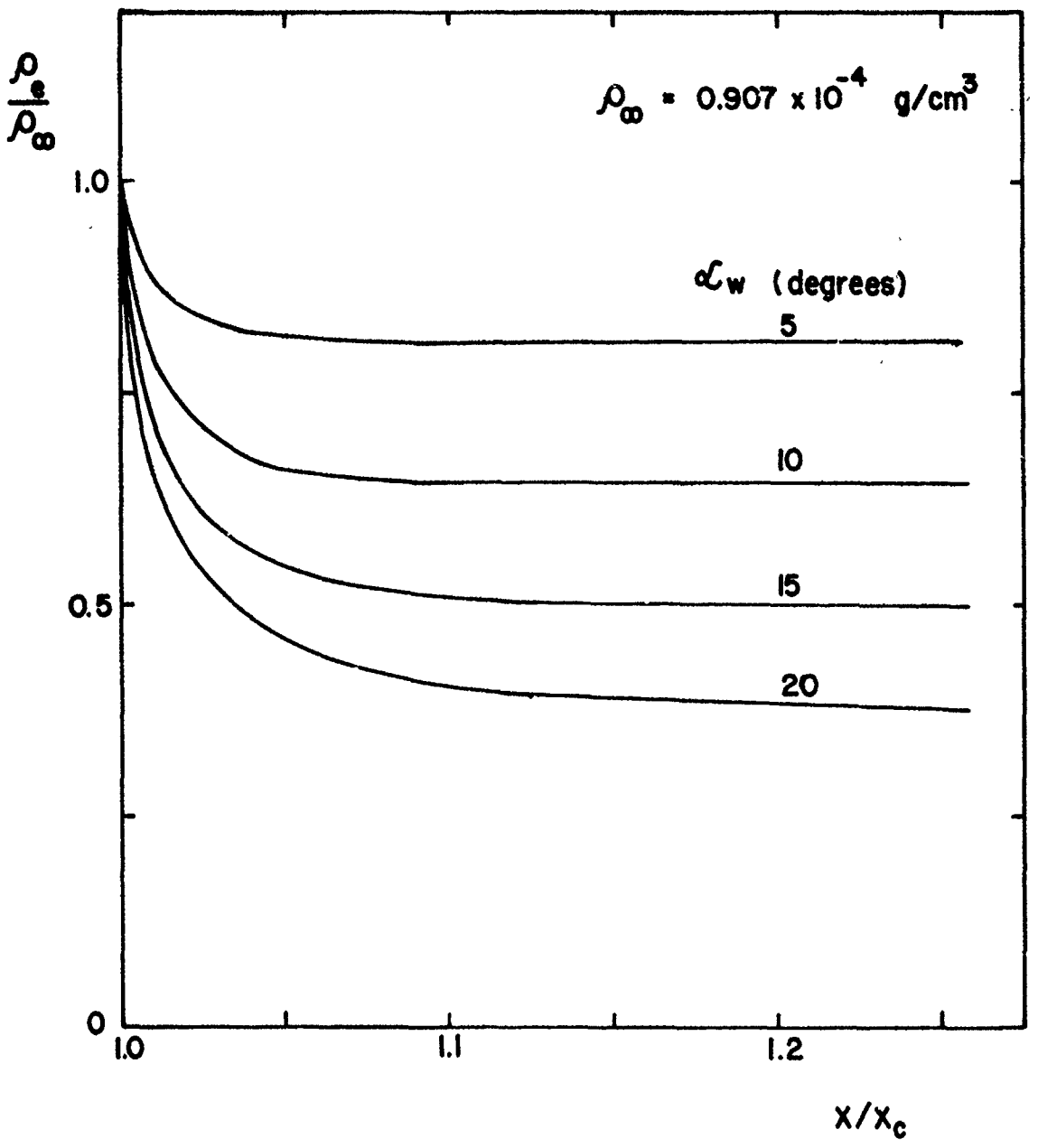

FIG. 31 DENSITY VARIATION WITH DISTANCE FOR A BOUNDARY LAYER-CORNER EXPANSION FLOW.

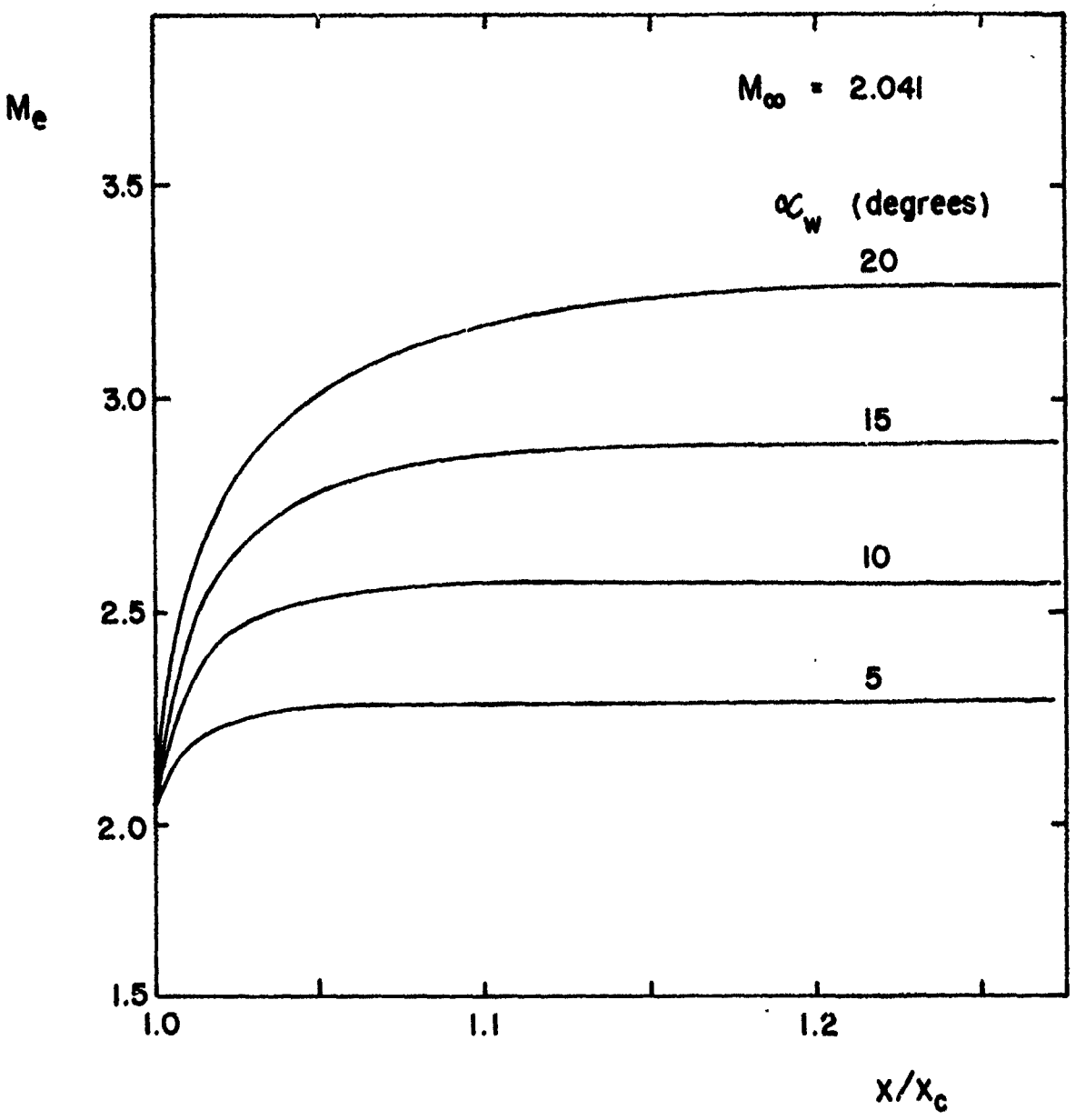

FIG. 32 MACH NUMBER VARIATION WITH DISTANCE FOR A BOUNDARY LAYER-CORNER EXPANSION FLOW.

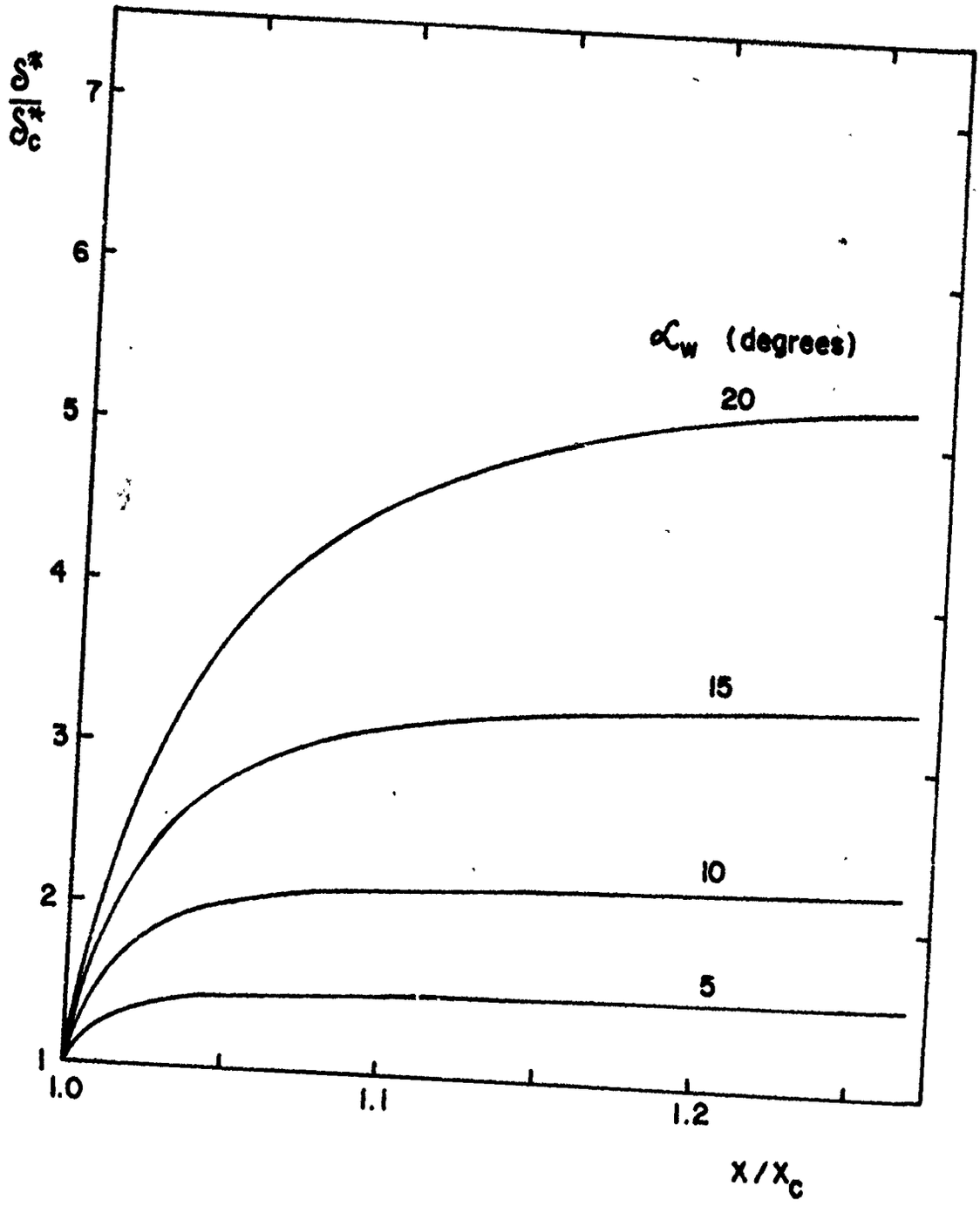

FIG. 33 DISPLACEMENT THICKNESS WITH DISTANCE FOR A BOUNDARY-LAYER, CORNER-EXPANSION FLOW.

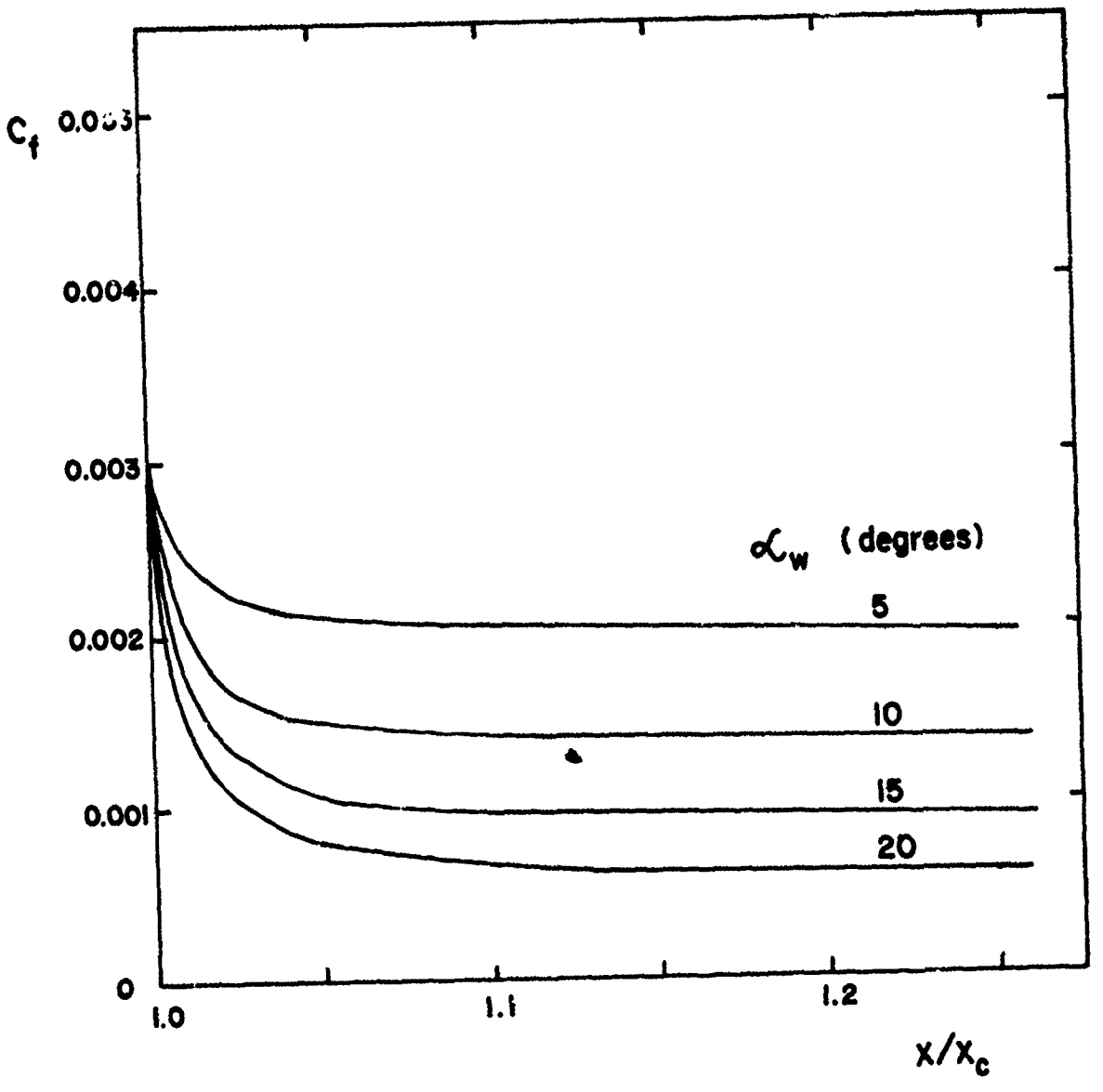

FIG. 34 SKIN FRICTION COEFFICIENT VARIATION WITH DISTANCE FOR A BOUNDARY-LAYER, CORNER-EXPANSION FLOW.

APPENDIX A: METHOD OF SOLVING BOUNDARY-LAYER EQUATIONS

The partial differential equations describing the boundary layer for each problem encountered in this study have been transformed by mathematical techniques into ordinary differential equations. Among the vast number of numerical methods available for solving boundary-value problems of ordinary differential equations the Runge-Kutta method is probably used most frequently. Standard Runge-Kutta computer programs are available and are quite easy to utilize.

The ordinary differential equations of Section 4.8 (Eqs. 4.66 and 4.67) for the equilibrium flow problem can be expressed in terms of five first-order ordinary differential equations with three initial conditions: $f_B(0) = 0$, $f'_B(0) = 0$, $g(0) = g_w$, and two boundary conditions: $f'_B(\infty) = 1$, $g(\infty) = 1$. For the frozen and nonequilibrium flow cases, the basic equations (Eqs. 4.69 to 4.71) can be written as seven first-order ordinary differential equations with four initial conditions: $f_B(0) = 0$, $f'_B(0) = 0$, $g(0) = g_w$ and either $z(0) =$ constant or $z'(0) =$ constant, and three boundary conditions: $f'_B(\infty) = 1$, $g(\infty) = 1$ and $z(\infty) = 1$. A procedure is now given for finding the other initial conditions, $f''_B(0)$, $g'(0)$ and $z'(0)$ (or $z(0)$), for the frozen and nonequilibrium cases. A similar procedure can be used for the equilibrium-flow case.

For the calculations we assume the initial conditions,

$$\begin{aligned} f''_B(0) &= a \\ g'(0) &= b \\ z'(0) \text{ or } E(0) &= c \end{aligned} \tag{A1}$$

and define the following equations,

$$\begin{aligned} F_1(a,b,c) &= 1 - f'_B(\infty) \\ F_2(a,b,c) &= 1 - g(\infty) \\ F_3(a,b,c) &= 1 - z(\infty) \end{aligned} \tag{A2}$$

The solutions to these equations

$$\begin{aligned} F_1(a,b,c) &= 0 \\ F_2(a,b,c) &= 0 \\ F_3(a,b,c) &= 0 \end{aligned} \tag{A3}$$

can often be found by a simple procedure known as the Newton-Raphson method. The recurrence relation can be derived from the Taylor series expansion for $\underline{f}(\underline{x}_1)$

$$\underline{f}(\underline{x}_1) = \underline{f}(\underline{x}_0) + (\underline{x}_1 - x_0)\, \underline{f}'(\underline{x}_1) + \ldots \tag{A3}$$

where, $\underline{f}$ represents F_1, F_2, F_3 and $\underline{x}$ for a,b,c.

From Eq. A3, an iterative sequence can now be obtained as follows:

$$\begin{aligned} a_{i+1} &= a_i - \Delta_a/\Delta \\ b_{i+1} &= b_i - \Delta_b/\Delta \\ c_{i+1} &= c_i - \Delta_c/\Delta \end{aligned} \tag{A4}$$

where,

$$\Delta = \begin{vmatrix} \frac{\partial F_1}{\partial a_i} & \frac{\partial F_1}{\partial b_i} & \frac{\partial F_1}{\partial c_i} \\ \frac{\partial F_2}{\partial a_i} & \frac{\partial F_2}{\partial b_i} & \frac{\partial F_2}{\partial c_i} \\ \frac{\partial F_3}{\partial a_i} & \frac{\partial F_3}{\partial b_i} & \frac{\partial F_3}{\partial c_i} \end{vmatrix} \tag{A5}$$

$$\Delta_a = \begin{vmatrix} F_1(a_i,b_i,c_i) & \frac{\partial F_1}{\partial b_i} & \frac{\partial F_1}{\partial c_i} \\ F_2(a_i,b_i,c_i) & \frac{\partial F_2}{\partial b_i} & \frac{\partial F_2}{\partial c_i} \\ F_3(a_i,b_i,c_i) & \frac{\partial F_3}{\partial b_i} & \frac{\partial F_3}{\partial c_i} \end{vmatrix} \tag{A6}$$

$$\Delta_b = \begin{vmatrix} \frac{\partial F_1}{\partial a_i} & F_1(a_i,b_i,c_i) & \frac{\partial F_1}{\partial c_i} \\ \frac{\partial F_2}{\partial a_i} & F_2(a_i,b_i,c_i) & \frac{\partial F_2}{\partial c_i} \\ \frac{\partial F_3}{\partial a_i} & F_3(a_i,b_i,c_i) & \frac{\partial F_3}{\partial c_i} \end{vmatrix} \tag{A7}$$

$$\Delta_c = \begin{vmatrix} \frac{\partial F_1}{\partial a_i} & \frac{\partial F_1}{\partial b_i} & F_1(a_i,b_i,c_i) \\ \frac{\partial F_2}{\partial a_i} & \frac{\partial F_2}{\partial b_i} & F_2(a_i,b_i,c_i) \\ \frac{\partial F_3}{\partial a_i} & \frac{\partial F_3}{\partial b_i} & F_3(a_i,b_i,c_i) \end{vmatrix} \tag{A8}$$

and the partial derivatives $\partial F_1/\partial a_i$ can be approximated by

$$\frac{\partial F_1}{\partial a_i} = \frac{1}{2h}\left[F_1(a_i + h, b_i, c_i) - F_1(a_i - h, b_i, c_i) \right] \tag{A9}$$

where, h is some appropriate step size. Similarly, the other partial derivatives can be evaluated.

The above procedure is iterative, since an initial approximation $a = a_o$, $b = b_o$, $c = c_o$ to the root of Eq. A3 has to be made, and a sequence of approximations a_{i+1}, b_{i+1} and c_{i+1} are generated as the true root is approached.

The initial conditions (Eq. A1) used in the calculations of the exact similar solutions of Section 4.8 have been checked, and they agree with the values given in Refs. 23, 24 and 63.

UTIAS REPORT NO. 198

Institute for Aerospace Studies, University of Toronto

AN ANALYSIS OF SHOCK STRUCTURE AND NONEQUILIBRIUM LAMINAR BOUNDARY LAYERS INDUCED BY A NORMAL SHOCK WAVE IN AN IONIZED ARGON FLOW

Liu, W. S.   54 pages   4 tables   34 figures

1. Ionized argon shock structure 2. Ionized argon boundary layers 3. Ionized argon corner-expansion flows and interactions 4. Shock tube flows 5. Interferometry 6. Non-equilibrium flows 7. Collision cross-sections 8. Integral and similarity methods

I. Liu, W. S.   II. UTIAS Report No. 198

An analytical study was made to describe the structure of a strong normal shock wave moving into argon and the nonequilibrium flow of partially ionized argon in the laminar boundary layers induced behind the shock wave on the shock-tube walls and over a flat plate. The subsequent interaction of the laminar boundary layer with a corner-expansion flow was also considered. In order to determine the shock structure, the ionization and relaxation processes were based on a two-step model of the collisional processes. The excitation (or ionization) cross-section constant for the argon atom-atom collisions was determined to be 3.5×10^{-20} cm^2/eV from a comparison of theoretical and experimental shock-structure data. The effects of a small amount of hydrogen impurity in the argon test gas on shock-wave structure was evaluated and discussed, as the hydrogen impurity can markedly reduce the total relaxation length. A study of this effect was required in connection with stabilizing the experimental shock waves. An integral method was used in the analysis to study both the shock induced nonstationary laminar boundary layer on the shock-tube walls and the quasi-steady flat-plate laminar boundary layer for an ionized argon flow. The frozen, equilibrium and nonequilibrium flow solutions were obtained and compared with some existing experimental results. The calculated results based on the integral method were found to be in agreement with the experimental data for the shock-induced wall boundary layer, but they did not agree with the experimental data for the flat-plate quasi-steady boundary layer. The cold-wall similarity method of Sullivan was extended to apply to the interaction of a laminar boundary layer with a corner-expansion wave for a supersonic frozen flow. The validity of the extended method is discussed.

Available copies of this report are limited. Return this card to UTIAS, if you require a copy.

UTIAS REPORT NO. 198

Institute for Aerospace Studies, University of Toronto

AN ANALYSIS OF SHOCK STRUCTURE AND NONEQUILIBRIUM LAMINAR BOUNDARY LAYERS INDUCED BY A NORMAL SHOCK WAVE IN AN IONIZED ARGON FLOW

Liu, W. S.   54 pages   4 tables   34 figures

1. Ionized argon shock structure 2. Ionized argon boundary layers 3. Ionized argon corner-expansion flows and interactions 4. Shock tube flows 5. Interferometry 6. Non-equilibrium flows 7. Collision cross-sections 8. Integral and similarity methods

I. Liu, W. S.   II. UTIAS Report No. 198

An analytical study was made to describe the structure of a strong normal shock wave moving into argon and the nonequilibrium flow of partially ionized argon in the laminar boundary layers induced behind the shock wave on the shock-tube walls and over a flat plate. The subsequent interaction of the laminar boundary layer with a corner-expansion flow was also considered. In order to determine the shock structure, the ionization and relaxation processes were based on a two-step model of the collisional processes. The excitation (or ionization) cross-section constant for the argon atom-atom collisions was determined to be 3.5×10^{-20} cm^2/eV from a comparison of theoretical and experimental shock-structure data. The effects of a small amount of hydrogen impurity in the argon test gas on shock-wave structure was evaluated and discussed, as the hydrogen impurity can markedly reduce the total relaxation length. A study of this effect was required in connection with stabilizing the experimental shock waves. An integral method was used in the analysis to study both the shock induced nonstationary laminar boundary layer on the shock-tube walls and the quasi-steady flat-plate laminar boundary layer for an ionized argon flow. The frozen, equilibrium and nonequilibrium flow solutions were obtained and compared with some existing experimental results. The calculated results based on the integral method were found to be in agreement with the experimental data for the shock-induced wall boundary layer, but they did not agree with the experimental data for the flat-plate quasi-steady boundary layer. The cold-wall similarity method of Sullivan was extended to apply to the interaction of a laminar boundary layer with a corner-expansion wave for a supersonic frozen flow. The validity of the extended method is discussed.

Available copies of this report are limited. Return this card to UTIAS, if you require a copy.

UTIAS REPORT NO. 198

Institute for Aerospace Studies, University of Toronto

AN ANALYSIS OF SHOCK STRUCTURE AND NONEQUILIBRIUM LAMINAR BOUNDARY LAYERS INDUCED BY A NORMAL SHOCK WAVE IN AN IONIZED ARGON FLOW

Liu, W. S.   54 pages   4 tables   34 figures

1. Ionized argon shock structure 2. Ionized argon boundary layers 3. Ionized argon corner-expansion flows and interactions 4. Shock tube flows 5. Interferometry 6. Non-equilibrium flows 7. Collision cross-sections 8. Integral and similarity methods

I. Liu, W. S.   II. UTIAS Report No. 198

An analytical study was made to describe the structure of a strong normal shock wave moving into argon and the nonequilibrium flow of partially ionized argon in the laminar boundary layers induced behind the shock wave on the shock-tube walls and over a flat plate. The subsequent interaction of the laminar boundary layer with a corner-expansion flow was also considered. In order to determine the shock structure, the ionization and relaxation processes were based on a two-step model of the collisional processes. The excitation (or ionization) cross-section constant for the argon atom-atom collisions was determined to be 3.5×10^{-20} cm^2/eV from a comparison of theoretical and experimental shock-structure data. The effects of a small amount of hydrogen impurity in the argon test gas on shock-wave structure was evaluated and discussed, as the hydrogen impurity can markedly reduce the total relaxation length. A study of this effect was required in connection with stabilizing the experimental shock waves. An integral method was used in the analysis to study both the shock induced nonstationary laminar boundary layer on the shock-tube walls and the quasi-steady flat-plate laminar boundary layer for an ionized argon flow. The frozen, equilibrium and nonequilibrium flow solutions were obtained and compared with some existing experimental results. The calculated results based on the integral method were found to be in agreement with the experimental data for the shock-induced wall boundary layer, but they did not agree with the experimental data for the flat-plate quasi-steady boundary layer. The cold-wall similarity method of Sullivan was extended to apply to the interaction of a laminar boundary layer with a corner-expansion wave for a supersonic frozen flow. The validity of the extended method is discussed.

Available copies of this report are limited. Return this card to UTIAS, if you require a copy.

UTIAS REPORT NO. 198

Institute for Aerospace Studies, University of Toronto

AN ANALYSIS OF SHOCK STRUCTURE AND NONEQUILIBRIUM LAMINAR BOUNDARY LAYERS INDUCED BY A NORMAL SHOCK WAVE IN AN IONIZED ARGON FLOW

Liu, W. S.   54 pages   4 tables   34 figures

1. Ionized argon shock structure 2. Ionized argon boundary layers 3. Ionized argon corner-expansion flows and interactions 4. Shock tube flows 5. Interferometry 6. Non-equilibrium flows 7. Collision cross-sections 8. Integral and similarity methods

I. Liu, W. S.   II. UTIAS Report No. 198

An analytical study was made to describe the structure of a strong normal shock wave moving into argon and the nonequilibrium flow of partially ionized argon in the laminar boundary layers induced behind the shock wave on the shock-tube walls and over a flat plate. The subsequent interaction of the laminar boundary layer with a corner-expansion flow was also considered. In order to determine the shock structure, the ionization and relaxation processes were based on a two-step model of the collisional processes. The excitation (or ionization) cross-section constant for the argon atom-atom collisions was determined to be 3.5×10^{-20} cm^2/eV from a comparison of theoretical and experimental shock-structure data. The effects of a small amount of hydrogen impurity in the argon test gas on shock-wave structure was evaluated and discussed, as the hydrogen impurity can markedly reduce the total relaxation length. A study of this effect was required in connection with stabilizing the experimental shock waves. An integral method was used in the analysis to study both the shock induced nonstationary laminar boundary layer on the shock-tube walls and the quasi-steady flat-plate laminar boundary layer for an ionized argon flow. The frozen, equilibrium and nonequilibrium flow solutions were obtained and compared with some existing experimental results. The calculated results based on the integral method were found to be in agreement with the experimental data for the shock-induced wall boundary layer, but they did not agree with the experimental data for the flat-plate quasi-steady boundary layer. The cold-wall similarity method of Sullivan was extended to apply to the interaction of a laminar boundary layer with a corner-expansion wave for a supersonic frozen flow. The validity of the extended method is discussed.

Available copies of this report are limited. Return this card to UTIAS, if you require a copy.

UTIAS REPORT NO. 198

Institute for Aerospace Studies, University of Toronto

AN ANALYSIS OF SHOCK STRUCTURE AND NONEQUILIBRIUM LAMINAR BOUNDARY LAYERS INDUCED BY A NORMAL SHOCK WAVE IN AN IONIZED ARGON FLOW

Liu, W. S. 54 pages 4 tables 34 figures

1. Ionized argon shock structure 2. Ionized argon boundary layers 3. Ionized argon corner-expansion flows and interactions 4. Shock tube flows 5. Interferometry 6. Non-equilibrium flows 7. Collision cross-sections 8. Integral and similarity methods

I. Liu, W. S. II. UTIAS Report No. 198

An analytical study was made to describe the structure of a strong normal shock wave moving into argon and the nonequilibrium flow of partially ionized argon in the laminar boundary layers induced behind the shock wave on the shock-tube walls and over a flat plate. The subsequent interaction of the laminar boundary layer with a corner-expansion flow was also considered. In order to determine the shock structure, the ionization and relaxation processes were based on a two-step model of the collisional processes. The excitation (or ionization) cross-section constant for the argon atom-atom collisions was determined to be 3.5×10^{-20} cm^2/eV from a comparison of theoretical and experimental shock-structure data. The effects of a small amount of hydrogen impurity in the argon test gas on shock-wave structure was evaluated and discussed, as the hydrogen impurity can markedly reduce the total relaxation length. A study of this effect was required in connection with stabilizing the experimental shock waves. An integral method was used in the analysis to study both the shock induced nonstationary laminar boundary layer on the shock-tube walls and the quasi-steady flat-plate laminar boundary layer for an ionized argon flow. The frozen, equilibrium and nonequilibrium flow solutions were obtained and compared with some existing experimental results. The calculated results based on the integral method were found to be in agreement with the experimental data for the shock-induced wall boundary layer, but they did not agree with the experimental data for the flat-plate quasi-steady boundary layer. The cold-wall similarity method of Sullivan was extended to apply to the interaction of a laminar boundary layer with a corner-expansion wave for a supersonic frozen flow. The validity of the extended method is discussed.

Available copies of this report are limited. Return this card to UTIAS, if you require a copy.

UTIAS REPORT NO. 198

Institute for Aerospace Studies, University of Toronto

AN ANALYSIS OF SHOCK STRUCTURE AND NONEQUILIBRIUM LAMINAR BOUNDARY LAYERS INDUCED BY A NORMAL SHOCK WAVE IN AN IONIZED ARGON FLOW

Liu, W. S. 54 pages 4 tables 34 figures

1. Ionized argon shock structure 2. Ionized argon boundary layers 3. Ionized argon corner-expansion flows and interactions 4. Shock tube flows 5. Interferometry 6. Non-equilibrium flows 7. Collision cross-sections 8. Integral and similarity methods

I. Liu, W. S. II. UTIAS Report No. 198

An analytical study was made to describe the structure of a strong normal shock wave moving into argon and the nonequilibrium flow of partially ionized argon in the laminar boundary layers induced behind the shock wave on the shock-tube walls and over a flat plate. The subsequent interaction of the laminar boundary layer with a corner-expansion flow was also considered. In order to determine the shock structure, the ionization and relaxation processes were based on a two-step model of the collisional processes. The excitation (or ionization) cross-section constant for the argon atom-atom collisions was determined to be 3.5×10^{-20} cm^2/eV from a comparison of theoretical and experimental shock-structure data. The effects of a small amount of hydrogen impurity in the argon test gas on shock-wave structure was evaluated and discussed, as the hydrogen impurity can markedly reduce the total relaxation length. A study of this effect was required in connection with stabilizing the experimental shock waves. An integral method was used in the analysis to study both the shock induced nonstationary laminar boundary layer on the shock-tube walls and the quasi-steady flat-plate laminar boundary layer for an ionized argon flow. The frozen, equilibrium and nonequilibrium flow solutions were obtained and compared with some existing experimental results. The calculated results based on the integral method were found to be in agreement with the experimental data for the shock-induced wall boundary layer, but they did not agree with the experimental data for the flat-plate quasi-steady boundary layer. The cold-wall similarity method of Sullivan was extended to apply to the interaction of a laminar boundary layer with a corner-expansion wave for a supersonic frozen flow. The validity of the extended method is discussed.

Available copies of this report are limited. Return this card to UTIAS, if you require a copy.

UTIAS REPORT NO. 198

Institute for Aerospace Studies, University of Toronto

AN ANALYSIS OF SHOCK STRUCTURE AND NONEQUILIBRIUM LAMINAR BOUNDARY LAYERS INDUCED BY A NORMAL SHOCK WAVE IN AN IONIZED ARGON FLOW

Liu, W. S. 54 pages 4 tables 34 figures

1. Ionized argon shock structure 2. Ionized argon boundary layers 3. Ionized argon corner-expansion flows and interactions 4. Shock tube flows 5. Interferometry 6. Non-equilibrium flows 7. Collision cross-sections 8. Integral and similarity methods

I. Liu, W. S. II. UTIAS Report No. 198

An analytical study was made to describe the structure of a strong normal shock wave moving into argon and the nonequilibrium flow of partially ionized argon in the laminar boundary layers induced behind the shock wave on the shock-tube walls and over a flat plate. The subsequent interaction of the laminar boundary layer with a corner-expansion flow was also considered. In order to determine the shock structure, the ionization and relaxation processes were based on a two-step model of the collisional processes. The excitation (or ionization) cross-section constant for the argon atom-atom collisions was determined to be 3.5×10^{-20} cm^2/eV from a comparison of theoretical and experimental shock-structure data. The effects of a small amount of hydrogen impurity in the argon test gas on shock-wave structure was evaluated and discussed, as the hydrogen impurity can markedly reduce the total relaxation length. A study of this effect was required in connection with stabilizing the experimental shock waves. An integral method was used in the analysis to study both the shock induced nonstationary laminar boundary layer on the shock-tube walls and the quasi-steady flat-plate laminar boundary layer for an ionized argon flow. The frozen, equilibrium and nonequilibrium flow solutions were obtained and compared with some existing experimental results. The calculated results based on the integral method were found to be in agreement with the experimental data for the shock-induced wall boundary layer, but they did not agree with the experimental data for the flat-plate quasi-steady boundary layer. The cold-wall similarity method of Sullivan was extended to apply to the interaction of a laminar boundary layer with a corner-expansion wave for a supersonic frozen flow. The validity of the extended method is discussed.

Available copies of this report are limited. Return this card to UTIAS, if you require a copy.

UTIAS REPORT NO. 198

Institute for Aerospace Studies, University of Toronto

AN ANALYSIS OF SHOCK STRUCTURE AND NONEQUILIBRIUM LAMINAR BOUNDARY LAYERS INDUCED BY A NORMAL SHOCK WAVE IN AN IONIZED ARGON FLOW

Liu, W. S. 54 pages 4 tables 34 figures

1. Ionized argon shock structure 2. Ionized argon boundary layers 3. Ionized argon corner-expansion flows and interactions 4. Shock tube flows 5. Interferometry 6. Non-equilibrium flows 7. Collision cross-sections 8. Integral and similarity methods

I. Liu, W. S. II. UTIAS Report No. 198

An analytical study was made to describe the structure of a strong normal shock wave moving into argon and the nonequilibrium flow of partially ionized argon in the laminar boundary layers induced behind the shock wave on the shock-tube walls and over a flat plate. The subsequent interaction of the laminar boundary layer with a corner-expansion flow was also considered. In order to determine the shock structure, the ionization and relaxation processes were based on a two-step model of the collisional processes. The excitation (or ionization) cross-section constant for the argon atom-atom collisions was determined to be 3.5×10^{-20} cm^2/eV from a comparison of theoretical and experimental shock-structure data. The effects of a small amount of hydrogen impurity in the argon test gas on shock-wave structure was evaluated and discussed, as the hydrogen impurity can markedly reduce the total relaxation length. A study of this effect was required in connection with stabilizing the experimental shock waves. An integral method was used in the analysis to study both the shock induced nonstationary laminar boundary layer on the shock-tube walls and the quasi-steady flat-plate laminar boundary layer for an ionized argon flow. The frozen, equilibrium and nonequilibrium flow solutions were obtained and compared with some existing experimental results. The calculated results based on the integral method were found to be in agreement with the experimental data for the shock-induced wall boundary layer, but they did not agree with the experimental data for the flat-plate quasi-steady boundary layer. The cold-wall similarity method of Sullivan was extended to apply to the interaction of a laminar boundary layer with a corner-expansion wave for a supersonic frozen flow. The validity of the extended method is discussed.

Available copies of this report are limited. Return this card to UTIAS, if you require a copy.